NASA Contractor Report 168293

A THEOPETICAL AND EXPERIMENTAL STUDY OF TURBULENT PARTICLE-LADEN JETS

J-S. Shuen, A.S.P. Solomon, Q-F. Zhang and G. M. Faeth

The Pennsylvania State University
University Park, Pennsylvania

November 1983

Prepared for

NATIONAL AERONAUTICS AND SPACE ADMINISTRATION
Lewis Research Center
Under Grant NAG 3-190

TABLE OF CONTENTS

NOMENCLATURE

Symbol	Description
a	acceleration of gravity
C	particle concentration
C_D	drag coefficient
C_i	parameters in turbulence model
d	injector diameter
d_p	drop diameter
f	mixture fraction
G	particle mass flux
k	turbulence kinetic energy
L_e	dissipation length scale
m	particle mass
n	number of particle groups
n_i	number of particles per unit time in group i
r	radial distance
Re	Reynolds number
S	source term
S_p	particle source term
t	time
t_e	eddy lifetime
u	axial velocity
u_p	particle velocity vector
v	radial velocity
v^o	Favre radial velocity
x	axial distance
x_p	particle position vector
y	lateral distance of particle disp...
Δx_p	path length of particles in an eddy
Δt	time of particle residence in an eddy
ϵ	rate of dissipation of turbulence kinetic energy
μ_t	turbulent viscosity
ρ	density
σ_i	turbulent Prandtl/Schmidt number
ϕ	generic property
Subscripts	
c	centerline quantity
p	particle property
o	injector exit condition
∞	ambient condition
Superscripts	
$( )'$	fluctuating quantity
$(\bar{})$	time mean value
$\vec{( )}$	vector quantity

SUMMARY

A theoretical and experimental study of particle-laden jets is described. The objective of the work is to assist the development of spray models--considering multiphase flows which are readily made monodisperse and avoid problems of drop shattering and coalescence. Models of these processes, developed during the first phase of this study [1-5], were evaluated by comparison of predictions with the measurements completed during this investigation, as well as measurements of Elghobashi et al. [6,7]. Three models of the process were evaluated: (1) a locally homogeneous flow (LHF) model, where slip between the phases was neglected; (2) a deterministic separated flow (DSF) model, where slip was considered but effects of particle dispersion by the turbulence were ignored; and (3) a stochastic separated flow (SSF) model, where effects of interphase slip and turbulent dispersion were considered using random sampling for turbulence properties in conjunction with random-walk computations for particle motion. All three models used a k-ε turbulence model which was extensively evaluated for constant and variable density single-phase jets during earlier work in this laboratory.

Measurements were conducted in particle-laden jets, to supplement existing results in the literature. Particle Sauter mean diameters of 79, 119 and 207 μm, and loading ratios of 0.2 and 0.66 were considered. Measurements included mean and fluctuating velocities of both phases, particle mass fluxes, particle size distributions, and calibration of particle drag properties. Particular attention was given to defining initial conditions of the flows, since the absence of this information was a major limitation in obtaining definite model evaluation when using existing results.

The LHF and DSF models did not provide very satisfactory predictions for the present measurements. The DSF model generally underestimated the rate of spread of the dispersed phase as a result of ignoring effects of turbulent dispersion. The LHF model provided reasonably good predictions for flows containing tracer-like particles, but was unsatisfactory for most practical flows. The LHF model generally overestimated the rate of spread of dispersed phases due to neglect of slip. The SSF model, however, yielded satisfactory predictions of flow structure--except at high particle loadings.

Some effects of particles on turbulence properties (turbulence modulation) were observed at high particle mass loadings. A modified k-ε turbulence model, accounting for the

effects of interphase transport, was developed for particle-laden jets within the framework of SSF formulation. Computations using this model showed that the effects of turbulence modulation on the present measurments were small--on the order of 7% at most. This finding was expected, since the present test flows are relatively dilute.

A sensitivity study was conducted for predictions of the present measurements, to examine the effects of specification of initial conditions and particle properties on the calculated results. In general, the predictions of gas-phase properties were not sensitive to specifications of initial conditions, while variations of particle size exerted large effects on predictions of particle flow properties. Since the particle size distributions involved in this study had relatively small standard deviations, uncertainties due to the use of one average particle size, the Sauter mean diameter, for each size group were within experimental accuracy.

The particle-laden jet structure measurements by Elghobashi et al. [6,7] were also examined during the present investigation. It was found that axial pressure gradients and local recirculation zones probably were present in the flows studied by these authors. Since the information concerning the magnitude of pressure gradients and the extent of recirculation zones are not available, these measurements provided only for a qualitative evaluation of the models. Nevertheless, the models provided reasonable predictions of these measurements.

1. INTRODUCTION

The objective of this investigation was to complete measurements of the structure of particle-laden jets, useful for evaluation of models of the process. The experiments considered dilute solid-particle-laden jets in a still environment. This arrangement has simple geometry and well-defined boundary conditions, which facilitates model evaluation. Furthermore, dilute solid-particle-laden jets highlight effects of particle dispersion by turbulence in jets, while minimizing complications due to particle collisions, interphase heat and mass transfer, effects of adjacent particles on interphase transport rates and modifications of turbulence properties by particles.

During the first phase of this study [1-5]* models of nonevaporating sprays and particle-laden jets were developed and evaluated, using the existing measurements in particle-laden jets, as well as the new measurements in nonevaporating sprays. While predictions for some models were encouraging, the evaluation was inhibited throughout by insufficient information concerning initial conditions. Moreover, the flow structure data available in the existing measurements of particle-laden jets were not complete in most of the cases, which further hindered the model evaluation.

The present investigation supplements the data base of existing measurements, considering particle-laden jets involving three particle-size groups and two loading ratios. The injector properties were carefully characterized so that the measurements can be employed to evaluate separated flow models. The flow structure measurements included: mean and fluctuating velocities of both gas and solid phases, gas-phase Reynolds stress, particle mass fluxes and the calibration of particle drag.

During the course of this study, new measurements in particle-laden jets were reported by Elghobashi and his coworkers [6,7]. In contrast to all the other existing measurements, these authors provided some information on initial conditions of their test flows. Profiles of mean and fluctuating velocities of both phases and the Reynolds stress of gas phase were reported at x/d = 20. Limited information concerning particle concentration profiles was also reported.

The present new measurements, as well as measurements of Elghobashi et al. [6,7], were employed to evaluate particle-laden jet models developed earlier in this study. Since these flows only involve interphase momentum exchange, modeling efforts

*Numbers in brackets denote references.

concentrated on effects of turbulent fluctuations on momentum transfer between the phases, as well as the dispersion of the particulate phase by turbulent fluctuations.

The structure of sprays and other particle-laden flows is generally influenced by turbulent dispersion of the discrete phase. Turbulent dispersion of particles is examined during this investigation by comparing predictions of several theoretical models with existing measurements. The study is limited to solid-particle-laden jets in a still environment. These results are also of interest for spray modeling, however, since the geometry approximates near-injector conditions while consideration of solid particles avoids complications due to polydisperse drop size distributions and drop coalescence.

Past models of turbulent particle-laden jets often consider two limiting cases instead of treating turbulent particle dispersion [5]. At one limit the particles and the continuous phase are assumed to have equal rates of turbulent diffusion. The locally homogeneous flow (LHF) approximation provides a consistent formulation of this limit. This implies that interphase transport rates are infinitely fast, so that both phases have the same velocity at each point in the flow. The LHF approximation provides best results for flows containing small particles, where characteristic response times of particles are small in comparison to characteristic times of turbulent fluctuations. LHF models have been extensively evaluated during earlier work in this laboratory, but only yielded accurate predictions for particle sizes smaller than most practical applications [1-5,8-10].

Turbulent particle dispersion is neglected entirely at the other limit. This implies that particles follow deterministic trajectories since they only interact with mean properties of the continuous phase, yielding a deterministic separated flow (DSF) model. Such an approximation is appropriate for flows containing large particles, where characteristic particle response times to flow disturbances are large in comparison to characteristic turbulent fluctuation times. Several spray and solid-particle-laden flow models have been proposed along these lines, e.g., El Banhawy and Whitelaw [11], Mongia and Smith [12], and Boyson and Swithenbank [13], and Faeth and coworkers [1-5], among others [5]. DSF models generally underestimate the rate of flow development and particle dispersion for both sprays and particle-laden jets, due to the neglect of turbulent dispersion.

Most practical particle-laden flows exhibit properties between these limits and require consideration of turbulent particle dispersion. Early dispersion models, discussed by Yuu et al. [14] and Dukowicz [15], apply a gradient diffusion approximation with empirical correlations for turbulent particle exchange coefficients. This approach is not practical, however, since such exchange coefficients are influenced by both particle and turbulence properties--requiring excessive effort to

accumulate a data base sufficient for general application of the method.

Several recent studies of turbulent particle dispersion use stochastic separated flow (SSF) methods to circumvent the limitations of the gradient diffusion approach. Stochastic analysis requires an estimate of the mean and turbulent properties of the continuous phase. Particle trajectories are then computed by random sampling to find instantaneous continuous phase properties. Mean and fluctuating particle properties are found by Monte Carlo methods--where a statistically significant number of particle trajectories are averaged to obtain system properties.

SSF models have been applied to particle-laden jets. Yuu et al. [14] use empirical correlations of mean and turbulent properties for SSF analysis of their particle dispersion measurements. Gosman and Ioannides [16] propose a more comprehensive approach, where flow properties for the stochastic calculations are computed with a k-ε turbulence model. This approach has been adopted by the present authors in their study of particle-laden flows, after only minor modification [1-5].

In the following, the models are described first of all, followed by the discussion of experimental methods used for the measurements in particle-laden jets. The report concludes with an evaluation of the models using the present new measurements and measurements of Elghobashi et al. [6,7], along with the discussion of difficulties encountered in the experiments of Elghobashi et al. [6,7].

2. THEORY

2.1 General Description

The theoretical model considers a steady, axisymmetric, dilute solid particle-laden, turbulent jet in an infinite, stagnant media. It is assumed that the boundary layer approximations apply for the present flow. A k-ε turbulence model is used to find the properties of the continuous phase, since this approach has been thoroughly calibrated for both constant and variable density jets [8-10,17] and has moderate computation requirements. The injector exit Mach number is less than 0.3; therefore, kinetic energy and viscous dissipation of the mean flow, as well as gas-density variations, are neglected with little error.

2.2 Locally Homogeneous Flow Model

The formulation of the LHF model corresponds to the general treatment of the continuous phase for all three models. The LHF approximation implies that both phases have the same velocity at each point in the flow, i.e., local thermodynamic

equilibrium is maintained. Therefore, the flow corresponds to a variable density single-phase fluid due to changes in particle concentration even though the density of each phase is constant. Following Lockwood and coworkers [17,18] and Bilger [19,20], among others, it is assumed that the exchange coefficients of both phases are the same. This assumption implies that, f, the mixture fraction (defined as the fraction of mass at a given point which originated from the injector) is a passive scalar or conserved property of the flow and that all scalar properties of the flow are only a function of f.

The turbulent flow model is based on the approach used by Gosman, Lockwood and Syed [18] for single-phase jets. This involves the solution of Reynolds-averaged conservation equations. The transport of mean quantities is given by conservation equations for mass, momentum and mixture fraction. Turbulence characteristics are based on a second-order model requiring the solution of model equations for turbulent kinetic energy and its rate of dissipation. While gravitational force is considred in the mean momentum equation, its effect on turbulence production and dissipation is ignored.

The governing equations are written as follows:

$$\frac{\partial}{\partial x}\ (\bar{\rho}\bar{u}\phi) + \frac{1}{r}\frac{\partial}{\partial r}\ (r\bar{\rho}\bar{v}^{o}\phi) = \frac{1}{r}\frac{\partial}{\partial r}\ (r\ \frac{\mu_t}{\sigma_\phi}\ \frac{\partial \phi}{\partial r}) + S_\phi \qquad (2.1)$$

where

$$\bar{\rho}\bar{v}^{o} = \bar{\rho}\bar{v} + \overline{\rho' v'} \qquad (2.2)$$

The parameters ϕ and S_ϕ appearing in Eqs. (2.1) and (2.2) are summarized in Table 1, along with the appropriate empirical constants. The empirical constants were established for single-phase flows [8,9,17]. They were not changed during present calculations for particle-laden jets. The turbulent viscosity was calculated from the turbulent kinetic energy and its rate of dissipation as follows:

$$\mu_t = C_\mu \bar{\rho} k^2/\varepsilon \qquad (2.3)$$

For present assumptions, the instantaneous particle concentration and flow density are only functions of mixture fraction--corresponding to the equilibrium state reached when f and (1-f) kg of injected and ambient fluid, respectively, are adiabatically mixed. This yields

$$C/C_o = f \ ; \quad \rho^{-1} = f/\rho_o + (1-f)/\rho_\infty \qquad (2.4)$$

Since C and ρ^{-1} are linear functions of f in the domain $0 \leq f \leq 1$, their mean values can be found by substituting f in

Table 1 Source Terms in Eq. (2.1)[b]

ϕ	S_ϕ
1	0
$\bar{u}$	$\pm\, a\, (\rho_\infty - \bar{\rho})^a$
k	$\mu_t \left(\frac{\partial \bar{u}}{\partial r}\right)^2 - \bar{\rho}\varepsilon$
$\bar{f}$	0
ε	$C_{\varepsilon_1} \mu_t \frac{\varepsilon}{k} \left(\frac{\partial \bar{u}}{\partial r}\right)^2 - C_{\varepsilon_2} \bar{\rho} \frac{\varepsilon}{k}^2$

Notes:

a. Positive sign is used in $S_{\bar{u}}$ for vertical upward flow.

b. Turbulence model constants are assigned the following values:

$C_\mu = 0.09$, $C_{\varepsilon_1} = 1.44$, $\sigma_k = 1.0$,

$\sigma_\varepsilon = 1.3$, $\sigma_f = 0.7$, and

$C_{\varepsilon_2} = 1.87$

Eq. (2.4). In this instance, it is not necessary to solve a transport equation for mixture fraction fluctuations and to adopt a probability density function (PDF) for f--which is usually necessary during LHF analysis when heat and mass transfer effects are considered [5,8-10].

Ambient values of u, f, k and ε are all zero for the flows treated here. Gradients of these quantities are also zero at the axis.

It was generally necessary to approximate initial conditions for existing measurements. When slug flow is assumed at the injector exit, all properties were taken to be constant, except for a shear layer having a thickness equal to 1 percent of the injector radius at the passage wall. The constant property portion of the flow was specified as follows:

$$x = 0 \quad , \quad r < 0.99d/2;$$

$$\bar{u}_o = \dot{M}_o/\dot{m}_o \quad , \quad \bar{f}_o = 1 \quad , \quad k_o = (0.02\bar{u}_o)^2 \quad , \tag{2.5}$$

$$\varepsilon_o = 2.84 \times 10^{-5}\, \bar{u}_o{}^3/d$$

Equation (2.5) provides the inner boundary conditions of the shear layer until it reaches the jet axis. The initial variation of u and f is taken to be linear in the shear layer. Initial values of k and ε in the shear layer were found by solving their transport equations while neglecting convection and diffusion terms.

When fully-developed pipe flow was assumed at the injector exit, $\bar{f}_o$ was taken to be unity while $\bar{u}_o$ was obtained from power law expressions provided by Schlicting [21]--allowing for variations with Reynolds number. Initial values of k_o and ε_o were obtained from Hinze [22] for fully-developed pipe flow in the present Reynolds number range.

2.3 Deterministic Separated Flow Model

Both separated flow models adopt the main features of the LHF model for the continuous phase. The density of the continuous phase is constant, for the present flow, simplifying Eq. (2.1). Furthermore, a solution for f is no longer needed, since particle concentration is found from the discrete-phase solution.

The dispersed phase is treated by solving Lagrangian equations of motion for the particles. At the initial condition, the particles are divided into n groups (defined by initial position, size and velocity) to yield a statistically significant representation of dispersed-phase properties.

The void fraction of the flows considered in this study is always greater than 99.8%; therefore, the volume occupied by the discrete phase is ignored with little error. For present conditions, mass is not exchanged between the phases; therefore, the conservation of mass equation for the continuous phase does not contain a source term. However, the interaction between the discrete and continuous phases yields an additional source term in Eq. (2.1) for $\underline{u}$. This term is found by computing the net change in momentum of each particle group i as it passes through a computational cell j (only one index is needed to define a cell since present calculations are parabolic and each cell is defined by its radial position). This yields the following source-term expression:

$$S_{\vec{pu}_j} = \left\{ \sum_{i=1}^{n} \dot{n}_1 \, m_{pi} \left[(\vec{u}_{pi})_{in} - (\vec{u}_{pi})_{out} \right]_j \right\} / V_j \qquad (2.6)$$

where $\dot{n}_i$ is the number of particles per unit time in each group, "in" and "out" denote conditions entering and leaving a computational cell, and V_j is the volume of computational cell j.

Source terms should also appear in the governing equations for k and ε--representing direct contributions of the relative motion of the particles to the production and dissipation of turbulence. These terms represent the turbulence modulation effects discussed by Al Taweel and Landau [23]. For dilute flows, it is reasonable to neglect direct effects of turbulence modulation; therefore, this approximation will be employed for most of the calculations conducted in this study.

The disperse-phase properties are obtained by solving the Lagrangian equation of motion for particles. The general form of the equation (the B-B-O equation which includes effects studied by Basset, Boussinesq and Oseen), after neglecting effects of particle rotation, can be written as follows [24]:

$$\frac{\pi}{6} d_p^3 \rho_p \frac{d\vec{u}_p}{dt_p} = \frac{\pi}{8} d_p^2 \rho C_D |\vec{u} - \vec{u}_p| (\vec{u} - \vec{u}_p) - \frac{\pi}{6} d_p^3 \frac{\partial p}{\partial \vec{r}} \qquad (2.7)$$

$$+ \frac{\pi}{12} d_p^3 \rho \frac{d}{dt_p} (\vec{u} - \vec{u}_p) + \frac{3}{2} d_p^2 (\pi \rho \mu)^{\frac{1}{2}} \int_{t_{po}}^{t_p} \frac{d/d\xi (\vec{u} - \vec{u}_p)}{(t_p - \xi)^{1/2}} \, d\xi + F_e$$

where the time derivative is taken following the motion of the particle

$$\frac{d}{dt_p} = \frac{\partial}{\partial t} + \vec{u}_p \frac{\partial}{\partial \vec{r}} \qquad (2.8)$$

(2.8)

The term on the left-hand side of Eq. (2.7) represents the inertial force of the sphere. Taken in order, the terms on the right-hand side of Eq. (2.7) represent: the drag force on the sphere, which conventionally includes both skin friction and form drag; the force on the sphere due to static pressure gradients in the flow; the force on the sphere due to the inertia of fluid displaced by its motion, which is often called the virtual mass term; the Basset term, which allows for effects of the deviation of the flow from a steady flow pattern around the sphere; and the external or body force term, e.g., the force due to gravity.

The usual assumptions involved in particle trajectory calculations are as follows [5,15,25,26]: dilute-particle flow with drag equivalent to a single particle in an unbounded environment and particle collisions neglected; drag treated empirically, assuming quasisteady flow for spherical particles and negligible effects of turbulent fluctuations, similar to most separated flow models; since $\rho_p/\rho \geq 200$ for conditions treated here, effects of static pressure gradients, virtual mass, Basset forces, Magnus forces, etc., can be neglected with little error; and ambient conditions of the particles were taken to be local mean flow properties. The last assumption is characteristic of the DSF formulation and will be relaxed for the SSF model. The remaining assumptions are typical of separated flow models of dilute particle-laden flows and are discussed more completely elsewhere [5,25,26].

After adopting these assumptions, Eq. (2.7) can be greatly simplified and the position and velocity of each particle group is found by integrating

$$\frac{dx_{pi}}{dt} = u_{pi} \quad , \quad i = 1,2,3 \tag{2.9}$$

$$\frac{du_{pi}}{dt} = \left(\frac{3\,\rho C_D}{4\,d_p\,\rho_p} \right) (\bar{u}_i - u_{pi}) |\vec{\bar{u}} - \vec{u}_p| + a_i \quad , \quad i = 1,2,3 \tag{2.10}$$

Particle Reynolds numbers did not reach the supercritical flow regime; therefore, the standard drag coefficient for solid spheres was approximated as follows [5,25,26]:

$$C_D = \frac{24}{Re} \left(1 + \frac{Re^{2/3}}{6}\right) \quad , \quad Re < 1000$$

$$= 0.44 \quad , \quad Re > 1000 \tag{2.11}$$

The particle motion equations, Eqs. (2.9) and (2.10), were solved at the same time as the gas-phase equations, in a stepwise fashion. A second-order finite difference algorithm was employed for these computations. The computations employed no less than 200 particle groups.

2.4 Stochastic Separated Flow Model

The SSF model involves finding trajectories of a statistically significant sample of individual particles as they move away from the injector and encounter a random distribution of turbulent eddies--using Monte Carlo methods. The treatment of the continuous phase is identical to the DSF model.

Key elements in the SSF model are the method used to specify eddy properties and the time of interaction of a particle and a particular eddy. The approach used to find these properties follows Gosman and Ioannides [16], but differs in some details. Properties are assumed to be uniform within each eddy and to change randomly from one eddy to the next. Particle trajectory computations are the same as the DSF model, involving solution of Eqs. (2.9) and (2.10); however, mean-gas properties in these equations are replaced by the instantaneous properties of each eddy.

The properties of each eddy are found at the start of particle-eddy interaction by making a random selection from the probability density function (PDF) of velocity. Velocity fluctuations are assumed to be isotropic with a Gaussian PDF having a standard deviation of $(2k/3)^{1/2}$ and mean components u, v, 0. The cumulative distribution function for each velocity component is constructed and sampled. This involves randomly selecting three numbers in the range 0-1 and computing the velocity components for each three values of the cumulative distribution function. This procedure provides a random selection of eddy properties which satisfies the PDF for velocity fluctuations.

A particle is assumed to interact with an eddy for a time which is the minimum of either the eddy lifetime or the transit time required for the particle to cross the eddy. These times are estimated assuming that the characteristic size of an eddy is the dissipation length scale, which is given as [16,27]

$$L_e = C_\mu^{3/4} k^{3/2}/\varepsilon \tag{2.12}$$

Eddy lifetime is computed using

$$t_e = L_e/(2k/3)^{1/2} \tag{2.13}$$

Particles are assumed to interact with an eddy as long as the time of interaction, Δt, and the distance of interaction $|\Delta x_p|$, satisfy the following criteria

$$\Delta t \leq t_e \quad , \quad |\vec{\Delta x}_p| \leq L_e \tag{2.14}$$

Particle capture by an eddy corresponds to ending the interaction with the first criterion while a particle traverses an eddy when the interaction is ended with the second criterion.

The remaining computations are similar to the DSF model, except that more particle trajectories must be considered to obtain statistically significant particle properties (generally 2000 trajectories were used). A by-product of the additional calculations, however, is that the SSF model yields both mean and fluctuating particle properties. This provides an additional test of model performance.

2.5 Turbulence Modulation Model

The models discussed in the preceding sections ignore direct contributions of interphase transport on turbulence properties, i.e., turbulence production, dissipation and scale. The comparison between predictions and measurements suggests that this approach is acceptable in dilute, lightly-loaded flows. However, effects potentially due to turbulence modulation can be significant when particle loading ratios are large [5-7,28-31], requiring modification of the turbulence model to account for the direct contributions to turbulence properties due to interactions with the discrete phase.

Several two-phase versions of turbulence models have been reported; however, they are limited in application mainly due to the assumption of a linear drag law [32-35]. The introduction of several new empirical constants which must be calibrated is another difficulty with most of the existing turbulence modulation models.

In contrast, the SSF formulation provides a convenient means for treating the nonlinear interphase transport with minimal empiricism. Therefore, a modified k-ε turbulence model accounting for effects of turbulence modulation is derived in the following for particle-laden jets within the framework of the SSF formulation.

Since only free jets in stagnant air are considered in this study, the pressure gradient is neglected throughout the derivation. Following the procedures described by Hinze [22], Tennekes and Lumley [36], and Daily and Harlow [37], the exact k and ε equations are obtained from the instantaneous continuous phase momentum equations--considering the particle source terms. The exact equations are then approximated by the boundary layer assumptions. Closure of these time-averaged equations is achieved by modeling the turbulent correlations, following the work of Gosman, Lockwood and Syed [18]. The conventional k-ε model equations are recovered with only one added term due to the contribution of the discrete phase in each of the modeled k and ε equations. The detailed derivation can be found in Appendix A. The final form of the equations is as follows

k-equation

$$\frac{\partial}{\partial x}(\bar{\rho}\,\bar{u}\,k) + \frac{1}{r}\frac{\partial}{\partial r}(r\,\bar{\rho}\,\bar{v}^{o}\,k) = \frac{1}{r}\frac{\partial}{\partial r}\left(r\,\frac{\mu_t}{\sigma_k}\frac{\partial k}{\partial r}\right)$$

$$+ \mu_t\left(\frac{\partial \bar{u}}{\partial r}\right)^2 - \bar{\rho}\,\varepsilon + \boxed{+\ \overline{u\,S_{pu}} - \bar{u}\,\bar{S}_{pu}} \qquad (2.15)$$

ε-equation

$$\frac{\partial}{\partial x}(\bar{\rho}\,\bar{u}\,\varepsilon) + \frac{1}{r}\frac{\partial}{\partial r}(r\,\bar{\rho}\,\bar{v}^{o}\,\varepsilon) = \frac{1}{r}\frac{\partial}{\partial r}\left(r\,\frac{\mu_t}{\sigma_\varepsilon}\frac{\partial \varepsilon}{\partial r}\right)$$

$$+ C_{\varepsilon_1}\,\mu_t\,\frac{\varepsilon}{k}\left(\frac{\partial \bar{u}}{\partial r}\right)^2 - C_{\varepsilon_2}\,\bar{\rho}\,\frac{\varepsilon^2}{k} \boxed{- 2\,C_{\varepsilon_3}\,\mu\,\frac{\varepsilon}{k}\frac{\partial \bar{S}_{pu}}{\partial r}} \qquad (2.16)$$

Where the terms contained in the broken-line boxes are the added terms due to the interphase transport, and S_{pu} is the particle source term in the streamwise momentum equation for the continuous phase.

Since instantaneous flow properties are known in the SSF formulation, the added term in the k-equation is exact. The new term in the ε-equation, however, is modeled in a way consistent with conventional k-ε models. Only one new model constant has been introduced, which greatly reduces the effort of model calibration.

3. EXPERIMENTAL METHODS

3.1 Introduction

The experimental apparatus was used for measurements in both single-phase and particle-laden jets. The flows examined during the present study are as follows:

1. An isothermal air jet.

2. Four particle-laden jets (with Sauter mean diameters 79, 119 and 207 μm and loading ratios 0.2 and 0.66).

A variety of measurements were performed to define the flow. Axial and radial profiles of mean and fluctuating velocities for both phases, gas-phase Reynolds stress, and mean particle-mass flux were measured. Initial conditions were obtained at x/d = 1. Other measurements involved particle size distributions and particle drag properties.

3.2 Test Apparatus

The requirements for a monodisperse particle-laden gas jet having no zones of recirculation, a simple geometry and well-defined boundary conditions can be met with the apparatus illustrated in Fig. 1. The injection tube was mounted on a two-dimensional traversing mechanism at the center of the cage. For all the test flows, injection was downward into still room air. The test cage was 1 m square by 2.5 m high--enclosed with 16-mesh screens to reduce the influence of room disturbances. Traversing in the third dimension, to obtain radial profiles of flow quantities, involved moving the entire cage assembly, which was mounted on a bearing track. This configuration allows a fixed optical measurement station, minimizing alignment problems for the laser-Doppler anemometer (LDA) system.

Measurements from this arrangement should be attractive for those wishing to evaluate models. The flow is parabolic; therefore, its turbulence characteristics can be modeled more reliably than flows with recirculation. Also, parabolic flow greatly simplifies problems of obtaining accurate numerical solutions. Boundary conditions are well-defined, since there are no uncertainties regarding wall friction and inlet flow properties which are encountered in confined chambers.

The flow system is illustrated in Figure 2. The jet tube has an internal diameter of 10.9 mm and extends in the vertical direction for 90 injector diameters. Flow at the exit of the injector roughly corresponds to fully-developed turbulent pipe flow; however, the initial condition is completely measured in any event.

The air supply for the particle-laden jet apparatus was provided by an oil-free air compressor. The air flow was metered using a critical flow orifice. Seeding particles needed for LDA measurements of gas-phase quantities were added using a reverse-cyclone seeder. Sand particles for two-phase flows were introduced upstream of the injection pipe by a gear feeder powered by a variable speed motor. The particle mean flow rates were varied by changing motor speed, as determined by system calibration. Three size ranges of particles, with Sauter mean diameters 79, 119 and 207 μm, were used in the experiments. The sand was sifted to reduce the diameter variation within each size group. Typical size distributions are illustrated in Figure 3, where more than 1000 particles were sampled for each group. The density of the sand particles is 2620 kg/m^3.

3.3 Experimental Procedure

3.3.1 Gas-Phase Velocity Measurements

Table 2 is a summary of the instrumentation used for each measurements.

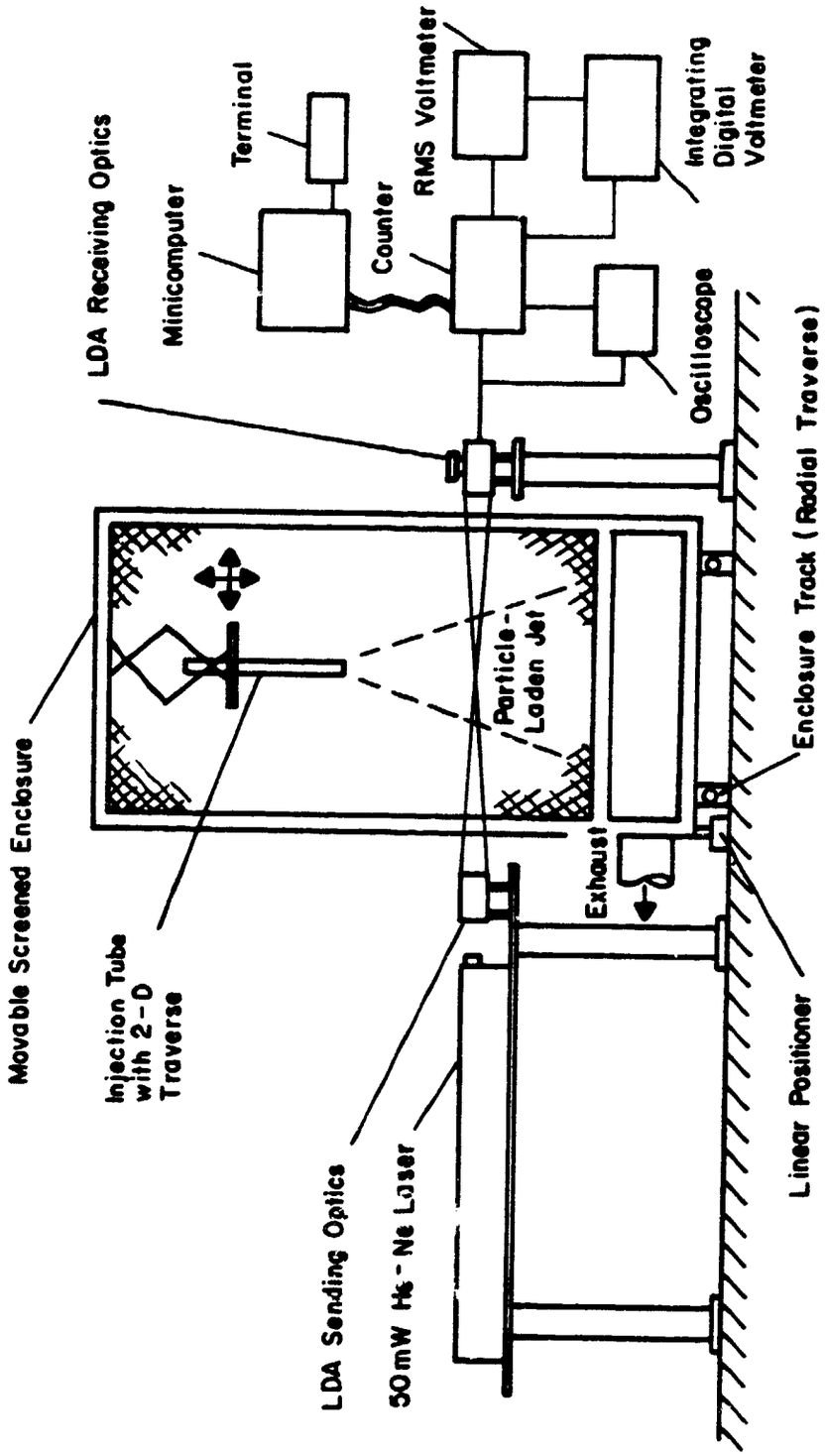

Fig. 1. Sketch of the apparatus for the particle-laden jet experiments.

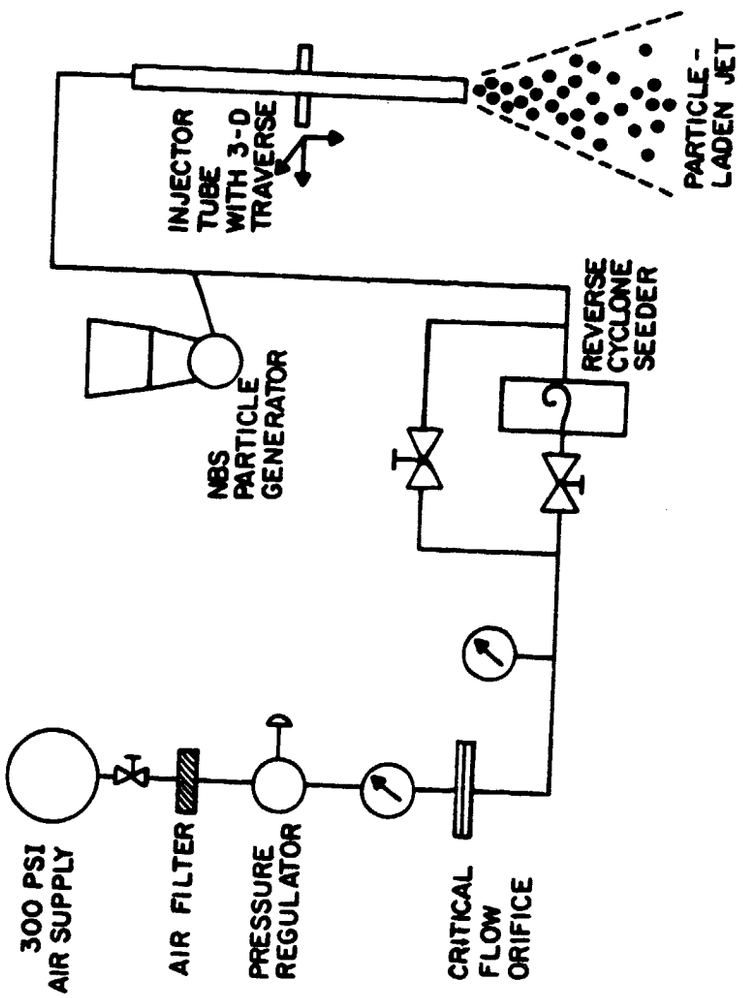

Fig. 2. Sketch of the flow system for the particle-laden jet experiment.

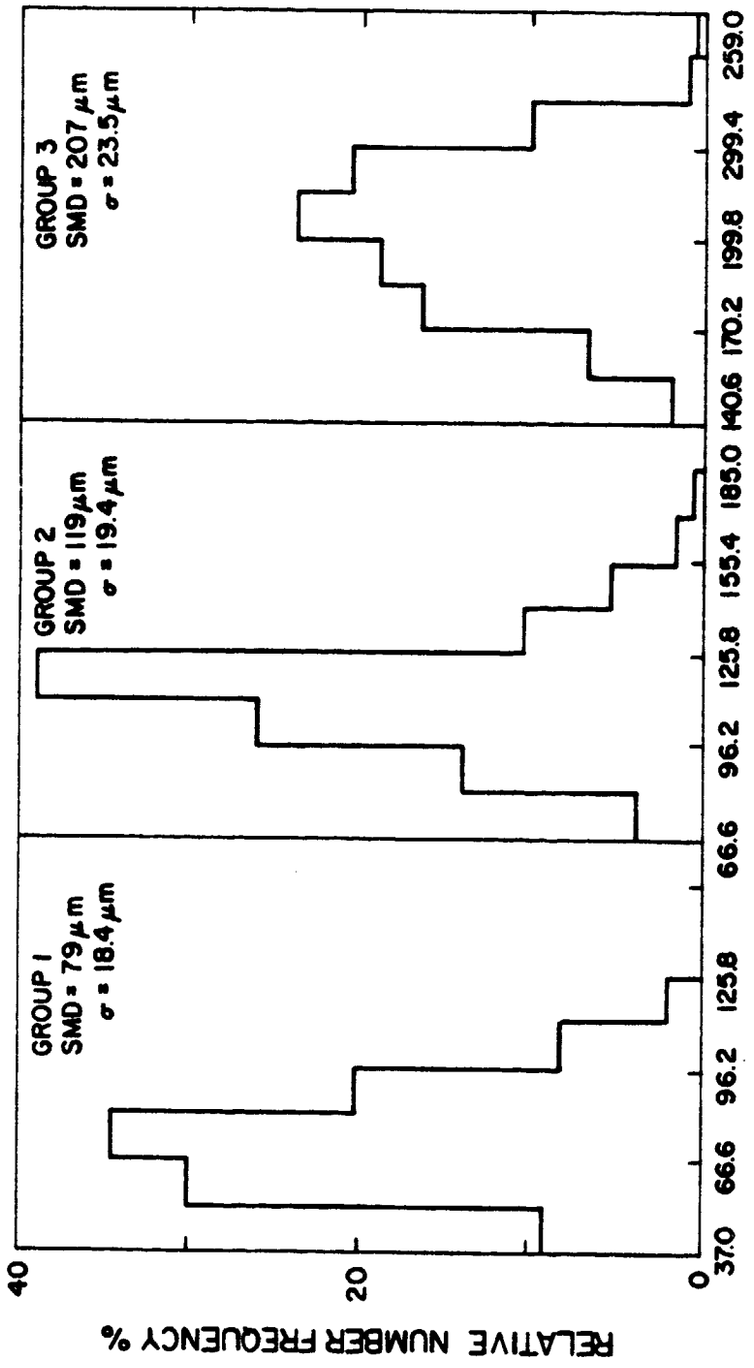

Fig. 3. Particle size distributions for the particle-laden jet experiments.

Table 2 Instrumentation

Measurement	Technique	Equipment
Mean and fluctuating gas velocities and Reynolds Stress	Dual-beam, forward scatter laser Doppler anemometer, frequency shifted with burst counter data processing.	Spectra Physics Model 125A (50 mW) He-Ne laser, rest TSI, Inc.
Mean and fluctuating particle velocities	Same techniques as for gas-phase velocity measurements, in conjunction with minicomputer for data processing.	Same as for gas-phase velocity measurements. MINC 11/23 minicomputer, Digital Equipment Company
Particle mass flux	Isokinetic sampling.	In-house design
Particle Drag Coefficient	Same techniques as for particle velocity measurement to determine particle terminal velocity and surrounding gas velocity.	Same as for particle velocity measurement

Mean and fluctuating gas velocities were measured using a single-channel, dual-beam, frequency-shifted LDA. An equipment list for the LDA system appears in Table 3. The sending and receiving optics had a focal length of 242 mm with a 11.61° angle between beams. The signal was focused on the photomultiplier with a 200 mm focal length lens. The aperture diameter of the photomultiplier was 0.25 mm. The receiving lens was masked with a beam-stop which provided a collection aperture of 25 mm diameter. The preceding optical configuration produced an ellipsoidal measuring volume of 0.470 mm in length and 0.098 mm in diameter, with a fringe spacing of 3.128 μm.

The injected flow was seeded with 0.2 μm Al_2O_3 particles, which was sufficient for most of the measurements. This primary seeding was supplemented by seeding the surroundings when measurements were taken near the edge of the jets, where the primary seeding level was low, in order to avoid biasing.

Mean and fluctuating velocity components were measured in the axial and radial directions at several axial distances from the injector for all test conditions. The use of several beam orientations allowed measurement of Reynolds stress. Reynolds stress measurements are valuable for checking model predictions and for locating the flow centerline (since Reynolds stress is zero at the centerline and doesn't exhibit the broad maxima encountered for other variables). Concentration biasing and interference from large particles were avoided by employing high concentrations of seeding particles. An integration time of one-minute or more was used to determine the time-averaged quantities. Each measurement was repeated three times to get a better averaging.

3.3.2 Particle Velocity Measurements

The particle velocity was measured using the same LDA arrangement as for gas-phase measurements. In this case, the gain settings of the photomultiplier and counter were adjusted to relatively low levels so that only strong scattering signals from large particles were recorded. The output of the data processor was then collected with a MINC 11/23 minicomputer and processed to yield mean and fluctuating particle velocities (by taking number-averaged velocities). When these tests were run, no seeding was used for the gas phase, in order to reduce potential bias errors of the measurements.

The centerline particle velocity for all the test flows was rechecked using the double-flash imaging technique developed by A.S.P. Solomon in a companion study. The photograph system consisted of two sub-microsecond flash sources, a lens system to focus the light and a camera. The flashes were fired consecutively at electronically controlled times so that two images of the moving particles were obtained on the same photograph. Measurement of the distance travelled by the

Table 3 LDA Equipment List

Component	Manufacturer	Model
Helium-Neon Laser	Spectra Physics	125 A
Integrated Optics	Thermo-Systems	900
Frequency Shifter	Thermo-Systems	9180
Photomultiplier	Thermo-Systems	960
Counter	Thermo-Systems	1980
RMS Voltmeter	Thermo-Systems	1060
Dual Beam Oscilloscope	Tektronix	561 A
Integrating Digital Voltmeter	Hewlett-Packard	240 IC

particles and the time interval between the two flashes provided the particle velocity.

3.3.3 Particle Flux Measurements

Particle fluxes were measured with an isokinetic sampling probe. The probe was a modified version of the particle collection probe used by Szekely and Faeth [38]. The tip of the probe had an ID of 3 mm, which provided sufficient spatial resolution for the measurements. Isokinetic conditions were maintained by applying suction to the probe and metering the sampling flow rate. The sampling flow rate was adjusted to match the local gas-flow rate determined from the velocity measurements.

The particles were collected on filter paper and weighed with a balance which had a sensitivity of one miligram. Sampling times varied from 1 minute to 30 minutes--depending on the location in the flow. The particle flux data--integrated over the cross-section of the jet at each axial position--was checked against the injector particle mass flow rate to determine the sampling efficiency.

3.3.4 Drag Measurements

Calibration of particle drag was necessary since the shape of the particles was somewhat irregular and the particles might not follow the standard drag law for solid spheres. These measurements involved determining terminal velocities of the particles in free-fall, as well as the local gas velocities resulting from particle drag, using the LDA. The drag coefficients were computed using the measured velocities and the Sauter mean diameter of each size group.

Particle drag properties at various particle Reynolds numbers were obtained by adjusting the standard drag law, using the ratio of measured drag to that of standard drag law at the free-fall Reynolds number for each particle group. The particle Reynolds numbers involved in the drag measurements were small, ranging from 1 to 10, compared to those encountered in the particle-laden jet measurements, where the particle Reynolds numbers varied in the range of 1 to 200 depending on the position in the flow and the particle size. However, the same scaling factors were used over the Reynolds number range for each particle group.

4. RESULTS AND DISCUSSION

4.1 Experimental Conditions

In order to generate a wide data base, a variety of test conditions were employed in the present study. A single-phase

air jet and four dilute particle-laden jets, involving three particle-size groups and two loading ratios, were chosen for study. The test conditions are summarized in Table 4 and all test results are tabulated in Appendix B.

The particles used in the experiments were Penn State C-30 foundry sand, which was sieved to obtain different size ranges. The material density of the particles was measured to be 2620 kg/m^3. The particle drag properties were calibrated against the standard drag law for spheres. A multiplication factor to the standard drag law was found for each of the size group, i.e., 1.0, 1.25 and 1.51 for particle groups having SMD of 79, 119 and 207 μm, respectively. The fact that the particles do not obey the drag law for spheres exactly is reasonable due to the somewhat irregular shape of the particles--particularly for larger sizes. The calibrated drag laws were used in the predictions.

The LDA measurements of mean particle velocities along the jet centerline were checked using the double-flash photographic technique. The agreement between the two techniques was reasonable for flows containing small and intermediate size particles, e.g., within 5% for case 1 jet and 15% for case 2 and case 3 jets. However, the particle velocities measured using LDA were significantly lower than those measured using double-flash photographic technique for case 4 particle-laden jet (SMD = 207 μm) downstream of x/d = 20. The discrepancies ranged from 40% at x/d = 20 to 57% at x/d = 30, where the LDA measurements yielded negligible slip velocities. The exact cause for the failure of LDA measurements for large particles is not clear. Due to this problem, the LDA measurements of mean and fluctuating particle velocities for case 4 particle-laden jet are not employed for evaluation of predictions in the following.

4.2 Initial Conditions

Initial conditions of both phases were measured at x/d = 1 for all five flows. The results are presented in Figures 4-12. The jets expanded well beyond r/x = 0.5, the injector radius, at this axial position due to shearing action. Gas-phase mean and fluctuating velocities, turbulence kinetic energy and Reynolds stress are shown in Figures 4, 5, 7, 9 and 11 for the five jets. The tangential component of velocity fluctuation, $\overline{(w'^2)}^{1/2}$, was not measured, and was assumed equal to $\overline{(v'^2)}^{1/2}$ when calculating the turbulence kinetic energy.

All the gas-phase results, except near the jet edge, were similar to the properties of the fully-developed pipe flow. Near the jet boundary, the flow behaved more like a free-mixing layer, yielding broad maxima for the turbulent quantities and a gradual change to ambient values for the mean velocity.

Table 4 Summary of Test Conditions[a]

Case	Single-Phase Air Jet	Dilute Particle-Laden Jets			
		Case 1	Case 2	Case 3	Case 4
Particle Sauter Mean Diameter (μm)	--	79	119	119	207
Particle Drag Ratio[b]	--	1.00	1.25	1.25	1.51
Loading Ratio[c]	--	0.2	0.2	0.66	0.66
Injector Exit Centerline Velocity (m/s)[d]					
Air	32.12	26.07	29.86	25.22	25.34
Particle	--	24.13	24.20	21.89	18.54
Injector Exit Centerline Particle Mass Flux (kg/m^2s)[d]	--	6.06	6.50	18.89	19.01

[a]Ambient temperature and pressure, 296°K, 97 kPa; injector inside diameter, 10.9 mm; particle material density, 2620 kg/m^3.

[b]Particle drag/drag of smooth sphere having the same diameter.

[c]Ratio of injected particle mass flow rate to air flow rate.

[d]Average across flow cross-section, measured at x/d = 1.

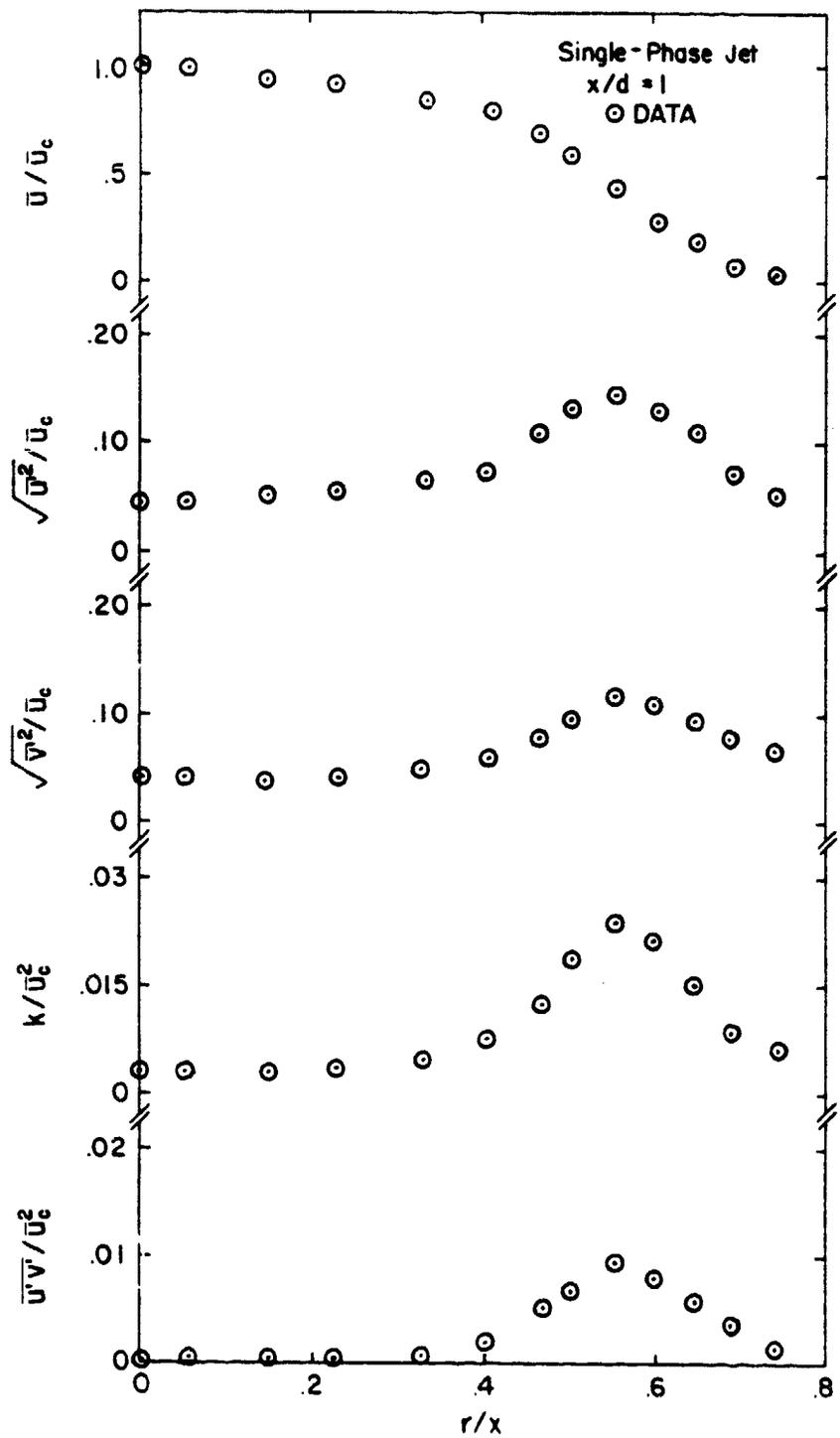

Fig. 4. The initial conditions for single-phase jet--- radial profiles of mean and turbulent quantities at x/d = 1.

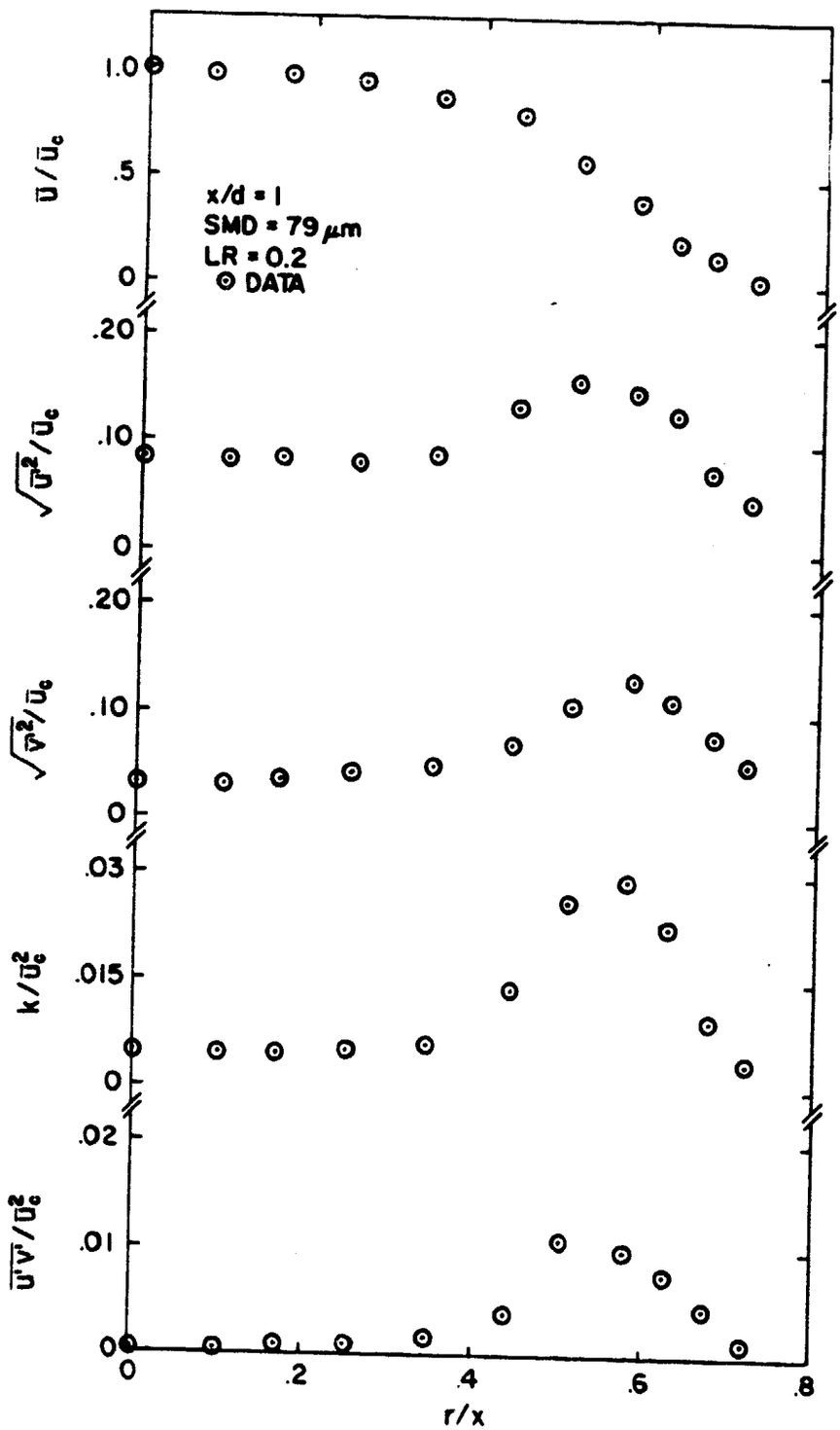

Fig. 5. The initial conditions for case 1 particle-laden jet---radial profiles of gas-phase mean and turbulent quantities at x/d = 1.

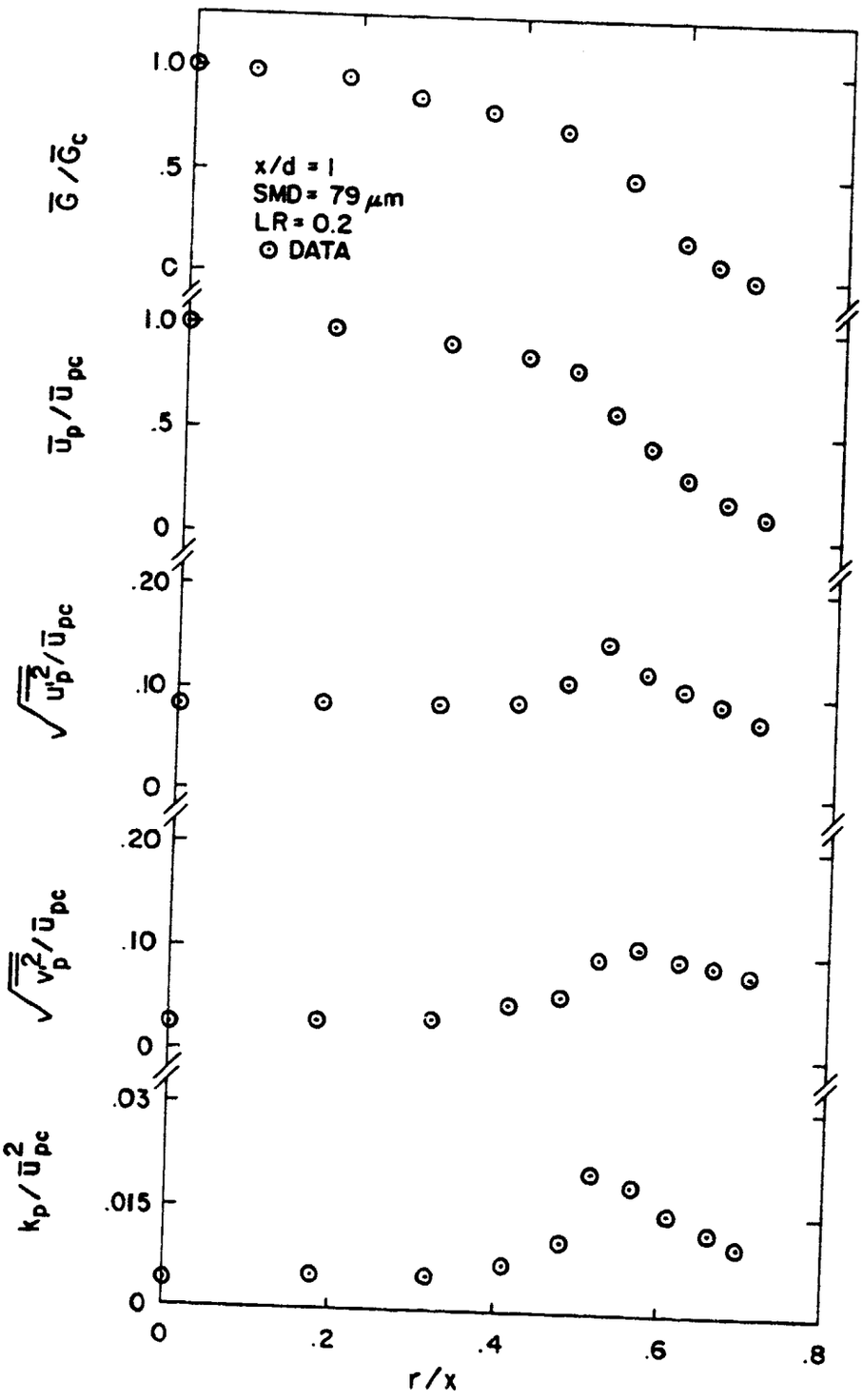

Fig. 6. The initial conditions for case 1 particle-laden jet---radial profiles of solid-phase mean and turbulent quantities at x/d = 1.

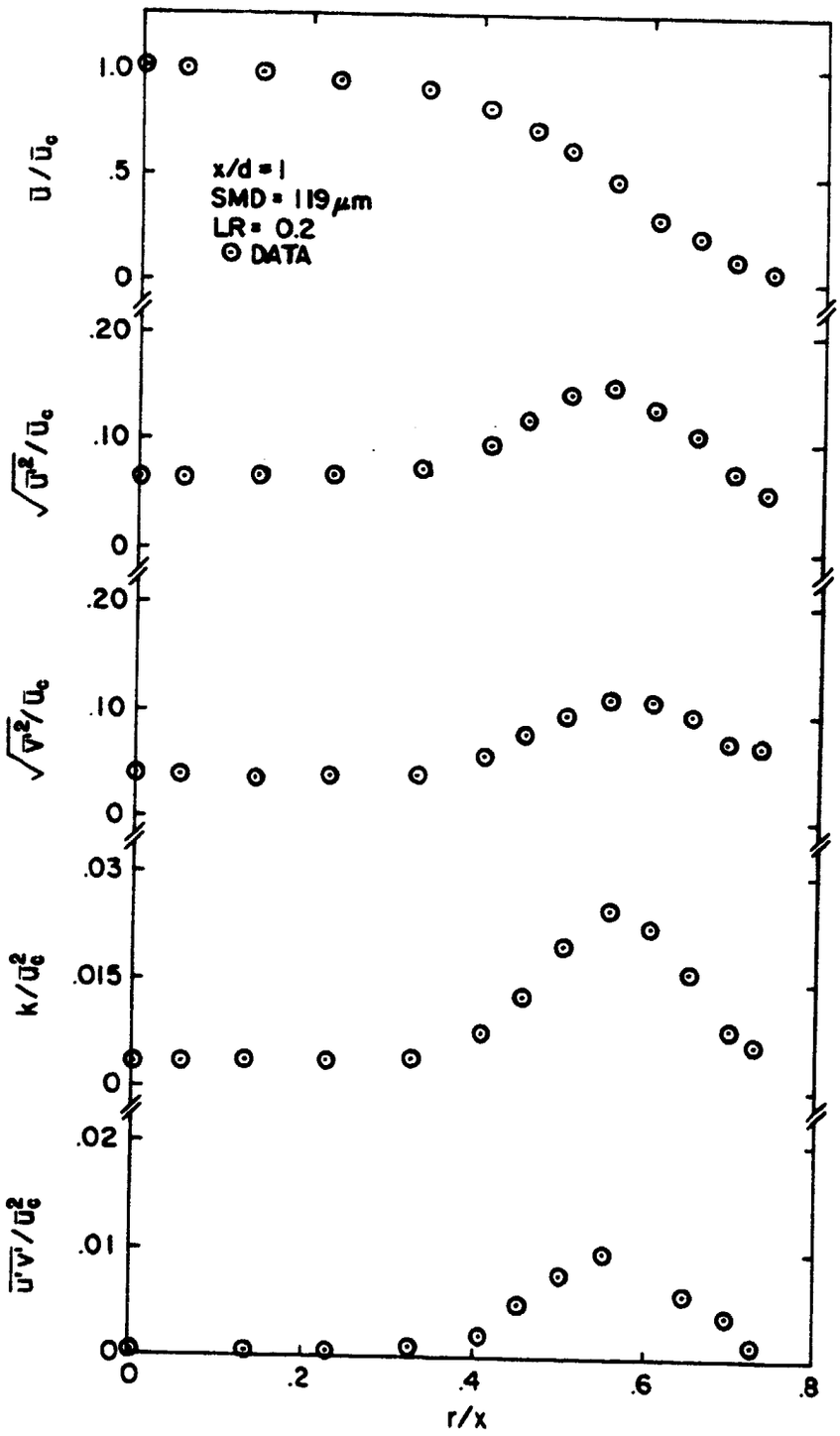

Fig. 7. The initial conditions for case 2 particle-laden jet---radial profiles of gas-phase mean and turbulent quantities at x/d = 1.

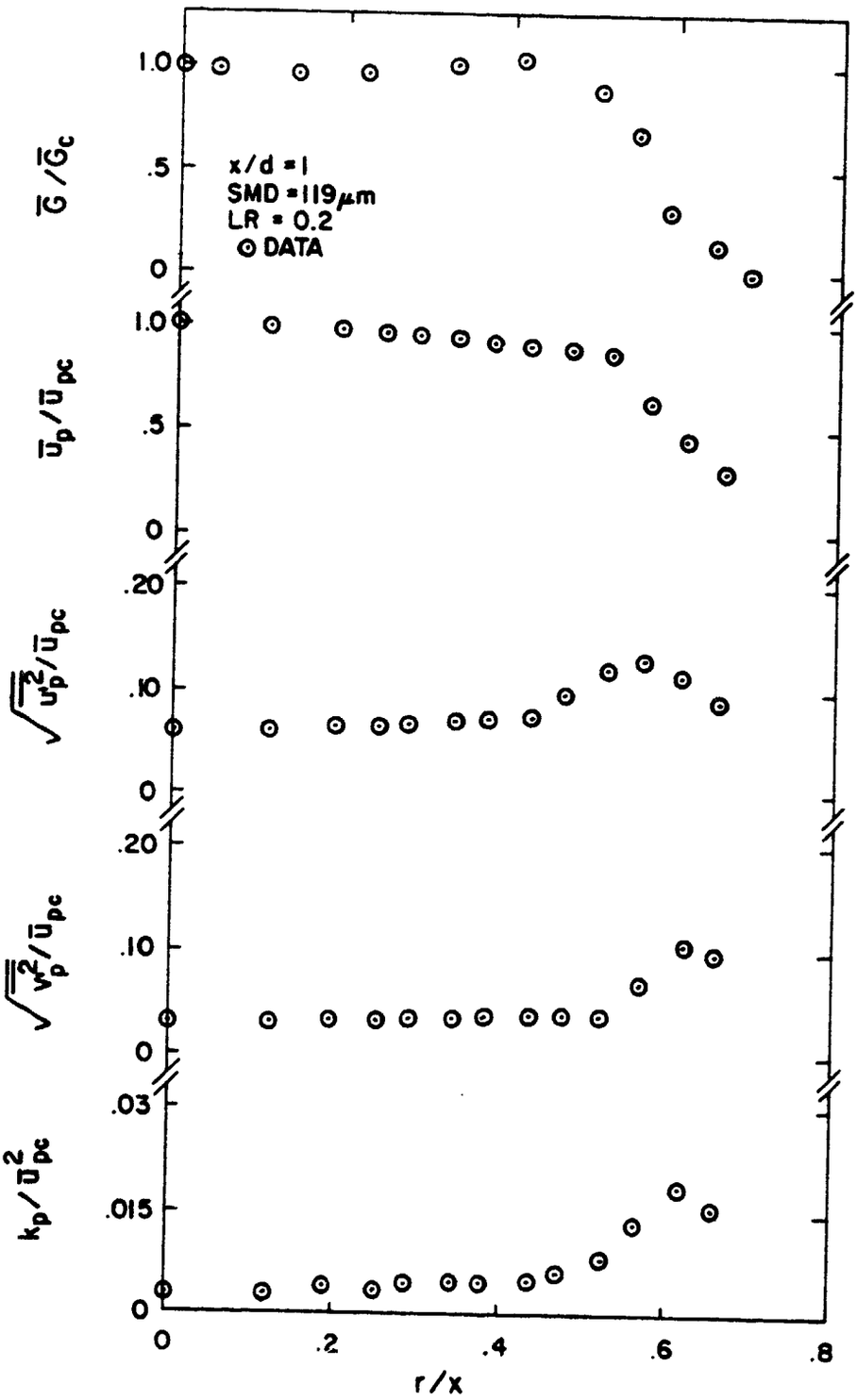

Fig. 8. The initial conditions for case 2 particle-laden jet---radial profiles of solid-phase mean and turbulent quantities at x/d = 1.

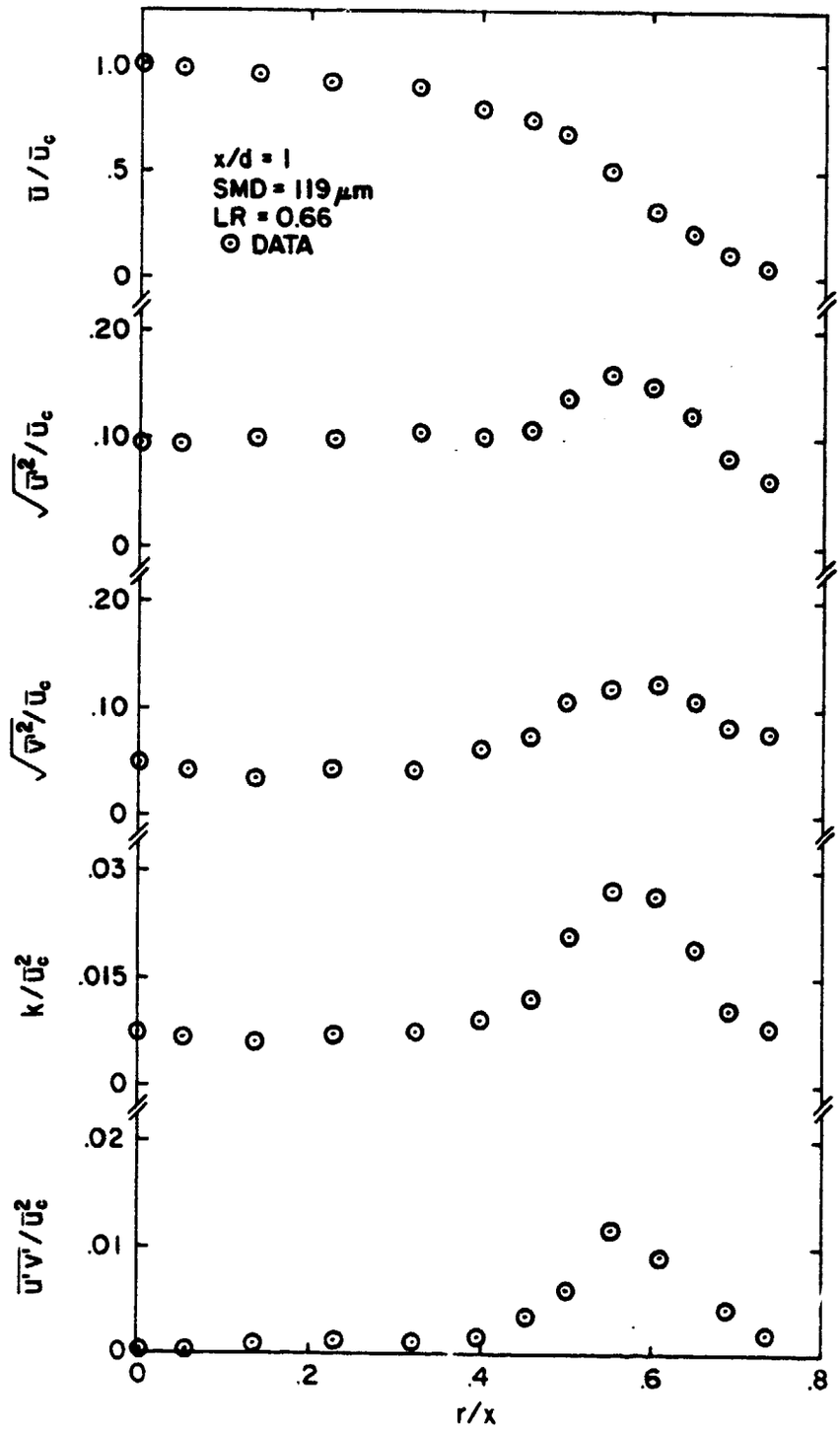

Fig. 9. The initial conditions for case 3 particle-laden jet---radial profiles of gas-phase mean and turbulent quantities at x/d = 1.

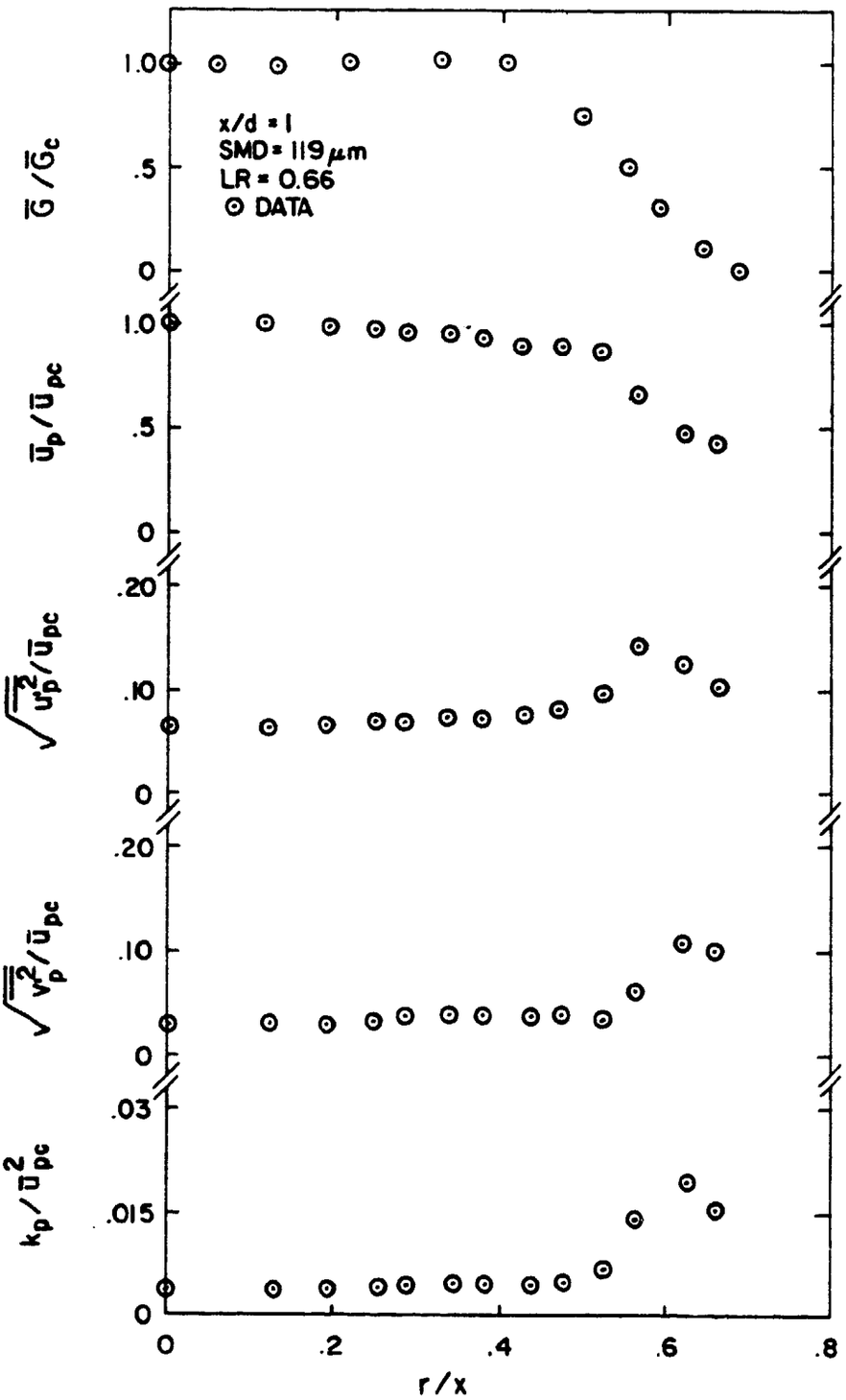

Fig. 10. The initial conditions for case 3 particle-laden jet---radial profiles of solid-phase mean and turbulent quantities at x/d = 1.

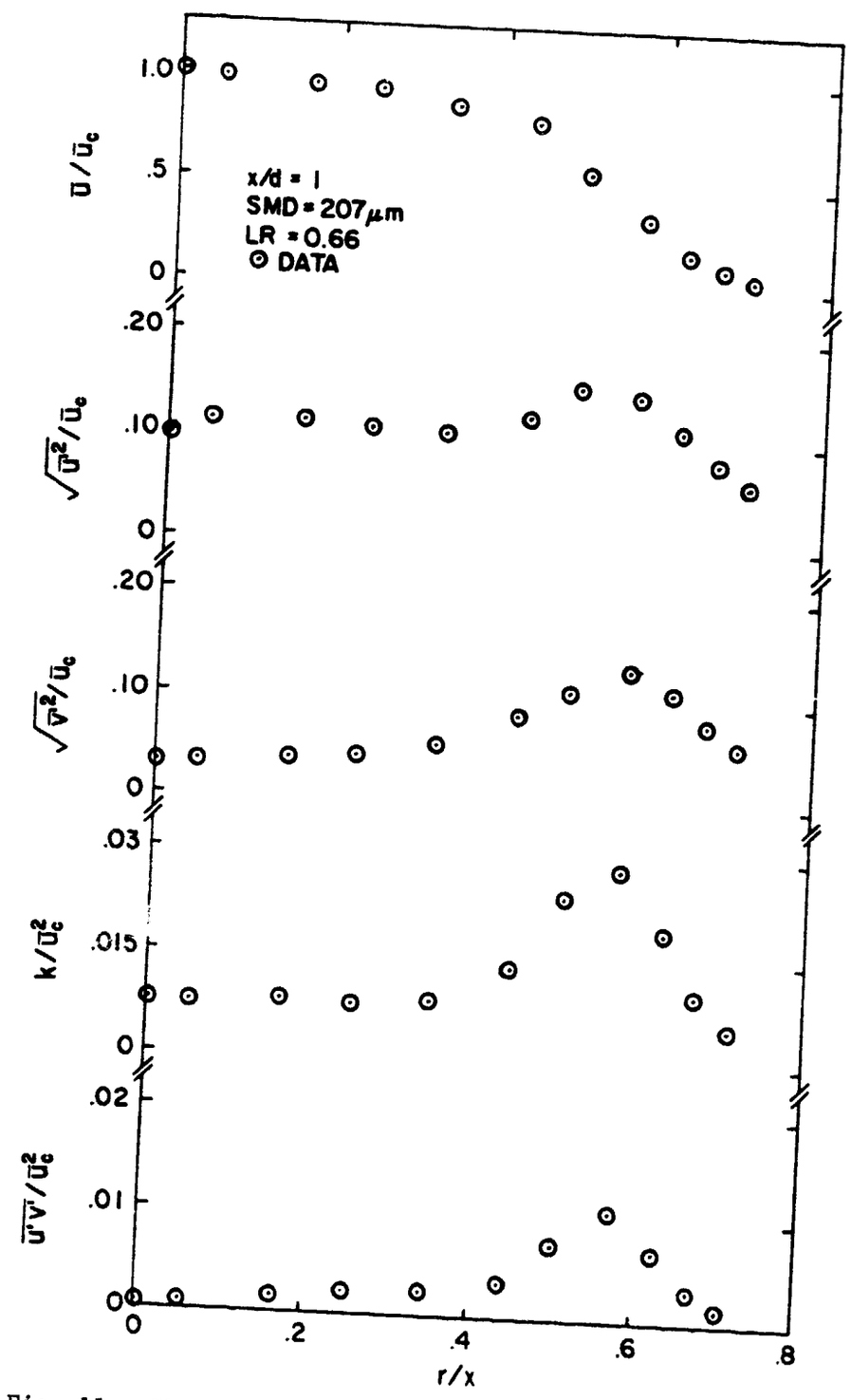

Fig. 11. The initial conditions for case 4 particle-laden jet---radial profile of gas-phase mean and turbulent quantities at x/d = 1.

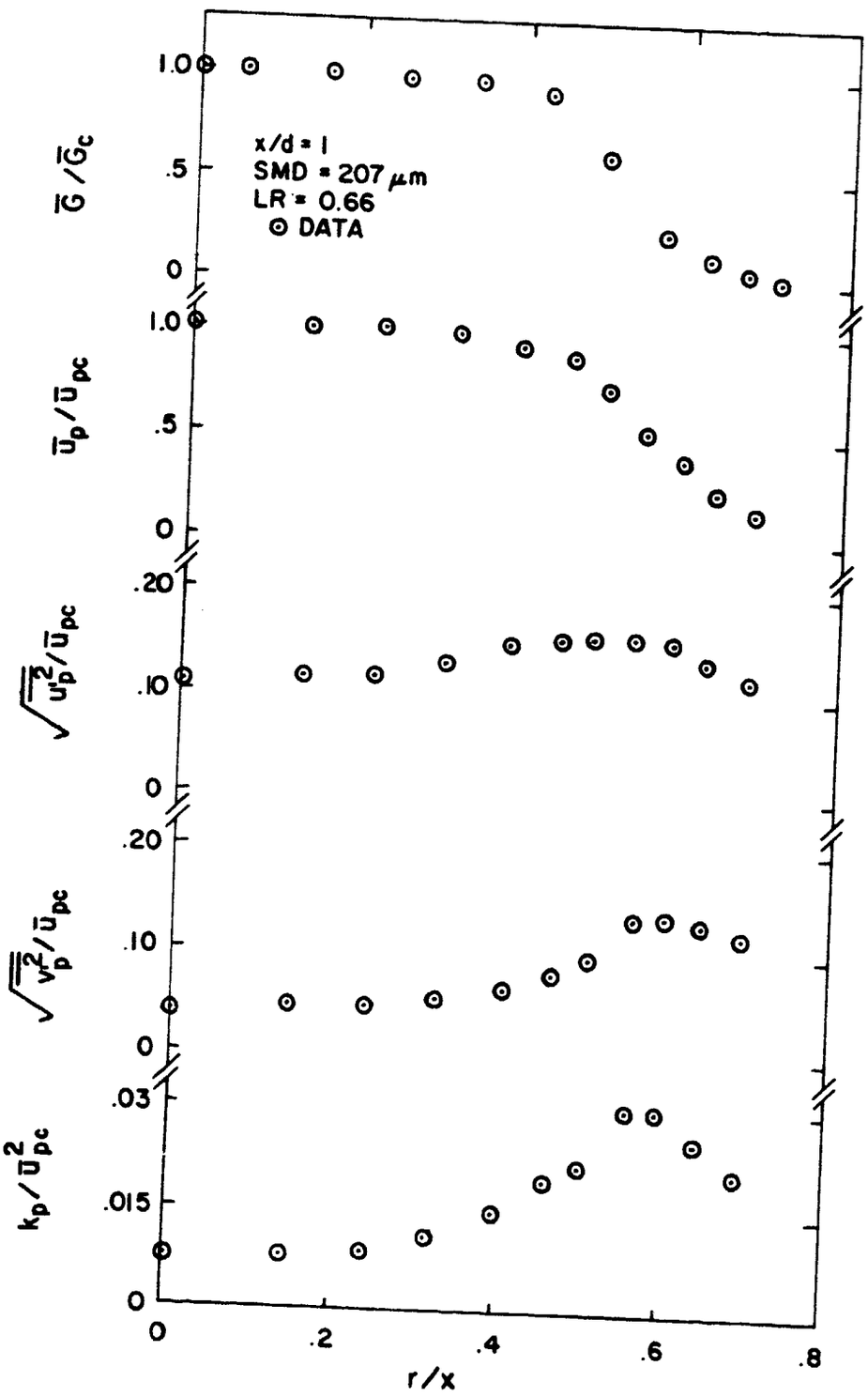

Fig. 12 The initial conditions for case 4 particle-laden jet---radial profile of solid-phase mean and turbulent quantities at x/d = 1.

The presence of particles resulted in no significant change for the gas-phase properties at x/d = 1. The mean velocity profiles were very similar for all the five test flows. However, the turbulence kinetic energies in the particle-laden jets were slightly higher than in the single-phase jet.

The profiles of mean particle mass flux, mean and fluctuating particle velocities and particle turbulence kinetic energy are shown in Figures 6, 8, 10 and 12. The mean slip velocity ratios, $(\bar{u}-\bar{u}_p)/\bar{u}$, at the jet axis were 7.4%, 18.9%, 13.2% and 26.8% for case 1 to case 4 particle-laden jets, respectively. The slip decreased with loading ratio for the jets having the same particle size (compare the case 2 and case 3 flows) which agrees with measurements in Refs. 6 and 7. The mean particle velocity profiles were wider than the mean-gas velocities, except for the case 4 flow due to the difficulties discussed previously.

The particle mass fluxes were nearly uniform up to r/x = 0.5 for particle-laden jets with larger particles, and then decreased to zero at edge, cf., Figures 8, 10 and 12. The jet with smallest particles, however, exhibited a continuous variation of particle-mass flux over the injector exit, cf., Figure 6. Particle-turbulent quantities were slightly smaller than comparable gas-phase quantities--except for the case 4 flow as discussed earlier.

4.3 Axial Variation of Flow Properties

Predictions of the SSF model will not include effects of turbulence modulation for results illustrated in Sections 4.3 and 4.4, since these effects are not large for the present test flows and we wish to consider model performance with all empirical factors established earlier. Turbulence modulation will be considered separately in Section 4.5.

Predicted and measured profiles of centerline mean gas-phase velocity along the axis are illustrated in Figure 13. Predictions for the single-phase jet, based on the model of Shearer et al. [8] developed earlier in this laboratory, agree well with measurements. This establishes an acceptable baseline for measurements in the particle-laden jets, since the single-phase jet model was well-calibrated [5,8,9]. The measured rates of decay of centerline velocity in the particle-laden jets are smaller than in the single-phase jet, with this effect more pronounced at higher loading ratio. Predictions of both the LHF and SSF models for particle-laden jets are in fair agreement with measurements, except for case 3 flow where both theories overestimate the rate of centerline velocity decay.

Predicted and measured mean-particle velocities along the jet axis are illustrated in Fig. 14. The SSF model predictions are in good agreement with the measurements in all cases. The LHF model, however, significantly overestimates the rate of velocity

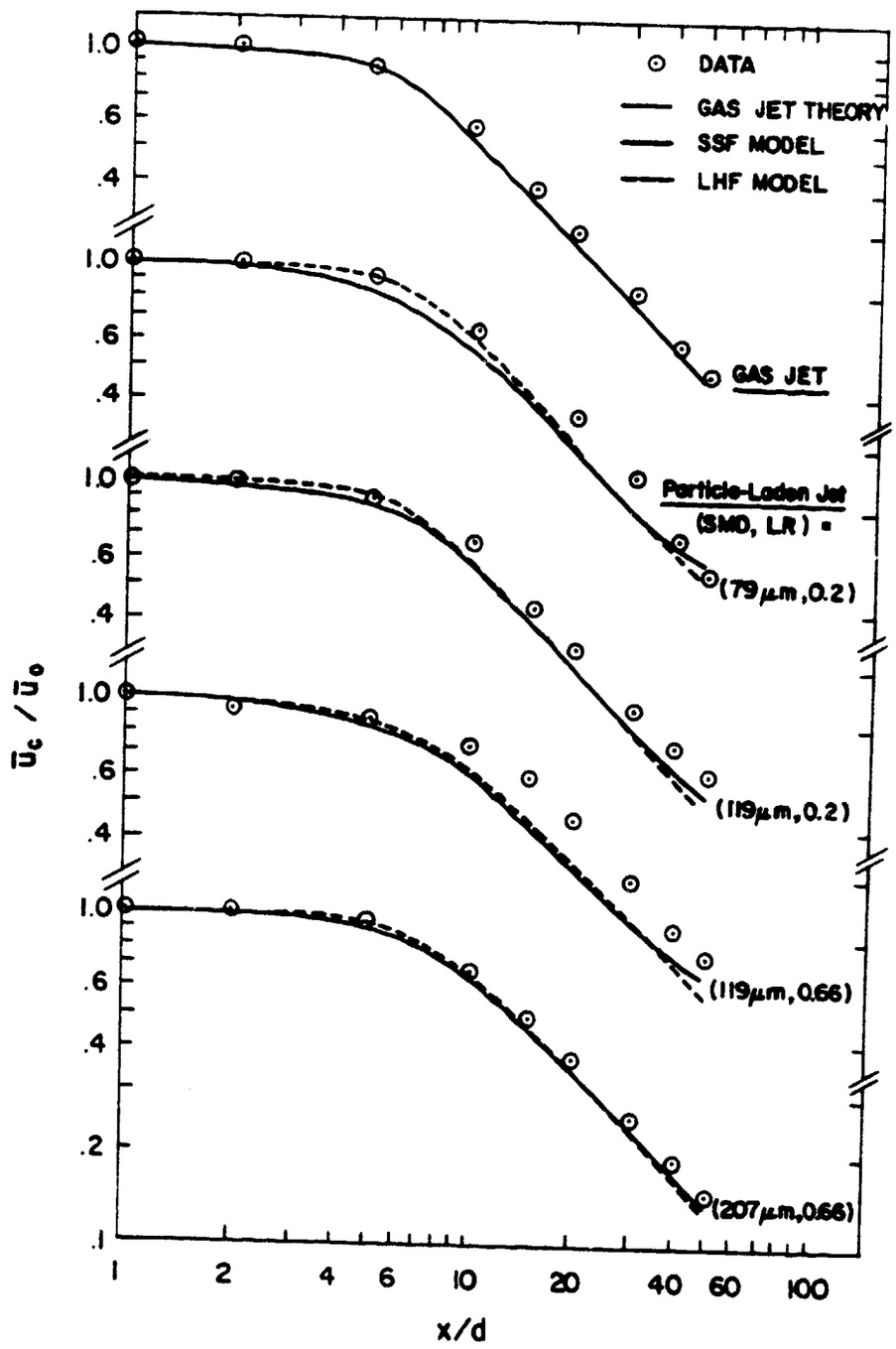

Fig. 13. Axial variation of centerline mean gas-phase velocity.

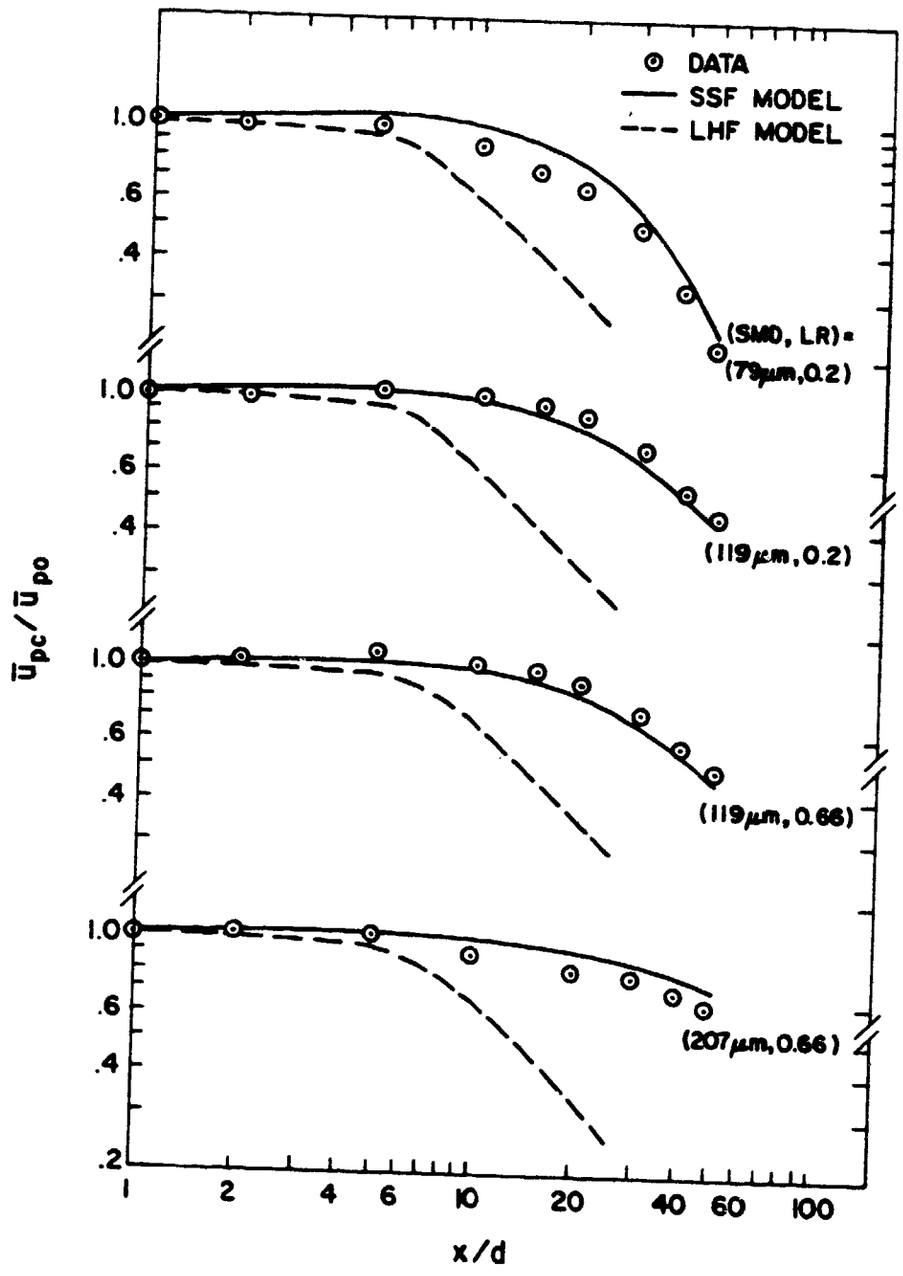

Fig. 14. Axial variation of centerline mean solid-phase velocity.

decay at all conditions, since the test particles have significant inertia.

The axial variation of gas-phase turbulence-kinetic energy is illustrated in Fig. 15. Results are shown for both particle-laden jets and the air jet. The theories agree well with measurements except in the near-injector region, where all the models underestimate turbulence levels. The underestimation of turbulence kinetic energy near the injector exit could be due to limitation of the k-ε model, since the turbulence is still developing in this region. The fact that turbulence levels in fully-developed regions, approaching x/d = 40, roughly correspond to values estimated from models which ignore effects of particle motion on turbulence properties, indicates that effects of turbulence modulation were small in these flows. This is reasonable, since all the test flows were dilute.

The axial variation of centerline particle turbulence kinetic energy is illustrated in Fig. 16. The results for the case 4 particle-laden jet are not shown, due to problems with the LDA measurements of large particles--discussed previously. The LHF model significantly overestimates the particle turbulence levels for all the cases considered here, since the particles cannot actually follow the gas-phase turbulent motion due to their inertia. In contrast, the SSF model yields fair agreement with measurements.

Predicted and measured particle-mass fluxes along the jet axis for the four particle-laden jets are illustrated in Fig. 17. The LHF model significantly overestimates the particle dispersion, due to neglect of effects of slip between the phases. In contrast, the SSF model provides satisfactory predictions in all cases.

4.4 Radial Variation of Flow Properties

Theoretical predictions of the radial variation of mean and fluctuating quantities for both phases were compared with measurements completed during the present study. The comparison involved profiles of mean velocity, axial and radial components of fluctuating velocity, turbulence kinetic energy and Reynolds stress for the gas phase; and profiles of mean velocity and mass flux, axial and radial components of fluctuating velocity, and turbulence kinetic energy for the particle phase. The tangential component of fluctuating velocity was not measured; therefore, it was assumed that $\overline{v'^2} = \overline{w'^2}$--which is usually true for jets and sprays [28]--to find measured turbulence kinetic energies for both phases. The predictions of gas-phase fluctuating velocity components were obtained by assuming $\overline{u'^2}:\overline{v'^2} = 1:0.5$ k--which is usually observed in single-phase jets.

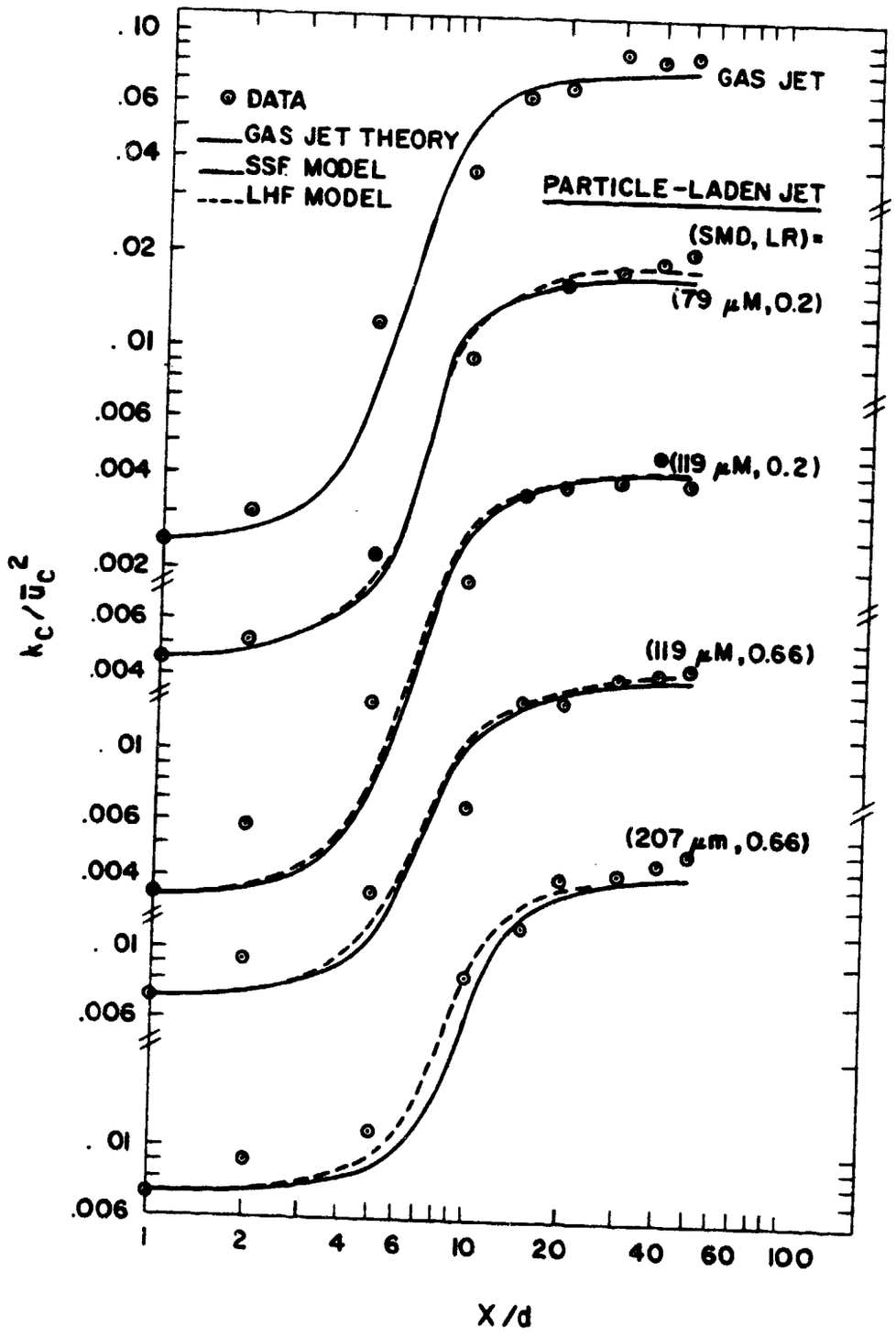

Fig. 15. Axial variation of centerline gas-phase turbulent kinetic energy.

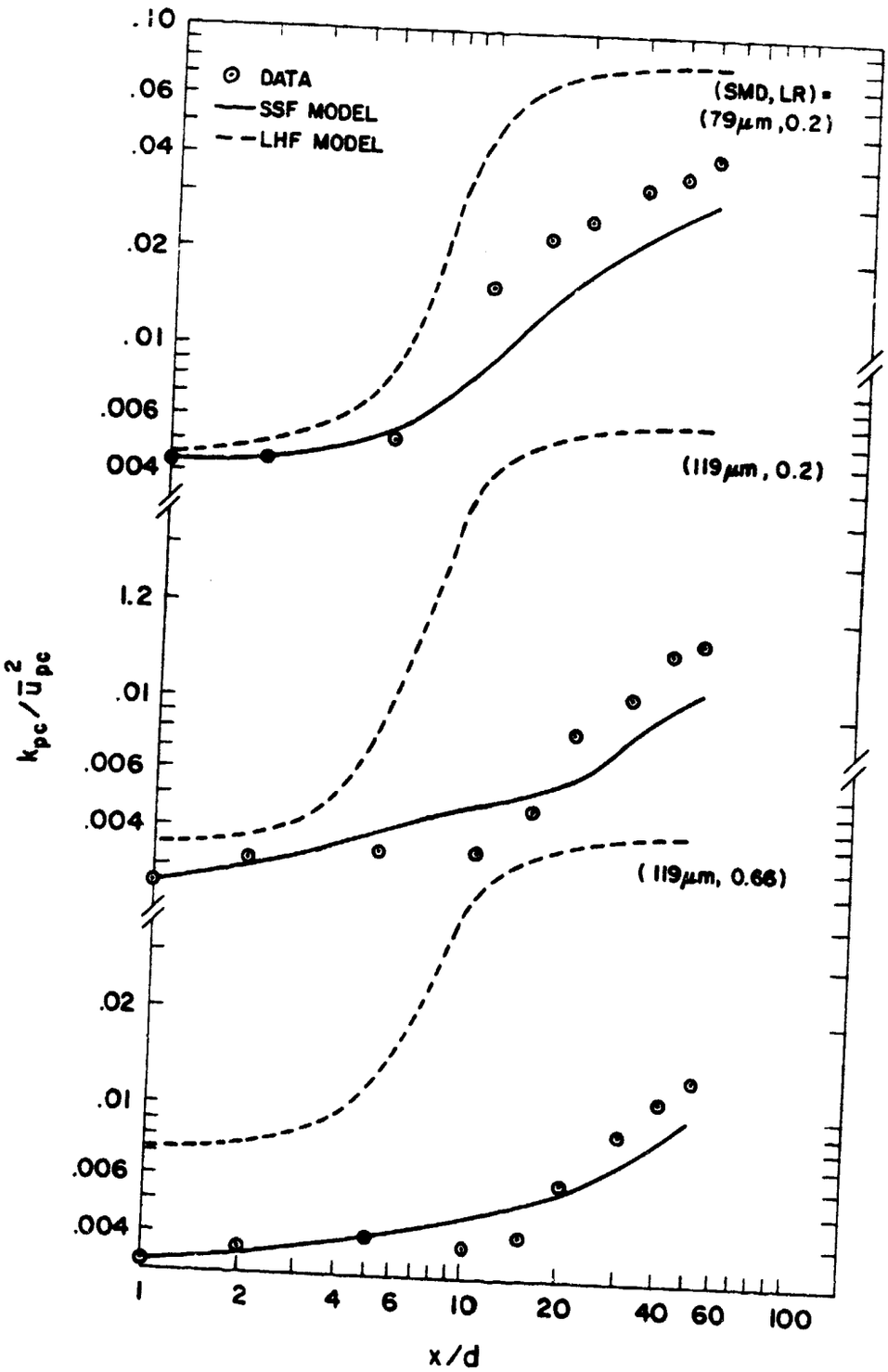

Fig. 16. Axial variation of centerline solid-phase turbulent kinetic energy.

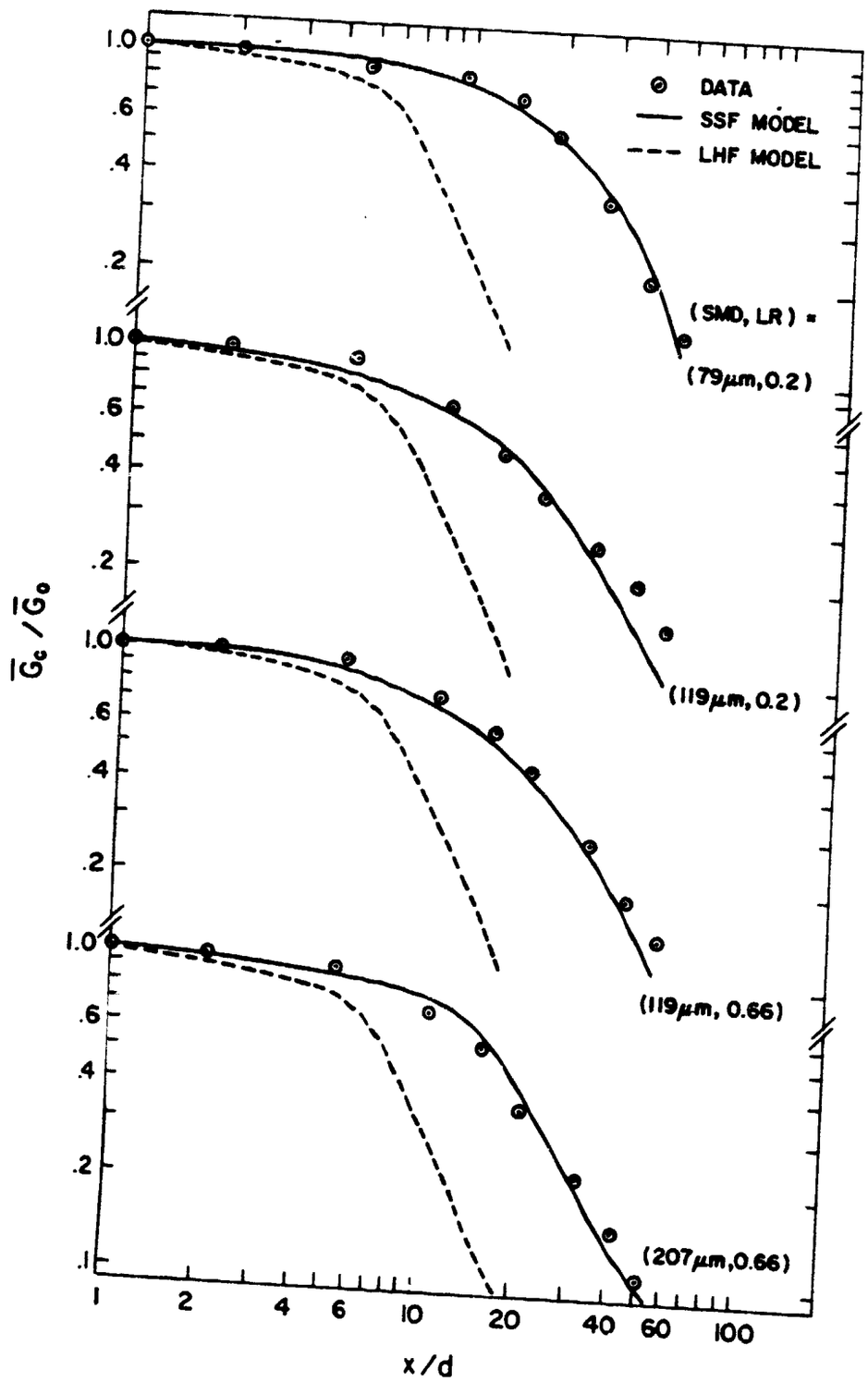

Fig. 17. Axial variation of centerline mean particle mass flux.

Predictions and measurements for air jet are compared in Figs. 18 and 19. Predictions agree well with measurements for all quantities, just as in the case of Shearer [8] and Mao [9].

Predictions and measurements for case 1 particle-laden jet are compared in Figs. 20-23. In this case, the loading ratio was quite low; therefore, gas-phase profiles approach the air-jet properties. Both LHF and SSF predictions are in good agreement with measurements for gas-phase properties at x/d = 20, except that the SSF model underestimates Reynolds stress at its maximum. The agreement between predicted and measured gas-phase properties is less satisfactory at x/d = 40. The predicted radial profiles are generally too wide compared to experimental results at this axial position. Predictions of particle properties are compared with measurements in Figs. 21 and 23. SSF predictions are in good agreement with data for all properties, except for the axial component of fluctuating velocity, where the model predictions are too low near the axis and too high away from the axis. Predictions of the LHF model are not satisfactory in this case. Results for the DSF model are also shown in Fig. 23. The DSF model yields poor results, similar to the findings when evaluating these models using existing measurements. Neglecting particle dispersion by turbulence causes the rate of spread of the flow to be substantially underestimated.

Comparison of radial profiles of mean and fluctuating quantities for the case 2 particle-laden jet is shown in Figs. 24-27. In this case, effects of particles on gas-phase properties are small due to the low loading ratio and the larger particle size. Predictions of gas-phase properties for both the LHF and SSF models are in reasonably good agreement with measurements at x/d = 20 and 40. The particle properties are also well predicted by the SSF model. In contrast, the LHF model overestimates all particle properties while the DSF model underestimates the flow spreading rate--similar to the case 1 flow.

The results for case 3 particle-laden jet are illustrated in Figs. 28-31. The loading ratio in this case is higher, resulting in greater effects of particles on the properties of the gas phase. The measured mean-gas velocity profiles for the case 3 jet are narrower than the case 2 jet, which has the same particle size, but a lower loading ratio. The fluctuating velocities, as well as the Reynolds stress, also decrease as the loading ratio increases. This may be attributed to the effects of turbulence modulation, i.e., turbulence intensity levels are attenuated by particle drag, resulting in a reduced jet spreading rate. This trend cannot be reproduced by the models, since effects of particle drag on turbulence structure are ignored for these predictions. As noted earlier, effects of turbulence modulation on the present test flows will be discussed in Section 4.5.

The particle properties are well predicted by SSF model, except for the profile of particle mass flux at x/d = 40 (Fig.

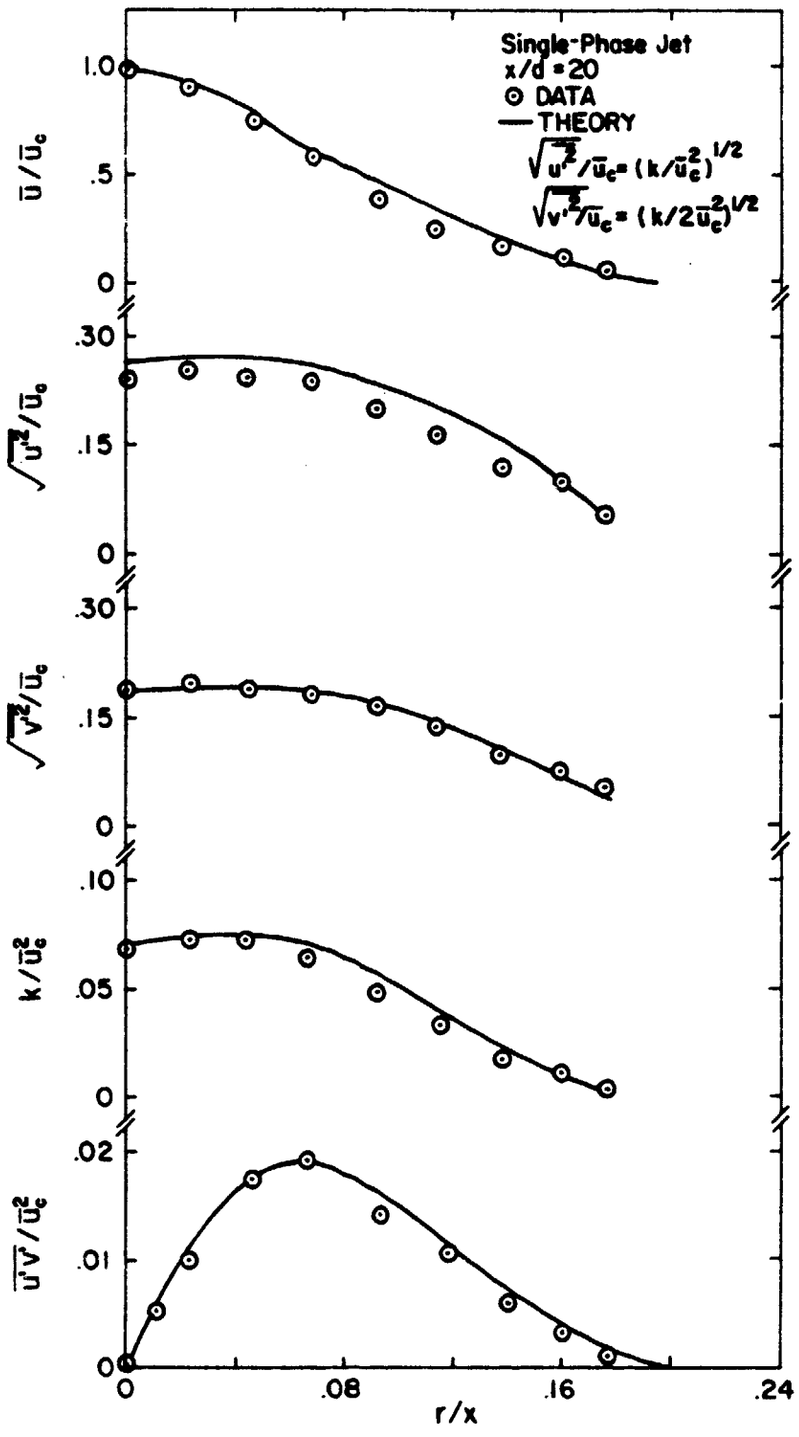

Fig. 18. Radial variation of mean and turbulent quantities in the single-phase jet at x/d = 20.

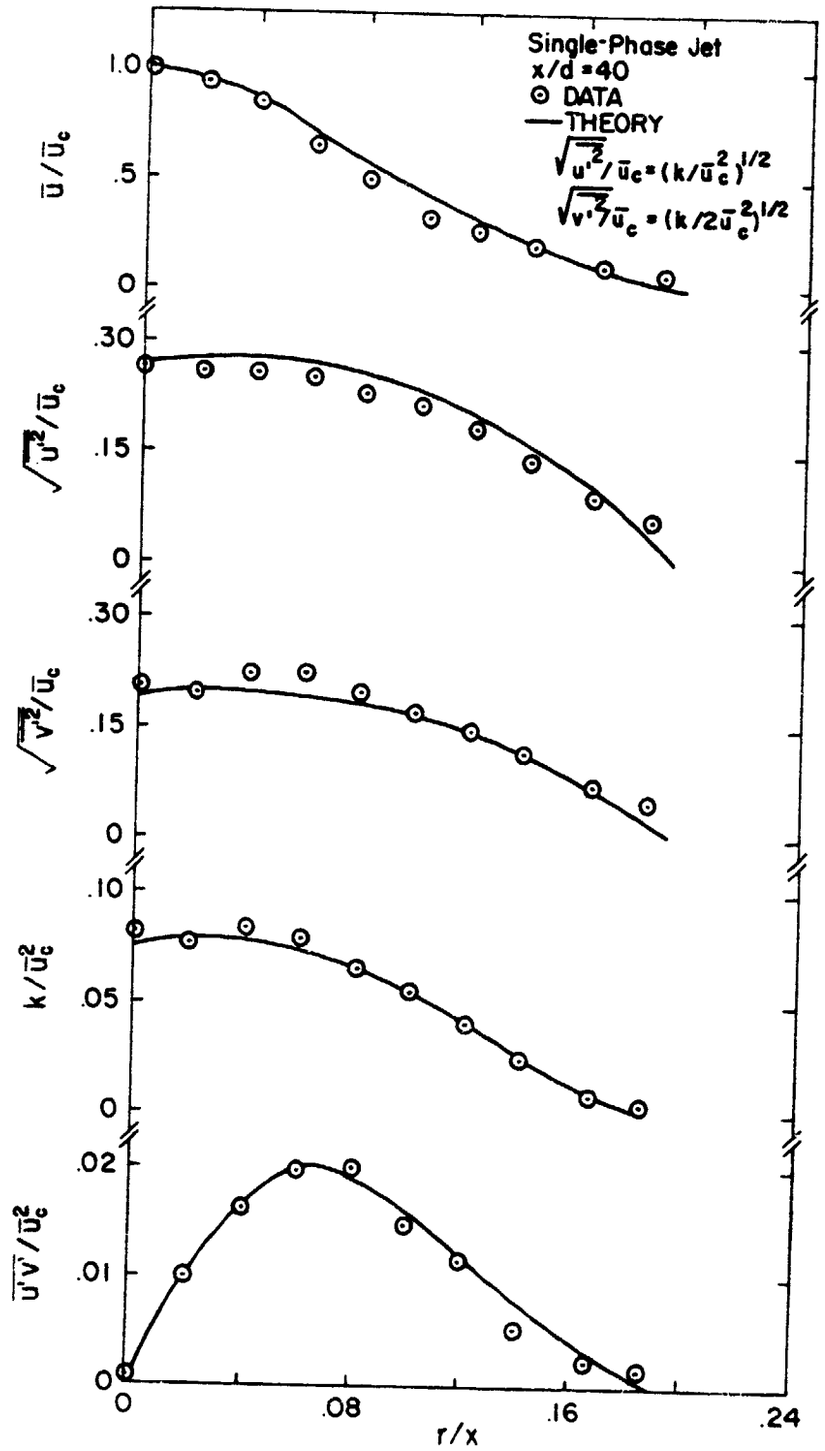

Fig. 19. Radial variation of mean and turbulent quantities in the single-phase jet at x/d = 40.

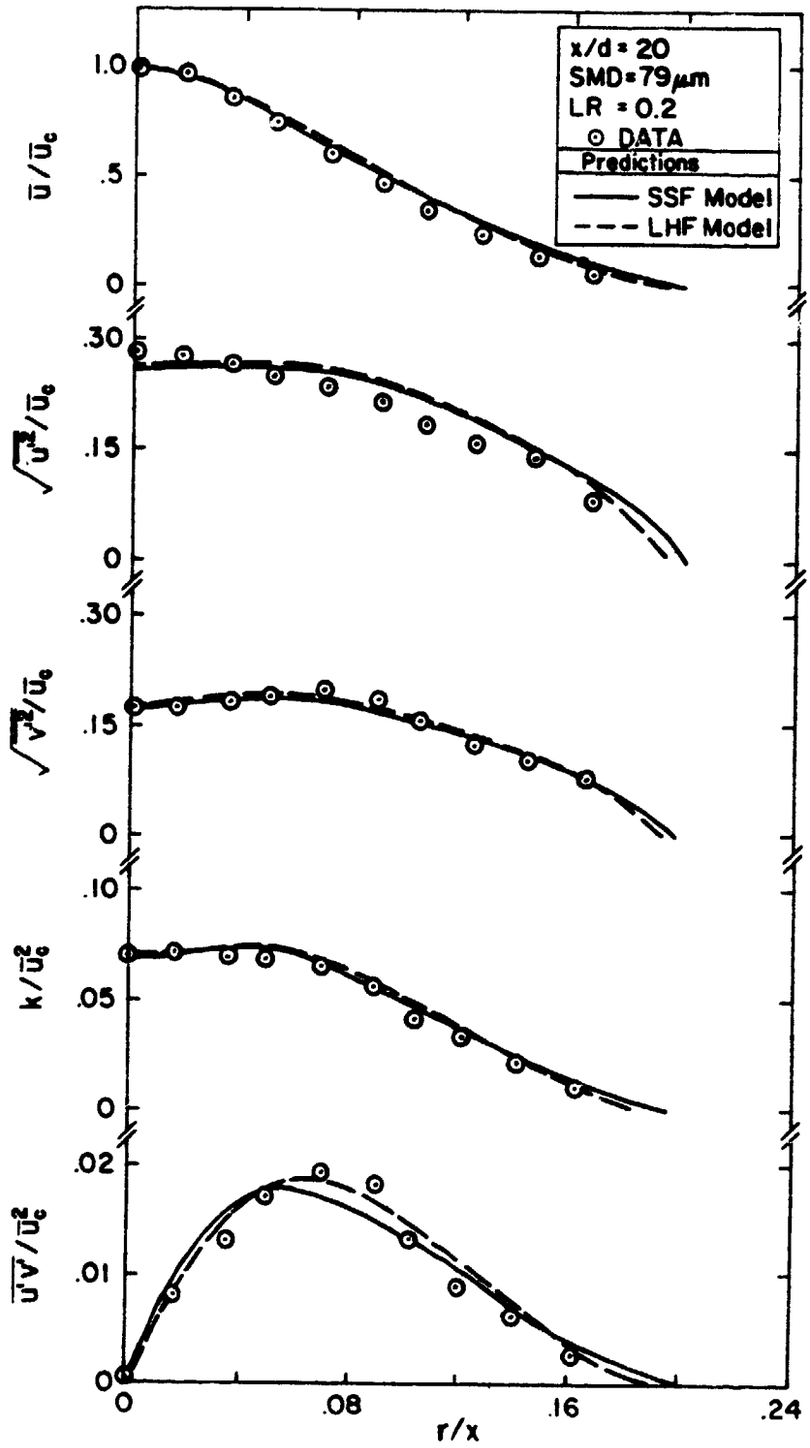

Fig. 20. Radial variation of gas-phase mean and turbulent quantities in case 1 particle-laden jet at x/d = 20.

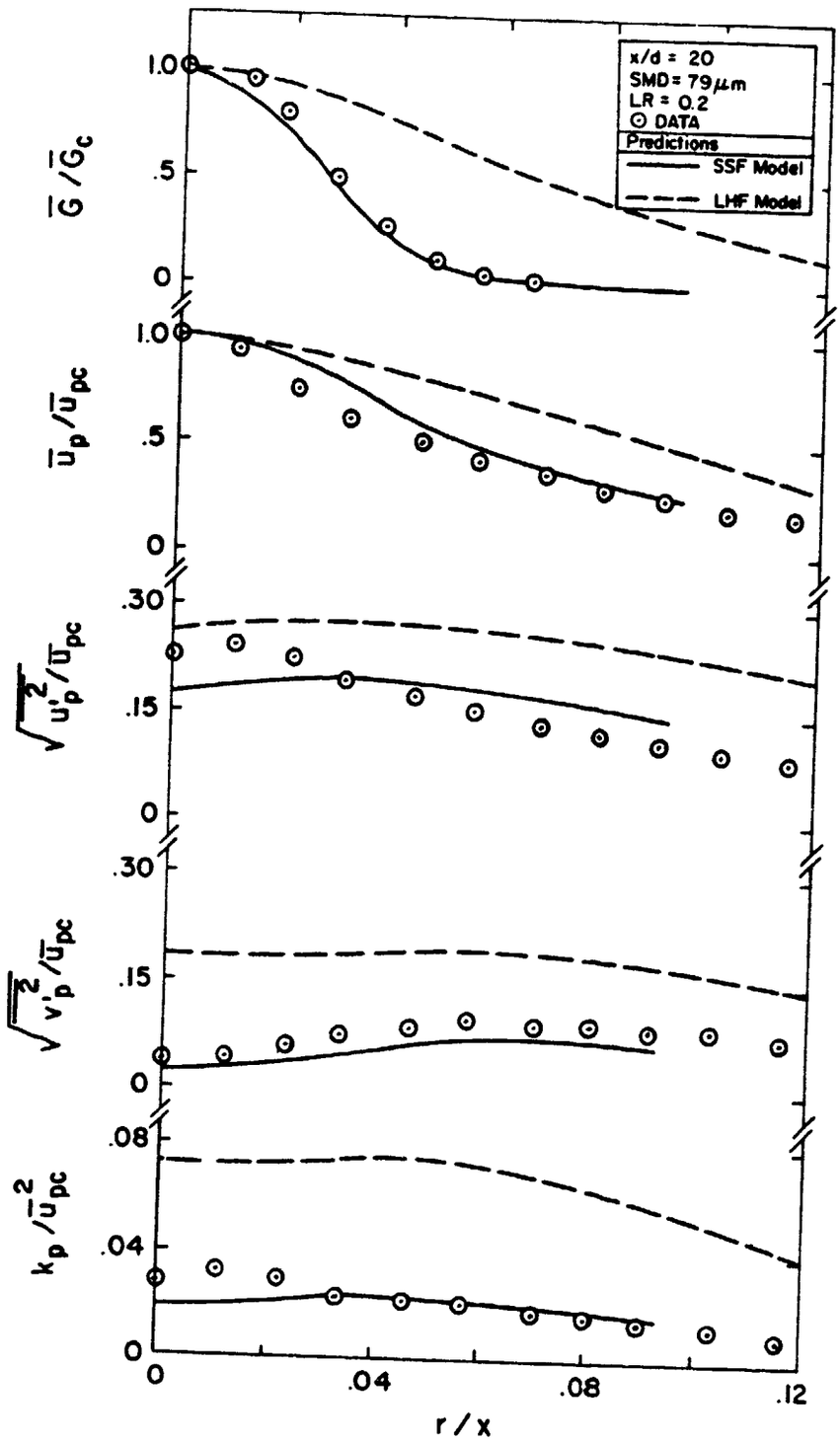

Fig. 21. Radial variation of solid-phase mean and turbulent quantities in case 1 particle-laden jet at x/d = 20.

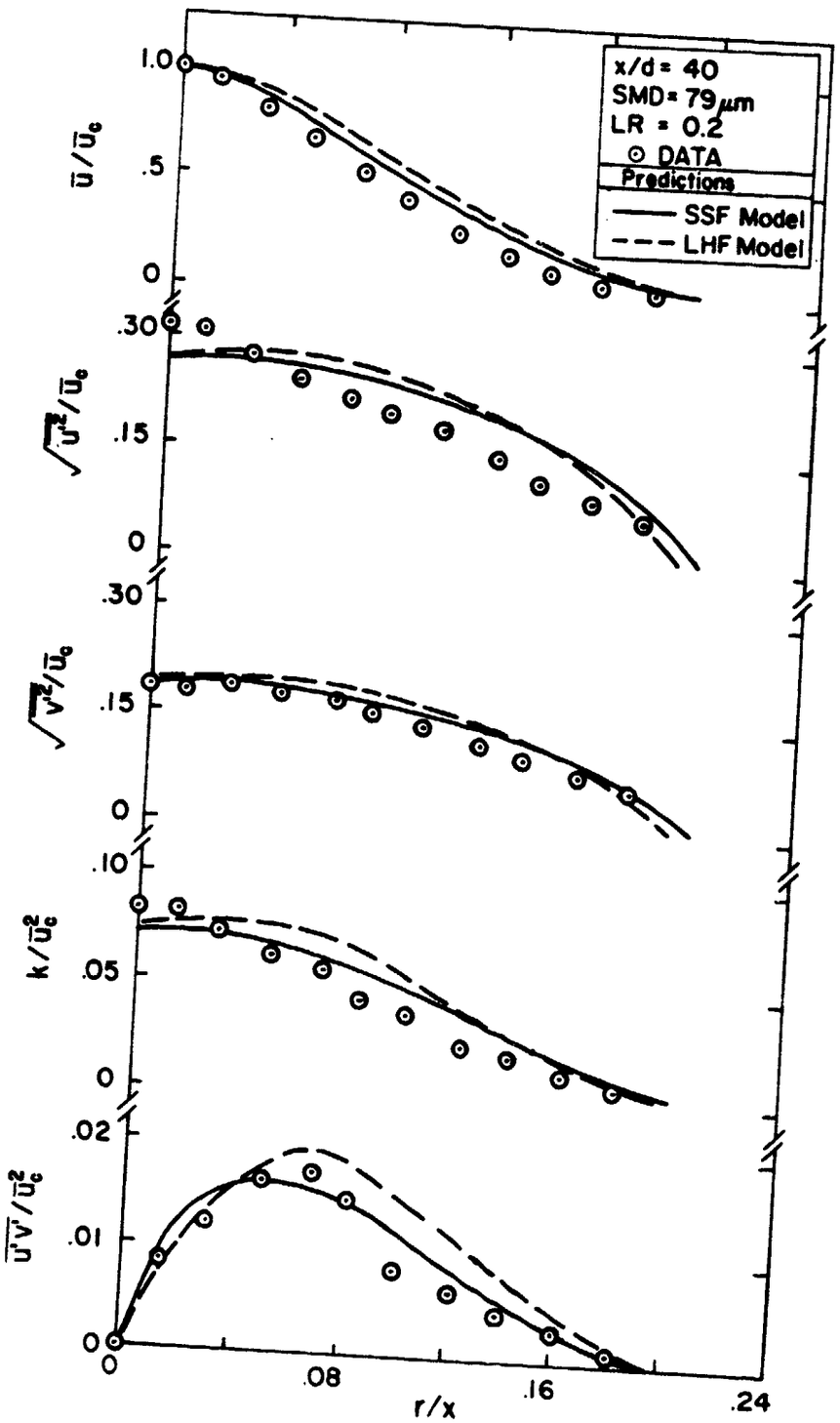

Fig. 22. Radial variation of gas-phase mean and turbulent quantities in case 1 particle-laden jet at x/d = 40.

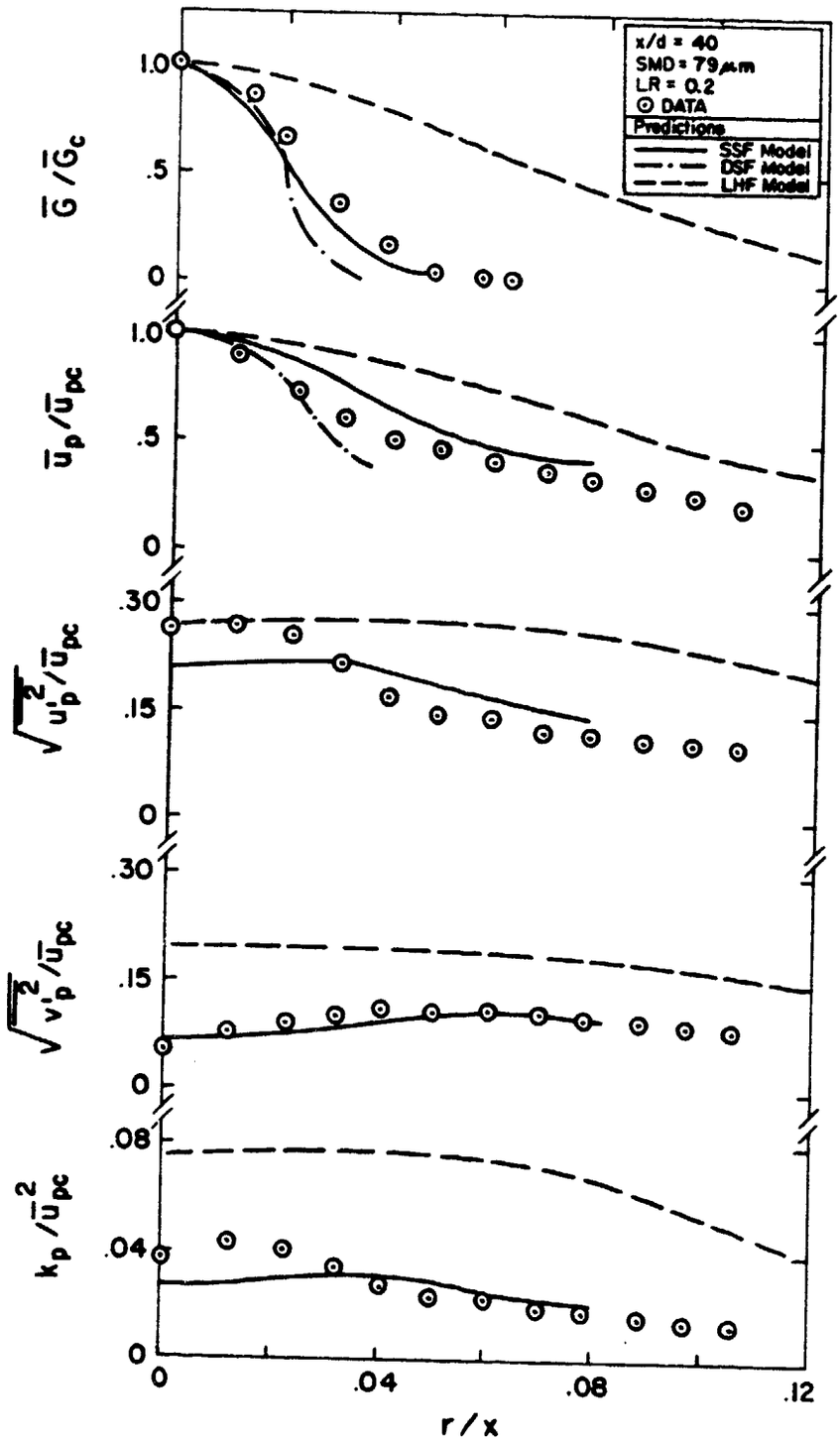

Fig. 23. Radial variation of solid-phase mean and turbulent quantities in case 1 particle-laden jet at x/d = 40.

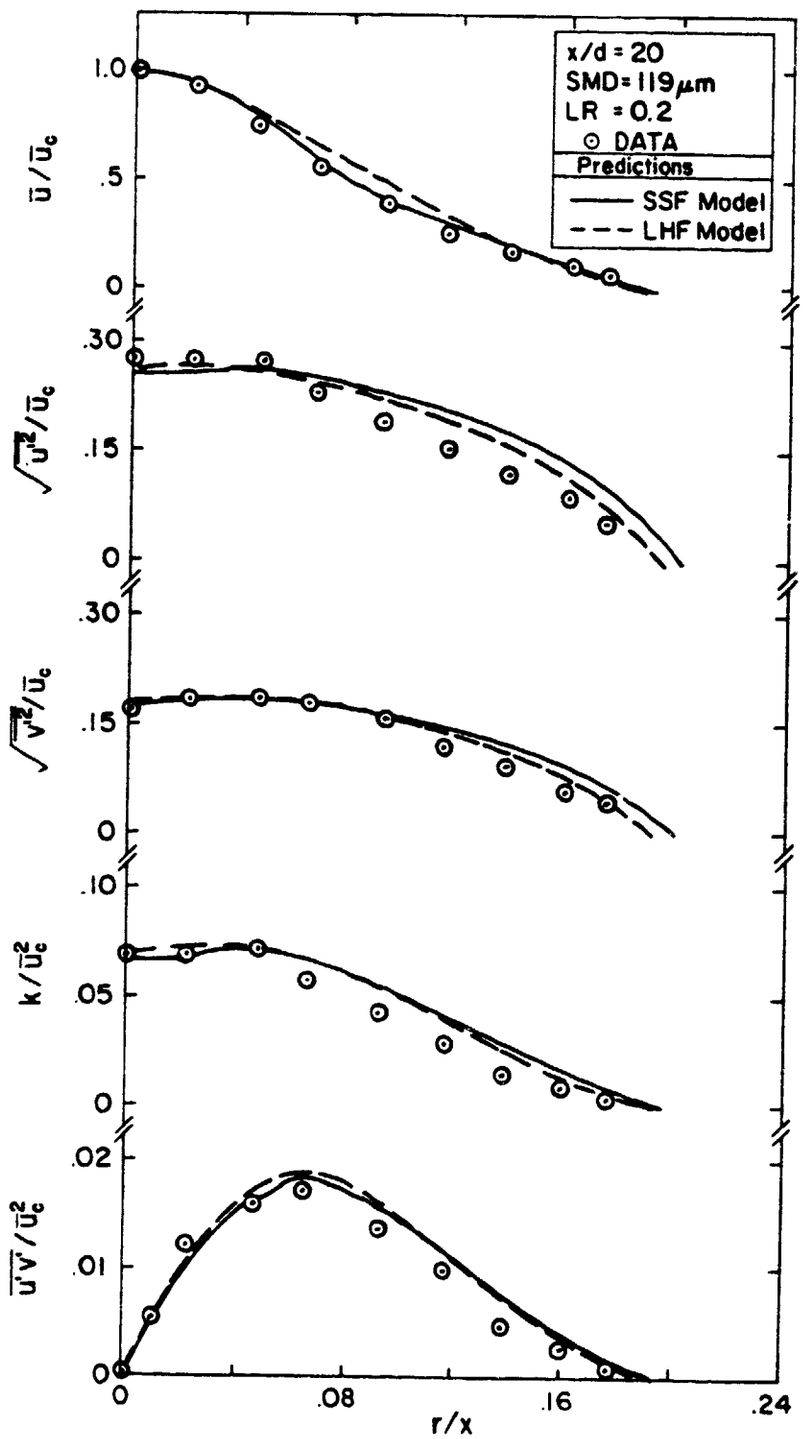

Fig. 24. Radial variation of gas-phase mean and turbulent quantities in case 2 particle-laden jet at x/d = 20.

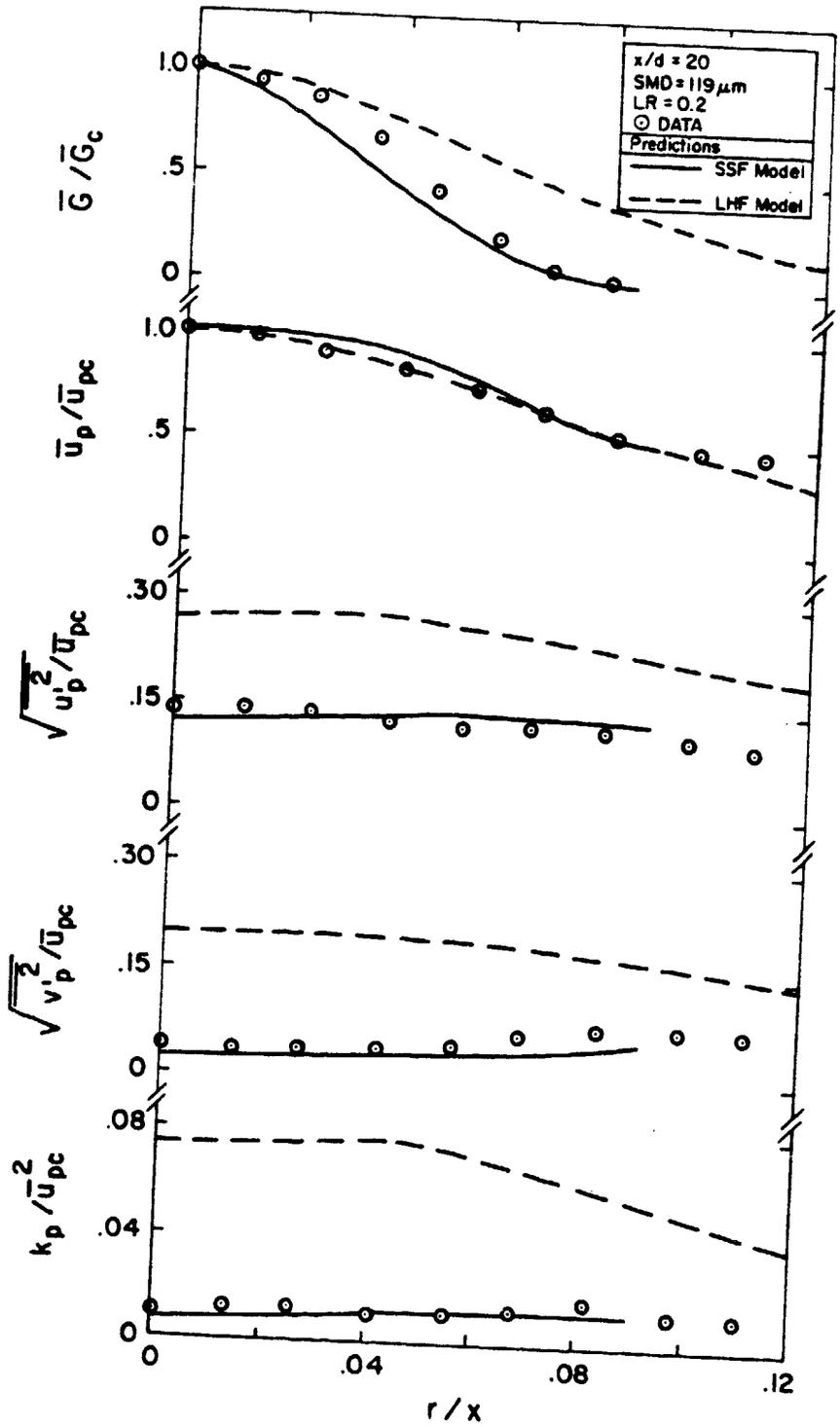

Fig. 25. Radial variation of solid-phase mean and turbulent quantities in case 2 particle-laden jet at x/d = 20.

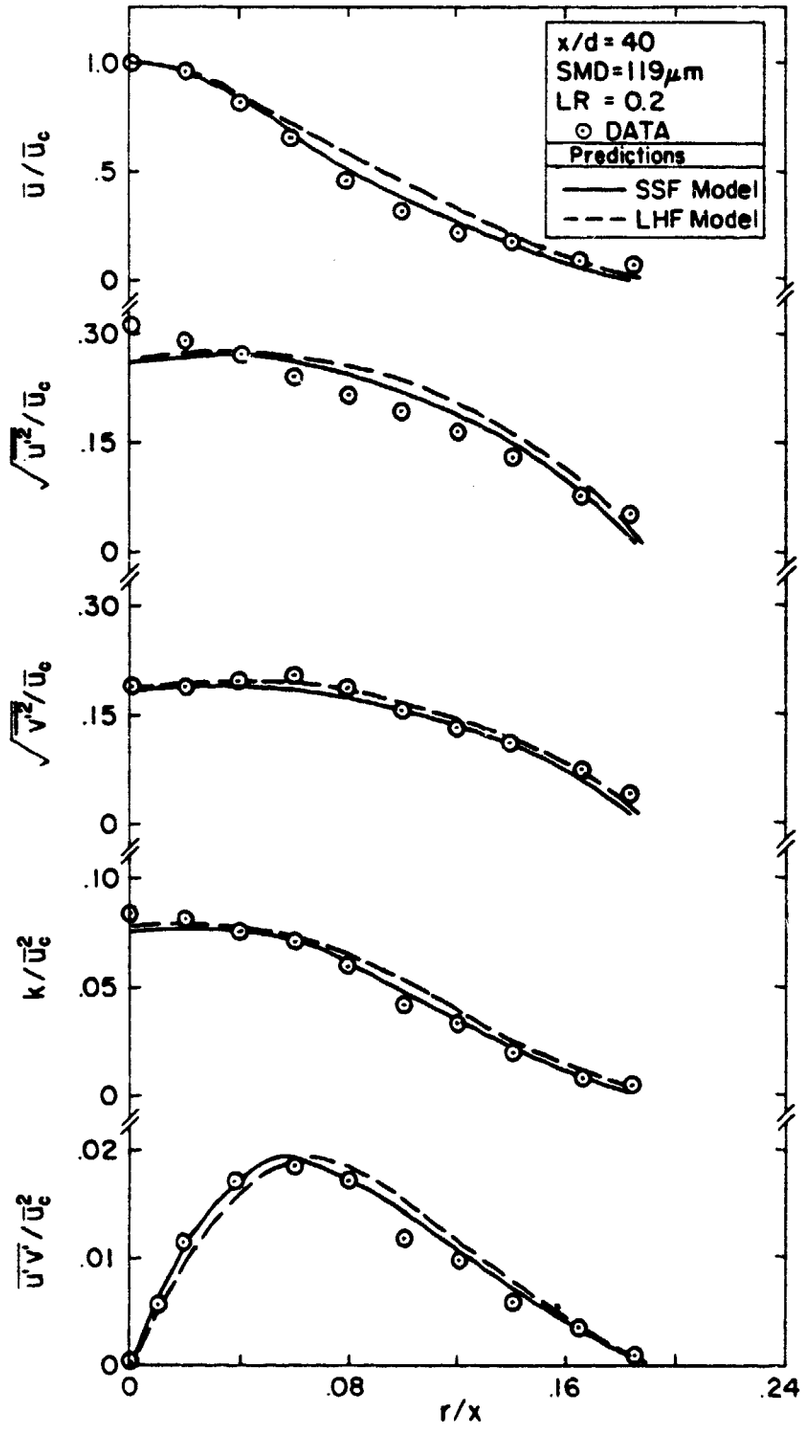

Fig. 26. Radial variation of gas-phase mean and turbulent quantities in case 2 particle-laden jet at x/d = 40.

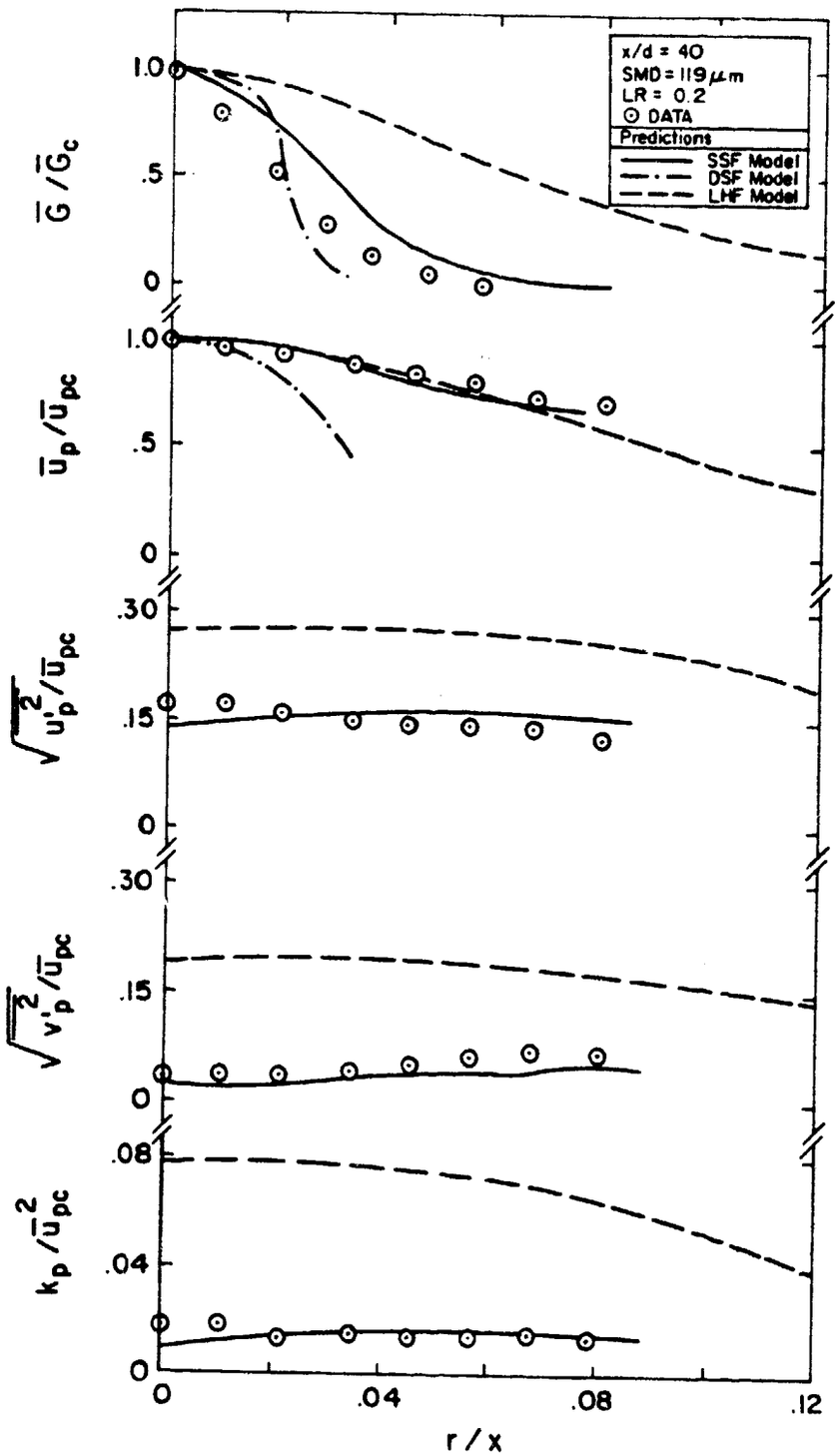

Fig. 27. Radial variation of solid-phase mean and turbulent quantities in case 2 particle-laden jet at x/d = 40.

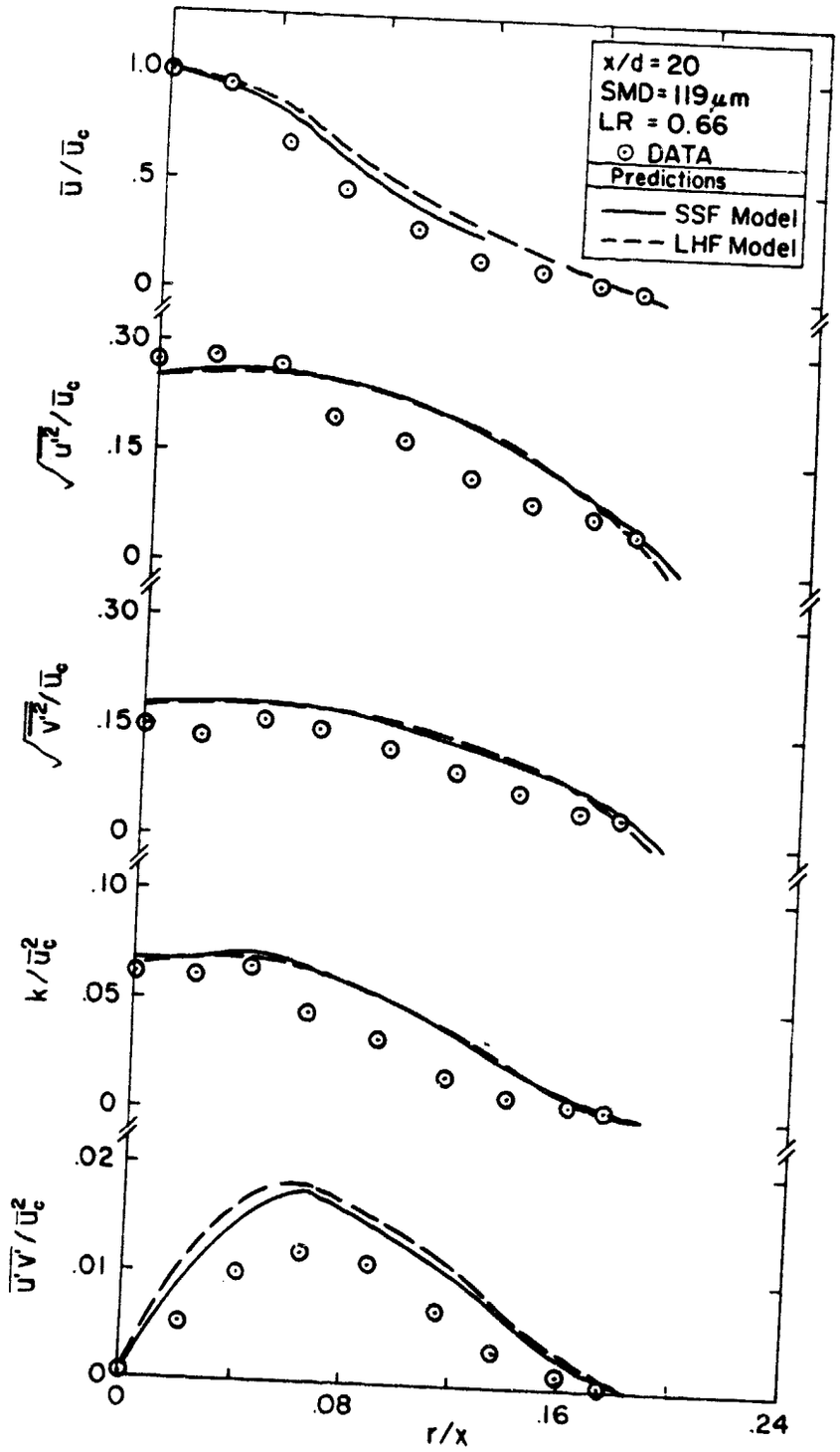

Fig. 28. Radial variation of gas-phase mean and turbulent quantities in case 3 particle-laden jet at x/d = 20.

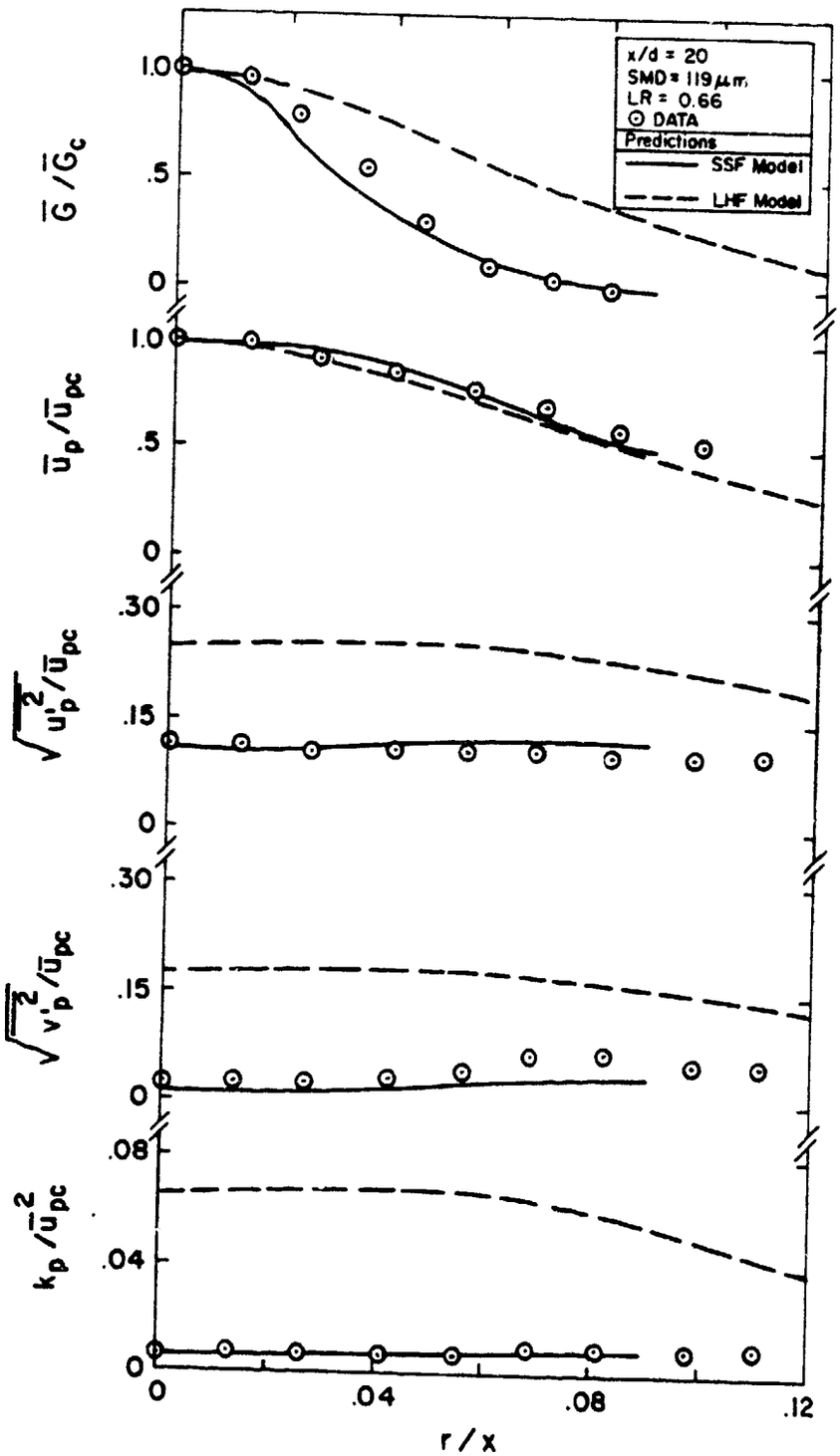

Fig. 29. Radial variation of solid-phase mean and turbulent quantities in case 3 particle-laden jet at x/d = 20.

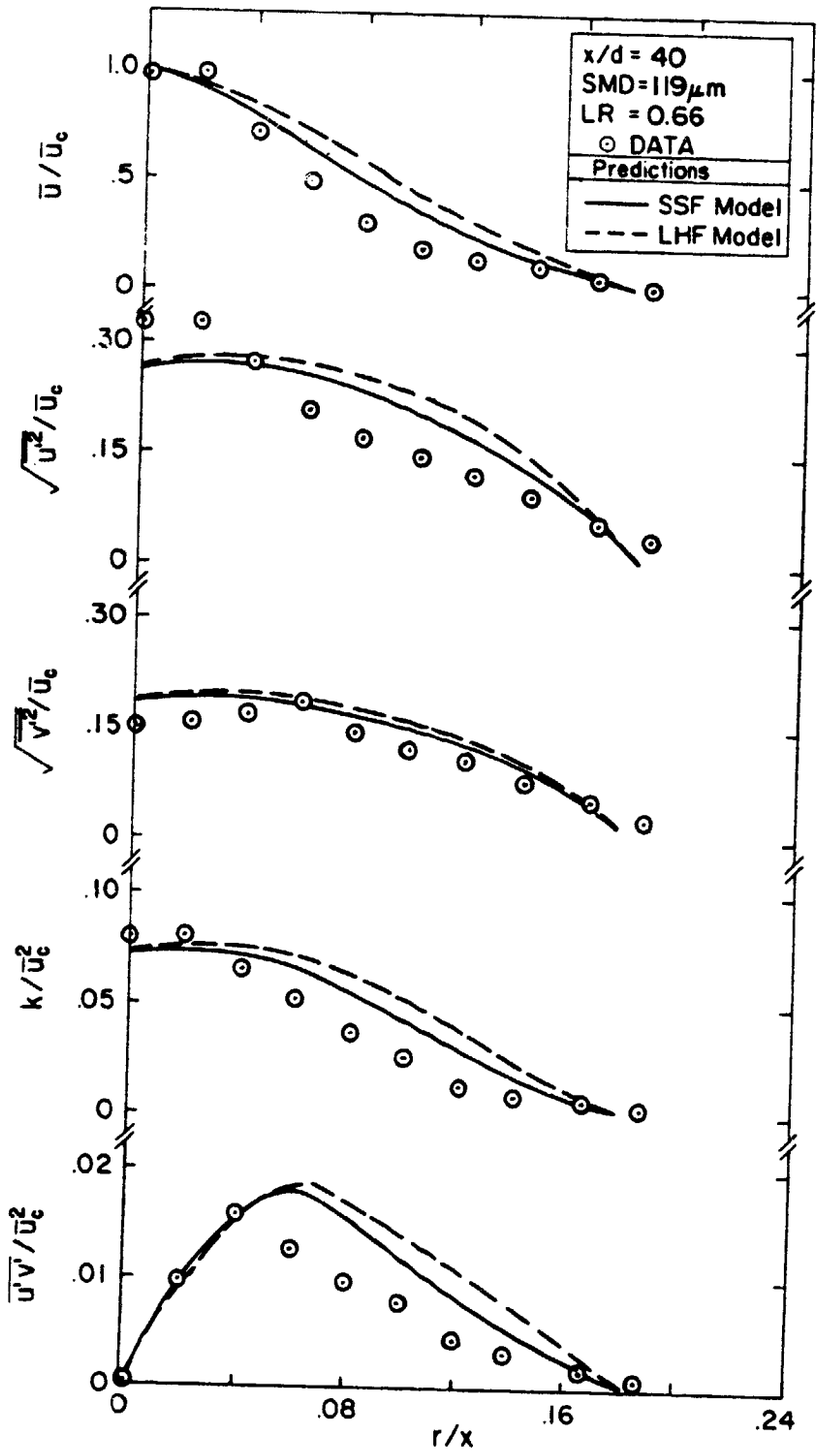

Fig. 30. Radial variation of gas-phase mean and turbulent quantities in case 3 particle-laden jet at x/d = 40.

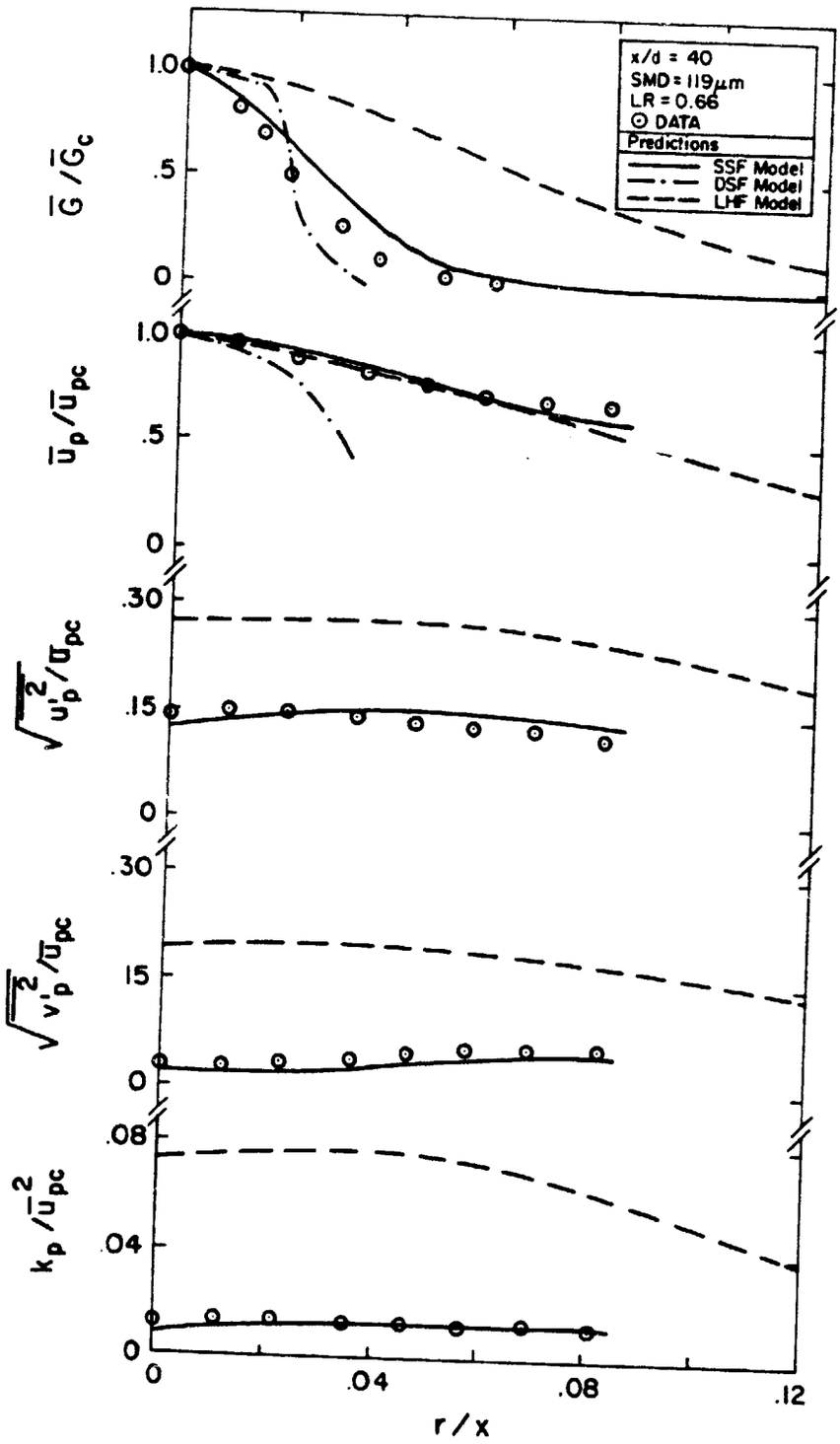

Fig. 31. Radial variation of solid-phase mean and turbulent quantities in case 3 particle-laden jet at x/d = 40.

31) where the SSF model somewhat overestimates the particle-spreading rate. The fact that good agreement is obtained for particle properties, in spite of errors in predictions for gas phase, indicate the particles in this test flow are relatively insensitive to the variation of gas properties due to their large inertia (large size and initial velocity).

Predictions of gas-phase properties for the case 4 particle-laden jet are compared with measurements in Figs. 32 and 33. The results for particle properties are not shown, since in this case velocity measurements for large particles using the LDA experienced difficulties. At this test condition, the large particles have a relatively small velocity change and short residence time from the jet exit to the measuring stations. Hence the influence of particles on gas-phase structure is small, even though the loading ratio is high. The predictions of the SSF model are in good agreement with measurements for all gas-phase properties, while the LHF model slightly overestimates both mean and fluctuating quantities.

In general, the SSF model provided reasonably good predictions of mean and turbulent quantities for both solid and gas phases. This is encouraging, in view of the simple formulation for treating the interphase transport processes. Although the LHF model yields poor predictions for solid-phase properties, it is capable of providing reasonable estimation for gas-phase properties of the flows examined in this study. However, it should be recalled that the present measurements were limited to dilute flows with relatively large particles, where the effects of interphase transport on gas-phase structure are not very significant. The DSF model is not attractive for the present flows, in view of the poor performance in predicting particle properties and the need for detailed information for initial conditions.

4.5 Effects of Turbulence Modulation

For results thus far, the SSF model has not considered direct contributions of interphase transport on turbulence properties. The comparison between predictions and measurements reveals that this approach is acceptable in dilute flows. However, effects of turbulence modulation can be large when particle-loading ratios were large, e.g., the results of Laats and Frishman [1] and the present study in Figs. 28 and 30.

Effects of turbulence modulation were studied for the measurements completed in the present investigation, using the model discussed in Section 2.5. The new model constant, C_3, which should be of order unity based on physical reasoning, was allowed to vary between 1 and 5. The calculated results for the fractional change of centerline flow properties, due to effects of turbulence modulation, are presented in Table 5, for $C_3 = 1$

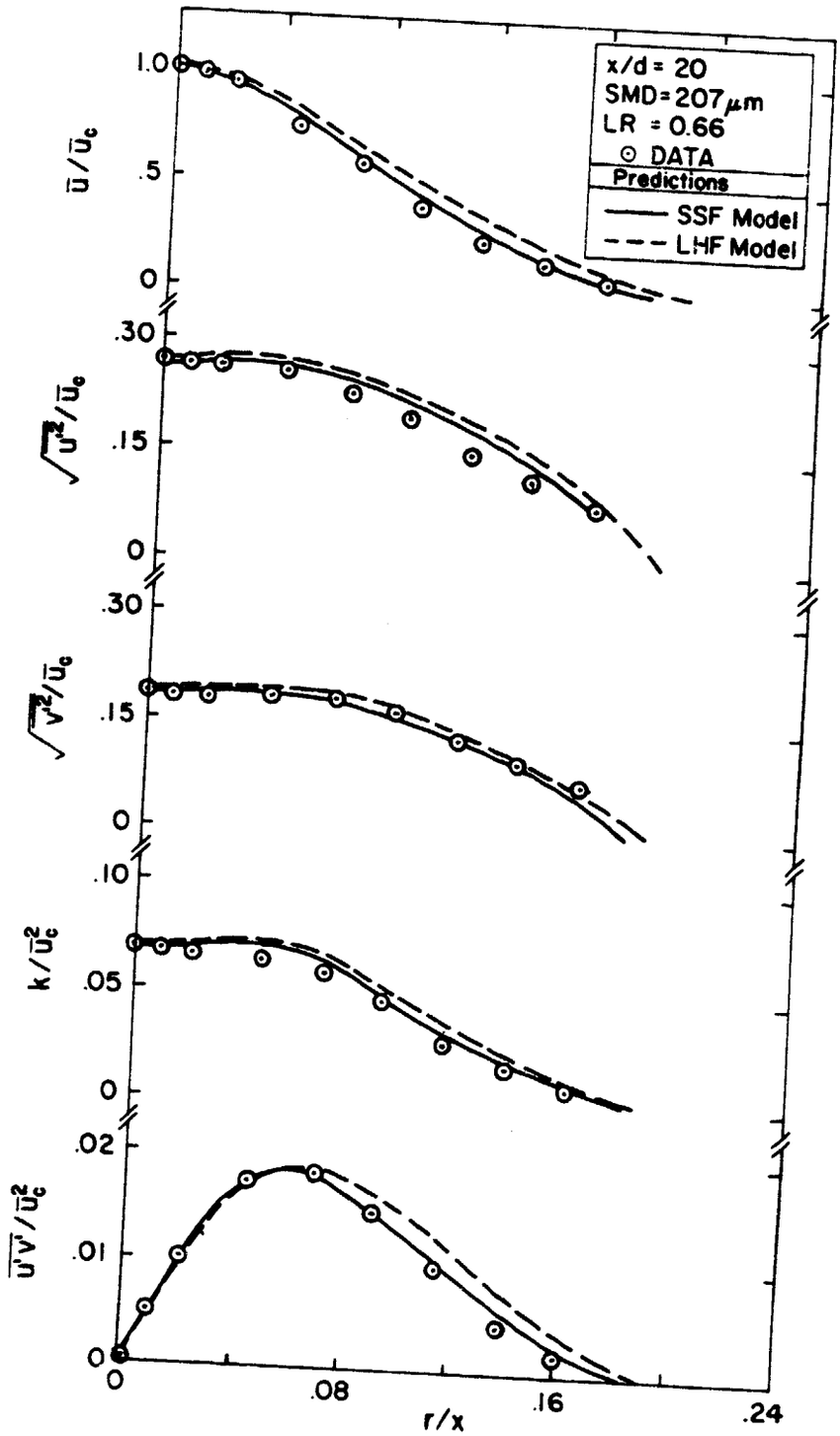

Fig. 32. Radial variation of gas-phase mean and turbulent quantities in case 4 particle-laden jet at x/d = 20.

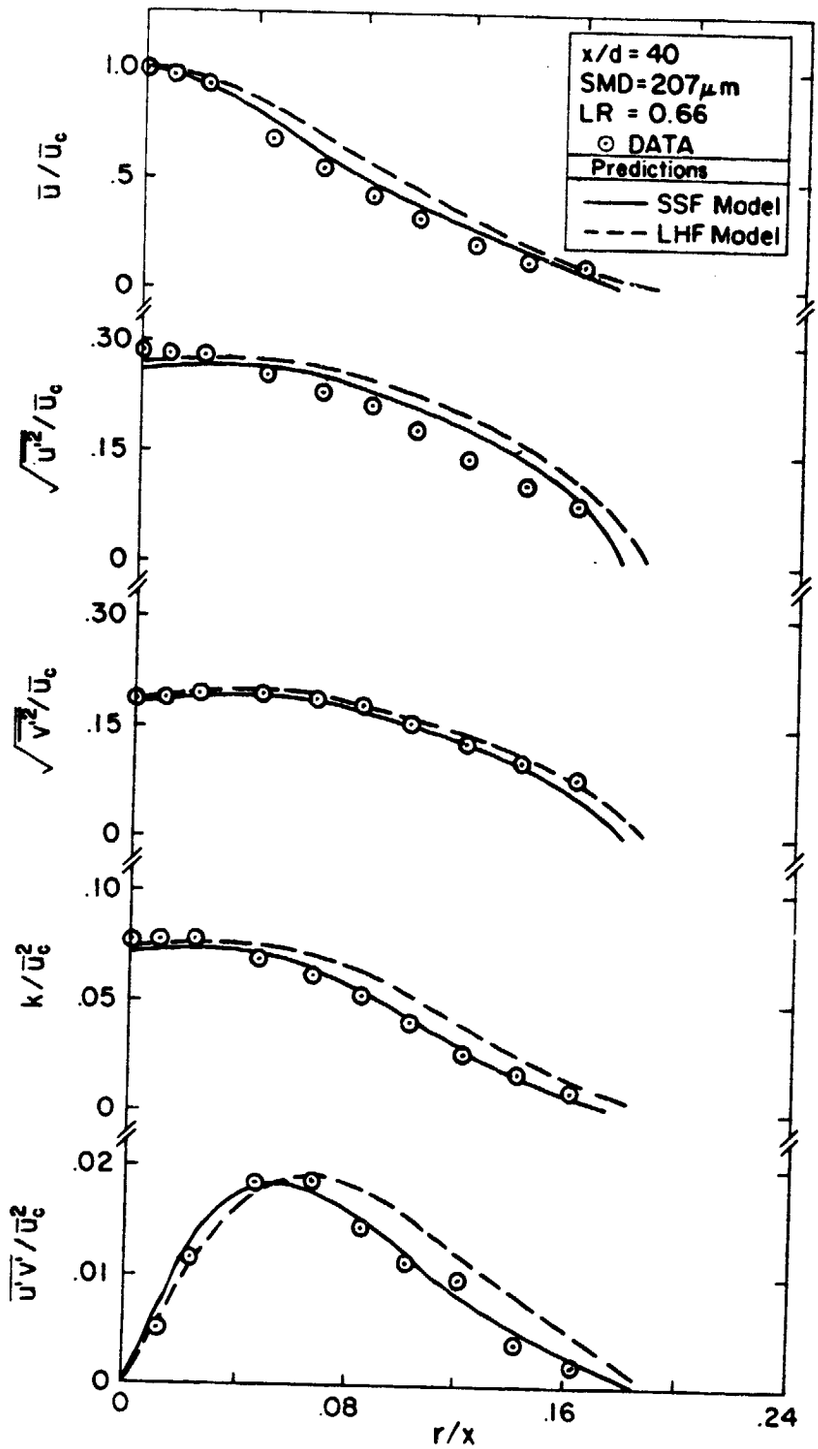

Fig. 33. Radial variation of gas-phase mean and turbulent quantities in case 4 particle-laden jet at x/d = 40.

Table 5 Summary of Results of the Turbulence Modulation Study[a]

ϕ	Case / x/d	1 C_{ε_3}=1.0	1 C_{ε_3}=5.0	2 C_{ε_3}= 1.0	2 C_{ε_3}=5.0	3 C_{ε_3}=1.0	3 C_{ε_3}=5.0	4 C_{ε_3}=1.0	4 C_{ε_3}=5.0
$\bar{u}_c$	10	.010	.008	.006	.006	.013	.012	.006	.004
	20	.013	.013	.007	.008	.020	.020	.008	.007
	30	.013	.015	.006	.007	.011	.011	.005	.007
	40	.010	.014	.004	.003	.005	.004	.010	.002
	50	.009	.014	.003	.002	.004	.004	.013	.004
$\frac{k_c}{\bar{u}_c^2}$	10	-.039	-.031	-.022	-.022	-.052	-.051	-.027	-.021
	20	-.041	-.046	-.021	-.021	-.066	-.059	-.018	-.014
	30	-.033	-.035	.012	.019	-.032	-.033	-.016	-.018
	40	-.010	-.018	.004	.005	-.018	-.019	-.036	.020
	50	-.010	-.027	.000	.008	-.005	-.008	-.047	.000
$\frac{(\overline{u'v'})_{max}}{\bar{u}_c^2}$	10	-.030	-.017	-.012	-.013	-.030	-.030	-.015	-.012
	20	-.031	-.034	-.021	-.023	-.051	-.058	-.006	-.008
	30	-.020	-.023	.003	.005	-.035	-.039	-.005	-.007
	40	-.011	-.011	.007	.009	-.026	-.029	-.021	-.006
	50	-.003	-.008	.006	.013	-.008	-.009	-.036	-.014
$\bar{G}_c$	10	.004	.003	.004	.004	.009	.007	.004	.003
	20	.016	.015	.008	.009	.012	.010	.006	.005
	30	.016	.016	.006	.005	.008	.007	.008	.008
	40	.013	.014	.004	.004	.007	.006	.015	.008
	50	.014	.016	.003	.003	.008	.005	.019	.006

[a]Results are the fractional change of properties when considering the effects of turbulence modulation, i.e., $(\phi_{w\ T.M.} - \phi_{w/o\ T.M.})/\phi_{w/o\ T.M.}$, where ϕ stands for $\bar{u}_c$, $k_c/\bar{u}_c^2$, $\overline{u'v'}_{max}/\bar{u}_c^2$ and $\bar{G}_c$.

and 5. The maximum change of flow properties from this calculation is 6.6%, which occurs in turbulence kinetic energy at x/d = 20 for case 3 particle-laden jet. Furthermore, the predictions were found to be relatively insensitive to the variations of C_3.

The small effect of particles on the turbulence structure of presently measured flows is expected, since these flows are all relatively dilute. The large particle inertia and small particle residence time may also reduce the effects of interphase transport on turbulence properties for these flows.

The relatively large discrepancies between predictions and measurements, shown in Figs. 28 and 30 cannot be rectified by only considering effects of turbulence modulation in the predictions. This deviation between theory and experiment is more likely to be due to experimental errors.

4.6 Sensitivity Study

In the preceding discussion, it was noted that specification of initial conditions is of vital importance to predictions using separated flow models. Because of this concern, special care was exercised to obtain reliable measurements of initial conditions for the test flows during the present experimental investigation. However, uncertainties still exist in the specification of particle properties, i.e., the particle-drag coefficient and mean-particle size used for initiating the computations. As discussed previously, the particle-drag coefficient for each size group used in the predictions was obtained by adjusting the standard drag law with a single scaling factor obtained from the free-fall experiment. Some uncertainties were introduced in this process, since the scaling factor for each particle group might vary over the Reynolds number range experienced in particle-laden jet experiments.

The particle size is another concern. The measured particle-size distributions for the three size groups have standard deviations varying from 11%, for largest particle-size group, to 23%, for smallest particle-size group. Only one average size, i.e., the Sauter mean diameter, was used for each group--to save computational effort.

Another potential source of uncertainty in predictions comes from the specification of ε_o, the rate of dissipation of turbulence kinetic energy at the jet exit. The k-ε model requires initial values of k and ε to start the computation. While k_o was measured directly, ε_o was calculated from measured values of turbulence kinetic energy, Reynolds stress and the mean velocity gradient at exit, using Equation (2.3) and the gradient transport assumption. Although this approach was consistent with the formulation of k-ε model, errors might be introduced due to

the small magnitude of the velocity gradient near the jet centerline at the exit.

Due to these uncertainties regarding specification of initial conditions and particle properties, the sensitivity of model predictions to the variation of these parameters was examined. The results of this study are presented in Tables 6, 7, 8 and 9 for the four particle-laden jets investigated in the present experiments. The entries show the fractional change in predictions brought about by raising the value of the indicated parameter by 100%--with all other parameters unchanged. These estimates were obtained using the SSF model without considering effects of turbulence modulation. The entries are computed for the major measurements stations considered in the experiments--x/d = 20 and 40.

In general, the predicted flow properties for both gas and particulate phases, are not sensitive to the variation of ε_o and k_o. This is expected, since the production and dissipation of turbulence kinetic energy are the prevailing mechanisms for the development of turbulence structure in free jets. In contrast, the calculated solid-phase properties show larger sensitivities to the variations of particle diameter and drag coefficient. This finding also illustrates the importance of defining initial particle properties in order to obtain a convincing evaluation of models.

Broadly, the most influential parameter for the predictions is particle size. For example, a 51% change in $\overline{u}_{pc}$ and -50% change in $k_p/\overline{u^2}_{pc}$ was obtained by raising the value of d_p by 100%. The large sensitivity of d_p is due to the fact that particle relaxation time (the time for the particle to change the slip velocity by a factor of e^{-1}) is roughly proportional to d_p^2. Since the standard deviations of the particle-size distributions involved in the present study are small (varying from 11% to 23% for the three size groups), the errors introduced by assuming monodisperse particle-laden flow are within experimental accuracy.

5. MODEL EVALUATION: MEASUREMENTS OF ELGHOBASHI ET AL.

5.1 General Description

Recently, Elghobashi and his coworkers [6,7] reported LDA measurements for particle-laden jets, with particle sizes of 50 μm and 200 μm and loading ratios from 0.32 to 0.85. The most important contribution of their experiments is that, in contrast to all the other existing measurements, they provided some information on initial conditions of their test flows. The authors also paid special attention to eliminating the cross-interference between the two phases in the velocity measurements. Flow structure measurements included: axial decay of streamwise mean velocities along the jet axis for both phases,

Table 6

Summary of Results of Sensitivity Study for Case 1 Particle-Laden Jet[a]

Input Parameter	Output Variables				
	$\bar{u}_c$	$k_c/\bar{u}_c^2$	$\bar{u}_{pc}$	$k_{pc}/\bar{u}_{pc}^2$	$\bar{G}_c$
x/d = 20					
ε_o	.09	-.01	.07	-.12	.06
k_o	-.12	.08	-.06	.09	-.06
C_D	.05	.02	-.13	.22	-.12
d_p	.04	-.03	.18	-.40	.13
x/d = 40					
ε_o	.05	~.00	.09	-.11	.08
k_o	-.06	.02	-.08	.13	-.08
C_D	.03	.04	-.30	.28	-.16
d_p	.06	-.04	.51	-.50	.18

[a]Entries show the fractional change in prediction brought about by raising the indicated input parameter by 100%.

Table 7

Summary of Results of Sensitivity Study for Case 2 Particle-Laden Jet[a]

Input Parameter	Output Variables				
	$\bar{u}_c$	$k_c/\bar{u}_c^2$	$\bar{u}_{pc}$	$k_{pc}/\bar{u}_{pc}^2$	$\bar{G}_c$
x/d = 20					
ε_o	.09	-.02	.02	-.03	.06
k_o	-.13	.05	-.06	.04	-.04
C_D	.02	-.01	-.09	.14	-.09
d_p	.02	-.02	.06	-.21	.08
x/d = 40					
ε_o	.04	~.00	.04	-.04	.06
k_o	-.07	.01	-.09	.07	-.07
C_D	.02	.01	-.32	.19	-.12
d_p	.02	-.03	.27	-.26	.13

[a]Entries show the fractional change in prediction brought about by raising the indicated input parameter by 100%.

Table 8

Summary of Results of Sensitivity Study for Case 3 Particle-Laden Jet[a]

Input Parameter	Output Variables				
	$\bar{u}_c$	$k_c/\bar{u}_c^2$	$\bar{u}_{pc}$	$k_{pc}/\bar{u}_{pc}^2$	$\bar{G}_c$
x/d = 20					
ε_o	.08	-.02	.02	-.04	.06
k_o	-.13	.04	-.07	.05	-.05
C_D	.04	-.02	-.10	.12	-.09
d_p	.03	-.02	.05	-.18	.08
x/d = 40					
ε_o	.03	~.00	.06	-.06	.07
k_o	-.06	.01	-.05	.06	-.07
C_D	.05	.03	-.31	.19	-.14
d_p	.05	-.02	.30	-.26	.16

[a]Entries show the fractional change in prediction brought about by raising the indicated input parameter by 100%.

Table 9

Summary of Results of Sensitivity Study for Case 4 Particle-Laden Jet[a]

Input Parameter	Output Variables				
	$\bar{u}_c$	$k_c/\bar{u}_c^2$	$\bar{u}_{pc}$	$k_{pc}/\bar{u}_{pc}^2$	$\bar{G}_c$
x/d = 20					
ε_o	.09	-.02	.01	-.02	.03
k_o	-.14	.04	-.06	.03	-.03
C_D	.02	-.02	-.06	.09	-.06
d_p	.01	-.02	.01	-.10	.05
x/d = 40					
ε_o	.04	~.00	.02	-.03	.03
k_o	-.07	~.00	-.03	.05	-.04
C_D	.04	.02	-.22	.15	-.08
d_p	.02	-.02	.18	-.14	.07

[a]Entries show the fractional change in prediction brought about by raising the indicated input parameter by 100%.

radial profiles of mean and fluctuating velocities for both phases and Reynolds stress of the gas phase, at x/d = 20. Limited information concerning particle concentration profiles was also reported.

The measurements of Elghobashi et al. are unusually complete. Sophisticated LDA and data processing systems were used to obtain initial conditions at the jet exit, as well as flow properties at downstream positions. However careful examination of the test apparatus employed in their experiment indicated that axial pressure gradients and local recirculation zones were very likely to be present in the flows investigated by Elghobashi et al. These undesirable phenomena were not defined in the measurements and altered the flow structure and complicated the specification of boundary conditions for predictions.

The test configuration of Elghobashi, et al. [6,7] consisted of a 2 cm jet issuing into a cylindrical glass chamber with very low velocity coflow. The chamber diameter was 60 cm. The jet air velocity at exit was 12.6 m/s, and the coflow air velocities were 0.05 m/s and 0.1 m/s for two test cases, respectively. All the air flow was discharged through the exhaust ducting system located at the bottom of the test chamber. This arrangement requires extreme care for operation of the exhaust and coflow feeding systems to balance the inflow and outflow to the test chamber, and to match the entrainment flow for the jet. Excessive exhaust flow yields an axial pressure gradient over the flow field, while insufficient supply of coflow air generates recirculation zones near the jet boundary.

5.2 Results and Discussions

The experiment of Elghobashi et al. [6,7] provided measurements in single-phase air jets, in addition to the measurements in particle-laden jets. This air jet data was first predicted using the single-phase jet model developed earlier in this laboratory, since this model has been extensively tested in the past [8,9]. No recirculation zone was assumed in the boundary condition specifications for predictions. The measured and predicted centerline velocity decay are summarized in Table 10 for several values of axial pressure gradient. It is evident that without adding a constant pressure gradient in the flow field, the model significantly overestimates the rate of centerline velocity decay. It is noted that the same model yielded satisfactory results over varieties of test conditions for flows similar to Elghobashi et al. [6,7] in the past [7,8,39].

Since maintaining balance between total inlet flow and exhaust flow is extremely difficult, it is believed that axial pressure gradients were present in the test chamber. In order to obtain more insight a study was conducted to investigate the potential presence of recirculation zones in the flow field. It is known that when the coflow falls short of the entrainment

Table 10

Centerline Velocity Decay of Single-Phase Jet--
Test Condition of Elghobashi et al.

	x/d			
	5	10	20	30
Measurements (m/s)	11.5	8.44	4.03	2.90
Predictions (m/s)				
$\frac{dp}{dx} = 0$	12.13	7.76	3.42	2.20
$\frac{dp}{dx} = -2\ N/m^3$	12.15	7.85	3.57	2.50
$\frac{dp}{dx} = -5\ N/m^3$	12.17	7.90	3.78	2.91
$\frac{dp}{dx} = -7\ N/m^3$	12.18	7.96	3.92	3.16

capacity of the jet in a confined duct, the balance is satisfied with recirculated fluid. The entrainment calculation, using the empirical expression of Abramovich [40], showed that all the coflow air was entrained at x/d = 14 and x/d = 26 for the jets with coflow air velocities of 0.05 m/s and 0.1 m/s, respectively. This finding suggested that recirculation zones were present in the regions where measurements were conducted. The results of the entrainment calculation was checked by testing for the presence of a recirculation zone using the technique described by Becker, Hottel and Williams [41]. The calculated front edge of the recirculation zones was found to be at x/d = 15 and x/d = 24 for coflow air velocities of 0.05 m/s and 0.1 m/s--neglecting the effect of the axial pressure gradient. These recirculation zones extend far downstream of the major measuring station.

From the preceding discussion, it is evident, due to the arrangement of test apparatus, the flow field investigated by Elghobashi et al. [6,7] was subjected to the influence of axial pressure gradients and local recirculation zones. Since the information concerning the magnitude of the pressure gradients and the extent of recirculation zones were not reported by the original authors, two pressure gradients, i.e., 0 N/m^3 and -5.0 N/m^3, were considered in the predictions discussed in the following. The recirculation zones were ignored, for lack of information.

Predicted and measured radial profiles of flow properties for both phases at x/d = 20 are illustrated in Fig. 34 for the particle-laden jet having a particle size of 50 μm and a loading ratio of 0.32. Predictions of the SSF model, both including and ignoring the effects of turbulence modulation, denoted SSFM and SSF respectively, are shown on the plot. The mean velocity profiles are normalized with the centerline velocity of the single-phase jet, to illustrate the magnitude of the slip velocity and the effects of particles on the gas phase velocity field. It is clear from the figure that improvement in the predictions of the SSF model is obtained by adding a -5.0 N/m^3 pressure gradient, which further suggests the presence of a pressure gradient in the flow field. The SSFM model generally yields better results than the SSF model for most of the flow properties illustrated in Fig. 34. This fact indicates that effects of turbulence modulation are important in this test flow. The overall agreement between SSFM model predictions and measurements is fair, except for axial particle fluctuation velocity, where the model underestimates the fluctuation level.

It is interesting to note that the effects of particulate phase on both mean and turbulent properties of the gas phase are larger in this case than those shown in Fig. 20 for the comparable particle-laden jet. This is due to the following: smaller particle size, larger particle residence time from the injector exit to the measuring station (roughly four times larger--half the initial particle velocity and twice the axial

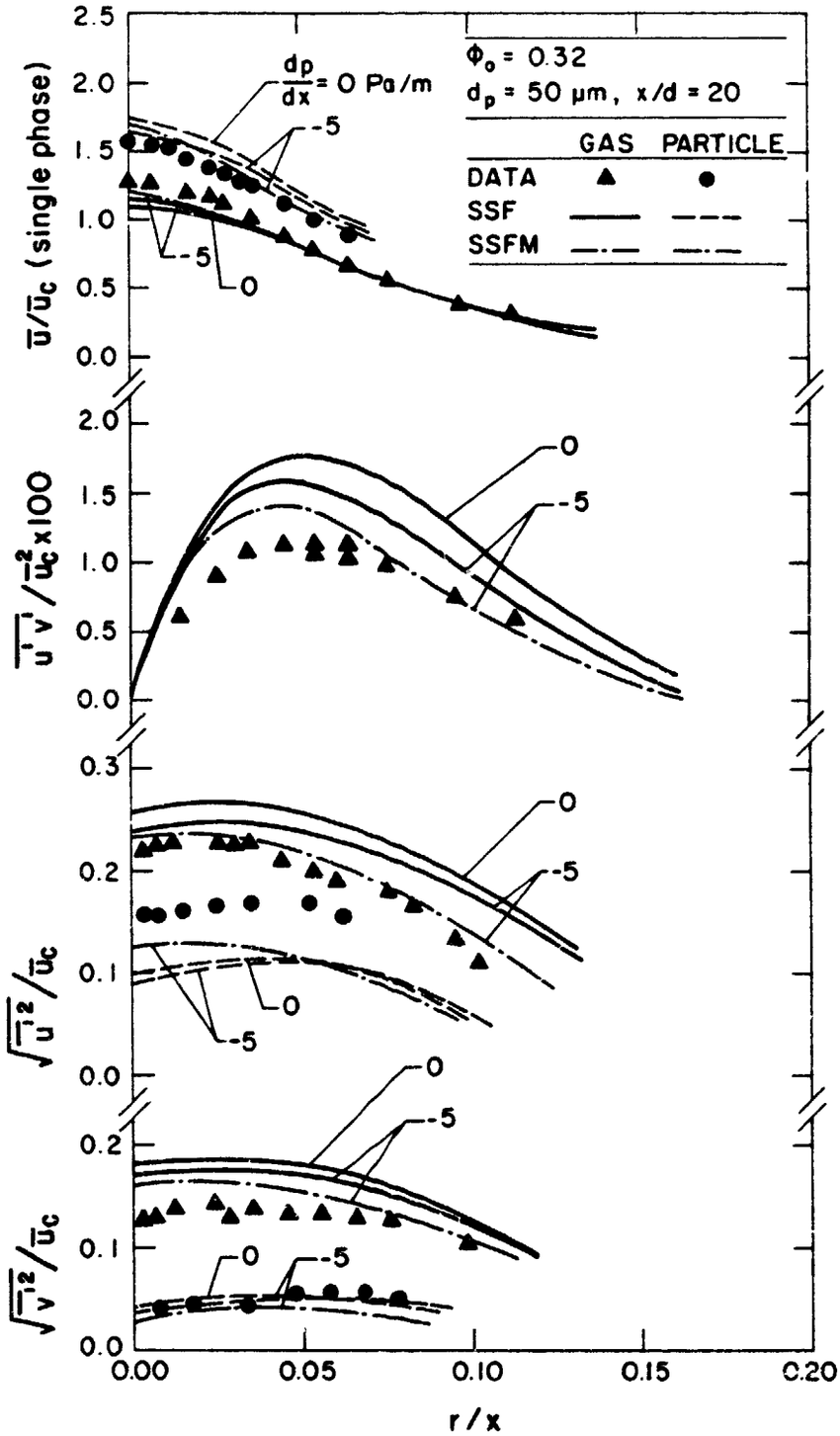

Fig. 34. Predicted and measured radial variation of flow properties at x/d = 20 for particle-laden jet with d_p = 50 μm and ϕ_o (loading ratio) = 0.32. Data of Elghobashi et al. [6,7].

distance), and the potential effects of the axial pressure gradient and recirculation zone, for this test condition.

Predicted and measured radial profiles of flow properties for both phases at x/d = 20 are compared in Fig. 35 for the particle-laden jet with 50 μm particles and 0.85 loading ratio. The agreement between model predictions and measurements is similar to the results with the lower loading ratio, illustrated in Fig. 34. However, as particle loading increases, the rate of decay of the gas-phase centerline velocity is reduced. This trend is reproduced by the SSFM model.

Results for larger particles, 200 μm in diameter, and loading ratio of 0.64 are illustrated in Fig. 36. Agreement between measurements and predictions from the SSFM and SSF models, with -5.0 N/m^3 pressure gradient, is satisfactory for all the flow properties, except for the mean particle velocity profile, where both models underestimate the particle velocity far from the jet axis. In this flow, effects of turbulence modulation are not important, since the large-size particles are less effective for interphase transport.

Agreement between predictions and measurements is generally better for the 200 μm particle jet than for the 50 μm particle jets. The main difference between these flows is that, besides the difference in particle size, the coflow velocity is 0.1 m/s for 200 μm particle jet and 0.05 m/s for 50 μm particle jets. This is interesting, since the recirculation zone, from the preceding discussion, extends to upstream of measuring station (x/d = 20) for the case with coflow velocity of 0.05 m/s. The front boundary of recirculation zone only reaches to slightly downstream of the measuring station for the case with 0.1 m/s coflow velocity. Therefore, the less satisfactory agreement for the cases with 50 μm particles may be due to effects of the recirculation flow penetrating upstream of the measuring station, since this phenomenon is not considered in the present model.

6. SUMMARY AND CONCLUSIONS

6.1 Summary

The overall objective of the present study was to develop and evaluate models of dilute turbulent particle-laden jets. Three models of these flows were developed: (1) a locally homogeneous flow (LHF) model, where interphase transport rates are assumed to be infinitely fast; (2) a deterministic separated flow (DSF) model, which allows for finite interphase transport rates (evaluated using mean properties of the continuous phase), but ignores dispersion of the particle phase by turbulent fluctuations; and (3) a stochastic separated flow (SSF) model, where finite interphase transport rates, and the turbulent dispersion of particles are considered by allowing particles to interact with a succession of eddies using a

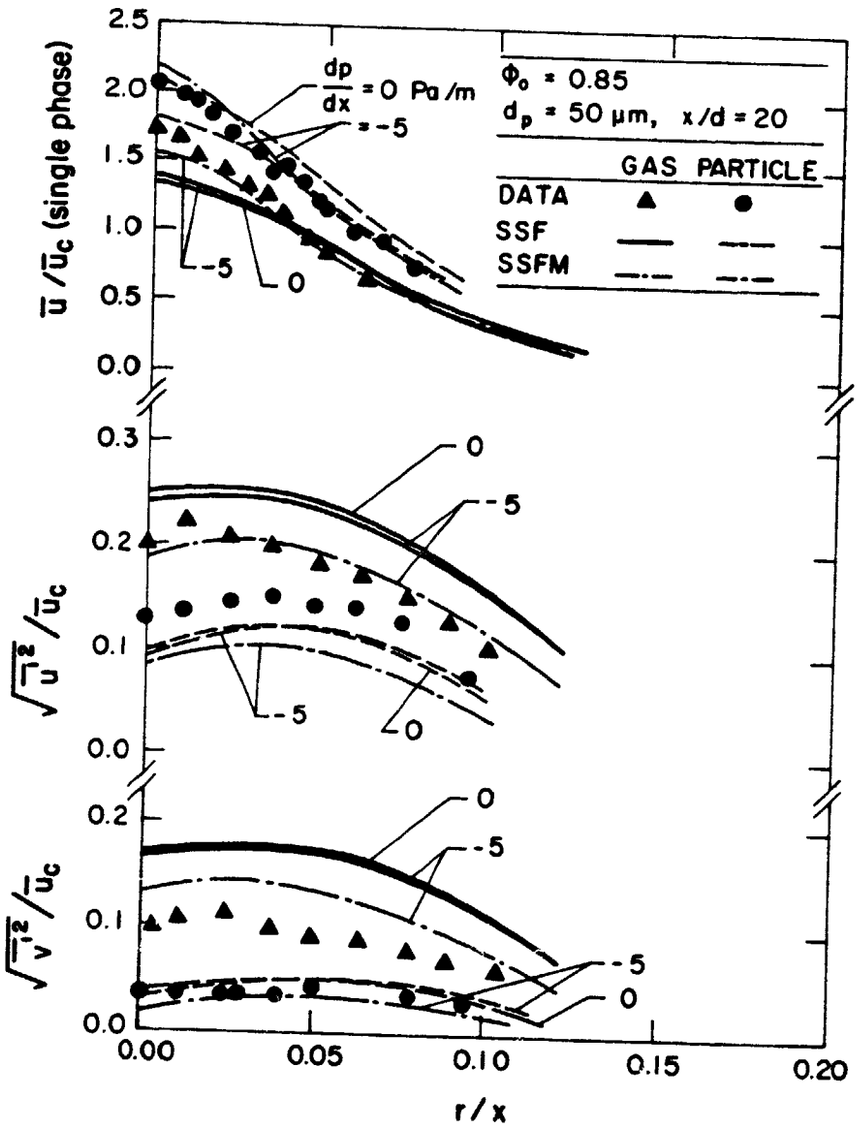

Fig. 35. Predicted and measured radial variation of flow properties at x/d = 20 for particle-laden jet with d_p = 50 μm and ϕ_o (loading ratio) = 0.85. Data of Elghobashi et al [6,7].

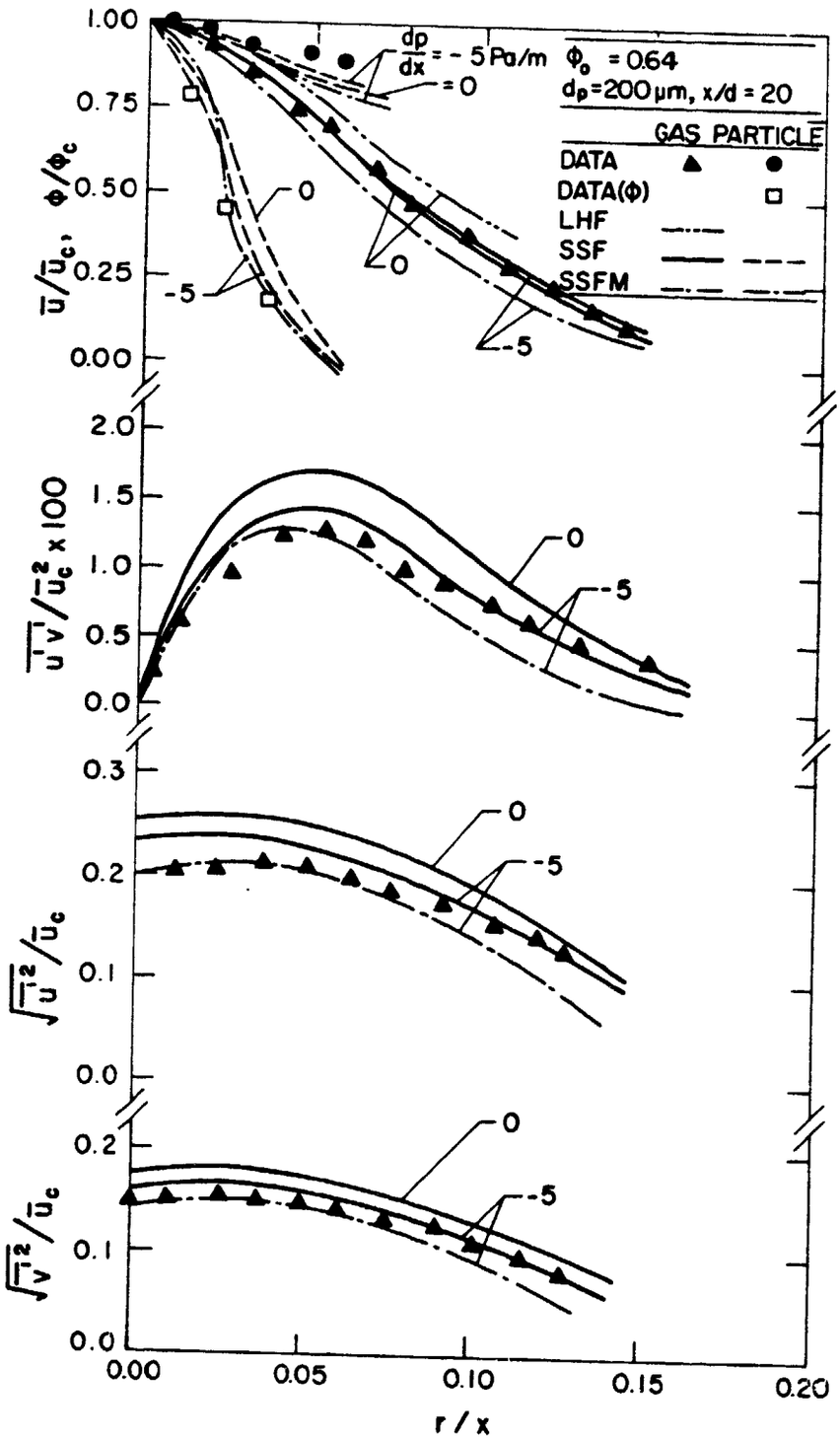

Fig. 36. Predicted and measured radial variation of flow properties at x/d = 20 for particle-laden jet with d_p = 200 μm and ϕ_o (loading ratio) = 0.64. Data of Elghobashi et al. [6,7].

random-walk procedure. Typical models of each type were described and evaluated using measurements in dilute particle-laden duct flows and round jets. All versions of these models used a well-calibrated k-ε model to estimate mean and fluctuating properties of the continuous phase.

The theoretical description of the continuous phase for all three models was based upon the Reynolds-averaged form of the conservation equations written in Eulerian coordinates. The dispersed phase is treated, for the separated flow models, by solving Lagrangian equations of motion for the particles. A modified version of the GENMIX program [42] combined with a second-order Runge-Kutta ordinary differential equation solver for particle motion were used to solve the governing equations.

Experiments were conducted for a single-phase air jet and four particle-laden jets, to supplement existing measurements in the literature. Particle Sauter mean diameters of 79, 119 and 207 μm, and loading ratios of 0.2 and 0.66 were considered. Measurements included mean and fluctuating velocities of both phases, particle mass fluxes, particle-size distributions, and calibration of particle-drag properties. A single-channel, dual-beam LDA was used to obtain velocity and drag measurements. Particles were examined with a microscope to find size distributions. The particle-laden flows were isokinetically sampled to obtain profiles of particle-mass flux. These measurements were compared with predictions of all three models discussed in this study.

A modified k-ε model, incorporating direct contributions of interphase transport on turbulence properties (turbulence modulation), was developed within the framework of the SSF model. The potential effects of turbulence modulation on the present measurements were examined using this model.

A sensitivity study was conducted to investigate the influence of uncertainties in specification of initial conditions and particle properties of model predictions. The results are useful in identifying potential sources of error for both predictions and measurements.

The measurements completed by Elghobashi, et al. present difficulties in obtaining a definitive evaluation of models. The shroud used around the experiment was the source of most of the difficulties. In the first place, the shroud causes an axial pressure gradient of unknown magnitude. Secondly, the coflow of air was insufficient to prevent recirculation of the flow beyond 20 jet diameters from the jet exit. Based on comparison between predictions and measurements for their single-phase experiments we find that the axial pressure gradient should be on the order of 2-5 N/m^3. The two-phase flow calculations were completed considering pressure gradients in the range of 0 to -5 N/m^3, but ignoring the effect of the recirculation pattern. Calculations were also conducted both including and ignoring the effects of

turbulence modulation. In view of the uncertainty in experimental conditions, the agreement between predictions and measurements is reasonably good.

6.2 Conclusions

The major conclusions and observations of this study are as follows:

1. The LHF and DSF models did not provide very satisfactory predictions for the data base considered in this evaluation. The LHF model was only satisfactory for flows containing tracer-like particles, where characteristic response times of the particles are small in comparison to all characteristic response times of the continuous phase. The DSF model generally underestimated the rate of flow development and particle dispersion over the entire data base. Both of these methods appear to have limited utility for modeling practical particle-laden flows.

2. The SSF model yielded reasonably good results over the entire data base (both existing and present measurements)--with no modification in the prescription for eddy properties from its original calibration. This result is encouraging, since the SSF method has the potential to treat nonlinear and complex interactions between the phases which are encountered in practical particle-laden flows, e.g., evaporating and combusting sprays, condensing and reacting vapor jets in liquid, pulverized coal combustion, etc. Additional development and evaluation of the SSF method will be required to determine if this potential can be realized.

3. Effects of turbulence modulation were small for the flows investigated in the present experiments, since these particle-laden flows were all lightly-loaded with particles having relatively large sizes and short residence times--which tends to inhibit interphase transport. However, results presented in Table 5 indicate the effects of turbulence modulation can be significant for applications involving higher loading ratios and smaller particle sizes than the present test fows.

4. In general, present model predictions are relatively insensitive to the specification of gas-phase initial conditions. The specification of particle properties, however, exerts much more pronounced effects on predictions. This emphasizes the importance of measurements of initial particle-phase conditions and particle properties, i.e., drag and size, in order to obtain a convincing evaluation of separated flow models.

5. Although the locally homogeneous flow model yields relatively poor predictions for particle-phase flow properties, it can still be a useful design tool. Initial conditions are easily specified for locally homogeneous flow models; therefore, these models can be applied to a wide range of flows to provide a rough initial estimate of flow characteristics.

APPENDIX A

DERIVATION OF k-EQUATION AND ε-EQUATION WITH PRESENCE OF DISPERSED PHASE

A.1 Derivation of k-Equation

Since free jets issuing into stagnant air are considered in this study, the pressure gradient is neglected throughout the following derivation. The governing equations are limited to steady, axisymmetric, constant property flows.

The gas-phase momentum equation, including the particle source term, is

$$\frac{\partial}{\partial x_j}(u_i u_j) = \nu \frac{\partial^2 u_i}{\partial x_j \partial x_j} + F_{pu_i} \qquad (A.1)$$

where $F_{pu_i} = S_{pu_i}/\rho$, and the repeated indices imply summation. Multiplying Eq. (A.1) by u_i and rearranging terms yields

$$\frac{\partial}{\partial x_j}\left[u_j\left(\frac{1}{2} u_i u_i\right)\right] = \nu \frac{\partial}{\partial x_j}\left(u_i \frac{\partial u_i}{\partial x_j}\right) - \nu \frac{\partial u_i}{\partial x_j}\frac{\partial u_i}{\partial x_j} + u_i F_{pu_i} \qquad (A.2)$$

The instantaneous quantities can be decomposed to mean and fluctuating components according to the following expressions

$$u_i = \bar{u}_i + u_i'$$

$$u_i u_i = \bar{u}_i \bar{u}_i + 2\bar{u}_i u_i' + q^2$$

$$\overline{\left(\frac{q^2}{2}\right)} \equiv k \qquad (A.3)$$

After decomposing and Reynolds-averaging, Eq. (A.2) may be written as

$$\frac{\partial}{\partial x_j}\left[\bar{u}_j\left(\frac{1}{2}\bar{u}_i\bar{u}_i\right)\right]$$

$$= -\frac{\partial}{\partial x_j}\overline{u_j'\left(\frac{1}{2}q^2\right)} - \frac{\partial}{\partial x_j}\bar{u}_j\overline{\left(\frac{1}{2}q^2\right)} - \frac{\partial}{\partial x_j}\left(\bar{u}_i\,\overline{u_i'\,u_j'}\right)$$

$$+\nu\frac{\partial}{\partial x_j}\left(\bar{u}_i\frac{\partial\bar{u}_i}{\partial x_j}\right) - \nu\frac{\partial\bar{u}_i}{\partial x_j}\frac{\partial\bar{u}_i}{\partial x_j} - \nu\frac{\partial}{\partial x_j}\overline{\frac{1}{2}\frac{\partial q^2}{\partial x_j}} - \nu\overline{\frac{\partial u_i'}{\partial x_j}\frac{\partial u_i'}{\partial x_j}}$$

$$+\overline{u_i\,F_{pu_i}} \qquad \text{(A.4)}$$

The Reynolds-averaged form of Eq. (A.1) is

$$\frac{\partial}{\partial x_j}\left(\bar{u}_i\bar{u}_j\right) = \frac{\partial}{\partial x_j}\left(\nu\frac{\partial\bar{u}_i}{\partial x_j} - \overline{u_i'\,u_j'}\right) + \bar{F}_{pu_i} \qquad \text{(A.5)}$$

Multiplying Eq. (A.5) by $\bar{u}_i$ and rearranging terms yields

$$\frac{\partial}{\partial x_j}\left[\bar{u}_j\left(\frac{1}{2}\bar{u}_i\bar{u}_i\right)\right] = \nu\frac{\partial}{\partial x_j}\left(\bar{u}_i\frac{\partial\bar{u}_i}{\partial x_j}\right) - \nu\frac{\partial\bar{u}_i}{\partial x_j}\frac{\partial\bar{u}_i}{\partial x_j}$$

$$+\overline{u_i'\,u_j'}\frac{\partial\bar{u}_i}{\partial x_j} - \frac{\partial}{\partial x_j}\left(\bar{u}_i\,\overline{u_i'\,u_j'}\right) + \bar{u}_i\,\bar{F}_{pu_i} \qquad \text{(A.6)}$$

Subtracting Eq. (A.6) from Eq. (A.4) the equation for turbulent kinetic energy is obtained

$$\frac{\partial}{\partial x_j}(\bar{u}_j\, k) = -\frac{\partial}{\partial x_j}\overline{u_j'\,(q^2/2)} - \overline{u_i'\,u_j'}\frac{\partial \bar{u}_i}{\partial x_j} + \nu\frac{\partial^2 k}{\partial x_j \partial x_j}$$

$$-\nu\,\overline{\left(\frac{\partial u_i'}{\partial x_j}\right)\left(\frac{\partial u_i'}{\partial x_j}\right)} + \overline{u_i\,F_{pu_i}} - \bar{u}_i\,\bar{F}_{pu_i} \qquad (A.7)$$

The viscous diffusion term in Eq. (A.7) is much smaller than the other terms and can be neglected. The fourth term in the RHS of the equation is the viscous dissipation of turbulent kinetic energy, ε.

After employing the modeling approach of Gosman et al. [18], the modeled thin shear layer form of Eq. (A.7) can be written as follows

$$\frac{\partial}{\partial x}(\bar{u}\,k) + \frac{1}{r}\frac{\partial}{\partial r}(r\,\bar{v}\,k) = \frac{1}{r}\frac{\partial}{\partial r}\left(r\,\frac{\nu_t}{\sigma_k}\frac{\partial k}{\partial r}\right) + \nu_t\left(\frac{\partial \bar{u}}{\partial r}\right)^2 - \varepsilon$$

$$+\overline{u\,F}_{pu} - \bar{u}\,\bar{F}_{pu} \qquad (A.8)$$

where the $(\overline{v\,F}_{pv} - \bar{v}\,\bar{F}_{pv})$ and $(\overline{w\,F}_{pw})$ terms have been neglected, since they are small compared to $(\overline{u\,F}_{pu} - \bar{u}\,\bar{F}_{pu})$.

Equation (A.8) is derived for constant density flows for simplicity and to highlight the derivation of the new terms due to interphase transport. However, the derivative of turbulent kinetic energy equation for variable density flows involves no fundamental difficulties.

Following past work [18,39], the following equation is obtained for variable density flow, after completion of the order of magnitude estimation

$$\frac{\partial}{\partial x}(\bar{\rho}\,\bar{u}\,k) + \frac{1}{r}\frac{\partial}{\partial r}(r\,\bar{\rho}\,\bar{v}^{o}\,k) = \frac{1}{r}\frac{\partial}{\partial r}\left(r\,\frac{\mu_t}{\sigma_k}\frac{\partial k}{\partial r}\right)$$

$$+ \mu_t\left(\frac{\partial \bar{u}}{\partial r}\right)^2 - \bar{\rho}\,\varepsilon + \overline{u\,S_{pu}} - \bar{u}\,\bar{S}_{pu} \qquad (A.9)$$

where $\bar{\rho}\,\bar{v}^{o} = \bar{\rho}\,\bar{v} + \overline{\rho' v'}$ and $S_{pu} = \rho\,F_{pu}$. In arriving at this equation, a number of density fluctuation terms are ignored and other terms are modeled according to the methods employed for uniform property flows. In fact, the only major difference between Eq. (A.9) and the constant density form, Eq. (A.8), involves retention of the $\overline{\rho' v'}$ correlation term on the LHS of the equation. The justification for this largely rests on the success of the method during earlier study of variable density flows [8,9,17,18,39].

A.2 Derivation of ε-Equation

The ε-equation, considering effects of interphase transport, was derived in the same manner as the k-equation. However, since the algebra is quite involved, only the procedure is outlined here. The first step in the derivation is to obtain a transport equation for the fluctuating velocity, u_i', by subtracting Eq. (A.5) from Eq. (A.1). The ε-equation is obtained by differentiating the u_i' equation with respect to x_k, multiplying throughout by $\nu\,\frac{\partial u_i'}{\partial x_k}$ and finally time averaging. The order of magnitude analysis is then conducted and

higher order terms are neglected, following the procedure by Tennekes and Lumley [36]. The resulting equation becomes

$$\frac{\partial}{\partial x_j}(\bar{u}_j\,\varepsilon) = -2\nu\frac{\partial \bar{u}_i}{\partial x_j}\left(\overline{\frac{\partial u_i'}{\partial x_k}\frac{\partial u_j'}{\partial x_k}} + \overline{\frac{\partial u_k'}{\partial x_j}\frac{\partial u_k'}{\partial x_i}}\right) - 2\nu\,\overline{\frac{\partial u_i'}{\partial x_k}\frac{\partial u_j'}{\partial x_k}\frac{\partial u_i'}{\partial x_j}}$$

$$-\frac{\partial}{\partial x_j}\overline{u_j'\,\varepsilon'} - 2\nu'\,\overline{\frac{\partial^2 u_i'}{\partial x_j\,\partial x_k}\frac{\partial^2 u_i'}{\partial x_j\,\partial x_k}} + 2\nu\,\overline{\frac{\partial u_i'}{\partial x_k}\frac{\partial F_i'}{\partial x_k}} \qquad (A.10)$$

Equation (A.10) is then transformed to thin shear layer form in Cartesian coordinates and modeled according to Gosman, Lockwood and Syed [18]. The modeled ε-equation can be written as

$$\frac{\partial}{\partial x}(\bar{u}\,\varepsilon) + \frac{1}{r}\frac{\partial}{\partial r}(r\,\bar{v}\,\varepsilon) = \frac{1}{r}\frac{\partial}{\partial r}\left(r\,\frac{\nu_t}{\sigma_\varepsilon}\frac{\partial \varepsilon}{\partial r}\right) + C_{\varepsilon_1}\nu_t\frac{\varepsilon}{k}\left(\frac{\partial \bar{u}}{\partial r}\right)^2$$

$$-C_{\varepsilon_2}\frac{\varepsilon^2}{k} + 2\nu\left(\overline{\frac{\partial u'}{\partial r}\frac{\partial F'_{pu}}{\partial r}} + \overline{\frac{\partial v'}{\partial r}\frac{\partial F'_{pv}}{\partial r}} + \overline{\frac{\partial w'}{\partial r}\frac{\partial F'_{pw}}{\partial r}}\right) \qquad (A.11)$$

The last term in the RHS of the above equation is the contribution from interphase transport and needs to be modeled. Employing the same method for single-phase flow [12], this term is modeled as follows

$$2\nu\left(\overline{\frac{\partial u'}{\partial r}\frac{\partial F'_{pu}}{\partial r}} + \overline{\frac{\partial v'}{\partial r}\frac{\partial F'_{pv}}{\partial r}} + \overline{\frac{\partial w'}{\partial r}\frac{\partial F'_{pw}}{\partial r}}\right) = -2\nu\,C_{\varepsilon_3}\frac{\varepsilon}{k}\frac{\partial \bar{F}_{pu}}{\partial r} \qquad (A.12)$$

where C_{ε_3} is the new model constant to be determined.

The variable density version of modeled ε-equation is obtained, following the same argument as for k-equation, as follows

$$\frac{\partial}{\partial x}(\bar{\rho}\,\bar{u}\,\varepsilon) + \frac{1}{r}\frac{\partial}{\partial r}(r\,\bar{\rho}\,\overline{v^{o}}\,\varepsilon) = \frac{1}{r}\frac{\partial}{\partial r}\left(r\,\frac{\mu_t}{\sigma_\varepsilon}\frac{\partial \varepsilon}{\partial r}\right)$$

$$+ C_{\varepsilon_1}\,\mu_t\,\frac{\varepsilon}{k}\left(\frac{\partial \bar{u}}{\partial r}\right)^2 - C_{\varepsilon_2}\,\bar{\rho}\,\frac{\varepsilon^2}{k} - 2\,C_{\varepsilon_3}\,\mu\,\frac{\varepsilon}{k}\,\frac{\partial \bar{S}_{pu}}{\partial r} \qquad (A.13)$$

APPENDIX B

EXPERIMENTAL DATA

B.1 Axial Variation of Flow Properties

Single-Phase Jet

x/d	$\bar{u}_c/\bar{u}_o$	$\left(\overline{u'^2}\right)^{\frac{1}{2}}/\bar{u}_c$	$\left(\overline{v'^2}\right)^{\frac{1}{2}}/\bar{u}_c$
1	1.0	.045	.039
2	.968	.056	.039
5	.890	.106	.081
10	.631	.189	.142
15	.418	.237	.188
20	.309	.248	.193
30	.193	.271	.225
40	.144	.268	.214
50	.117	.262	.221

Particle-Laden Jet SMD = 79 μm LR = 0.2

x/d	$\bar{u}_c/\bar{u}_o$	$\left(\overline{u'^2}\right)^{\frac{1}{2}}/\bar{u}_c$	$\left(\overline{v'^2}\right)^{\frac{1}{2}}/\bar{u}_c$	$\bar{u}_{p_c}/\bar{u}_{p_c}$	$\left(\overline{u_p'^2}\right)^{\frac{1}{2}}/\bar{u}_{p_c}$	$\left(\overline{v_p'^2}\right)^{\frac{1}{2}}/\bar{u}_{p_c}$	$\bar{G}_c/\bar{G}_o$
1	1.0	.082	.034	1.0	.086	.025	1.0
2	.998	.085	.038	1.003	.088	.024	.975
5	.942	.095	.069	1.005	.093	.033	.893
10	.648	.194	.145	.872	.152	.066	.858
15	--	--	--	.756	.192	.060	.744
20	.364	.286	.171	.658	.223	.036	.601
30	.235	.292	.188	.493	.240	.062	.374
40	.167	.312	.183	.324	.259	.056	.214
50	.120	.286	.217	.218	.275	.065	.145

Particle-Laden Jet SMD = 119 μm LR = 0.2

x/d	$\bar{u}_c/\bar{u}_o$	$\left(\overline{u'^2}\right)^{\frac{1}{2}}/\bar{u}_c$	$\left(\overline{v'^2}\right)^{\frac{1}{2}}/\bar{u}_c$	$\bar{u}_{p_c}/\bar{u}_{p_c}$	$\left(\overline{u_p'^2}\right)^{\frac{1}{2}}/\bar{u}_{p_c}$	$\left(\overline{v_p'^2}\right)/\bar{u}_{p_c}$	$\bar{G}_c/\bar{G}_o$
1	1.0	.063	.039	1.0	.059	.030	1.0
2	.974	.088	.044	1.009	.072	.027	.975
5	.896	.121	.082	1.013	.074	.026	.930
10	.660	.183	.138	.980	.074	.026	.677
15	.444	.254	.181	.932	.091	.024	.485
20	.336	.271	.181	.839	.123	.028	.369
30	.227	.269	.191	.669	.144	.024	.258
40	.176	.309	.190	.536	.167	.033	.195
50	.143	.237	.188	.445	.176	.026	.143

Particle-Laden Jet SMD = 119 μm LR = 0.66

x/d	$\bar{u}_c/\bar{u}_o$	$\left(\overline{u'^2}\right)^{\frac{1}{2}}/\bar{u}_c$	$\left(\overline{v'^2}\right)^{\frac{1}{2}}/\bar{u}_c$	$\bar{u}_{p_c}/\bar{u}_{p_o}$	$\left(\overline{u_p'^2}\right)^{\frac{1}{2}}/\bar{u}_{p_c}$	$\left(\overline{v_p'^2}\right)^{\frac{1}{2}}/\bar{u}_{p_c}$	$\bar{G}_c/\bar{G}_o$
1	1.0	.100	.048	1.0	.069	.030	1.0
2	.958	.131	.050	1.006	.075	.028	.984
5	.915	.140	.075	1.015	.080	.026	.938
10	.743	.162	.124	.996	.079	.023	.757
15	.600	.278	.194	.938	.085	.021	.603
20	.434	.279	.148	.855	.106	.021	.434
30	.289	.299	.162	.709	.128	.022	.269
40	.228	.338	.144	.579	.144	.025	.183
50	.177	.307	.179	.495	.156	.025	.135

Particle-Laden Jet SMD = 207 μm LR = 0.66

x/d	$\bar{u}_c/\bar{u}_o$	$\left(\overline{u'^2}\right)^{\frac{1}{2}}/\bar{u}_c$	$\left(\overline{v'^2}\right)^{\frac{1}{2}}/\bar{u}_c$	$\bar{u}_{p_c}/\bar{u}_{p_o}$	$\bar{G}_c/\bar{G}_o$
1	1.0	.113	.032	1.0	1.0
2	.999	.126	.037	1.001	.968
5	.972	.122	.063	1.005	.915
10	.680	.185	.136	.920	.654
15	.491	.237	.151	.869	.515
20	.373	.279	.177	.817	.341
30	.253	.284	.182	.783	.214
40	.193	.291	.187	.716	.149
50	.156	.312	.192	.640	.108

B.2 Radial Variation of Flow Properties

Single-Phase Jet

x/d = 1

r/x	$\bar{u}/\bar{u}_c$	$\left(\overline{u'^2}\right)^{\frac{1}{2}}/\bar{u}_c$	$\left(\overline{v'^2}\right)^{\frac{1}{2}}/\bar{u}_c$	$\overline{u'v'}/\bar{u}_c^{\,2}$
0.0	1.0	.045	.039	.0001
.046	.992	.045	.038	.00005
.138	.966	.051	.035	.00031
.229	.928	.056	.039	.00060
.333	.868	.069	.048	.00134
.413	.792	.088	.062	.00194
.459	.709	.115	.078	.00507
.505	.595	.137	.096	.00664
.551	.448	.147	.116	.00945
.596	.291	.132	.111	.00824
.642	.210	.110	.095	.00577
.688	.121	.077	.077	.00355
.734	.054	.059	.069	.00136

Single Phase Jet

x/d = 20

r/x	$\bar{u}/\bar{u}_c$	$\left(\overline{u'^2}\right)^{\frac{1}{2}}/\bar{u}_c$	$\left(\overline{v'^2}\right)^{\frac{1}{2}}/\bar{u}_c$	$\overline{u'v'}/\bar{u}_c^{\,2}$
0.0	1.0	.248	.193	.0003
.023	.924	.258	.200	.0105
.046	.781	.251	.204	.0189
.067	.590	.240	.188	.0188
.092	.408	.199	.166	.0140
.115	.274	.168	.138	.0107
.138	.190	.126	.101	.0056
.161	.142	.098	.081	.0027
.174	.089	.063	.057	.0010

Single Phase Jet

x/d = 40

r/x	$\bar{u}/\bar{u}_c$	$\left(\overline{u'^2}\right)^{\frac{1}{2}}/\bar{u}_c$	$\left(\overline{v'^2}\right)^{\frac{1}{2}}/\bar{u}_c$	$\overline{u'v'}/\bar{u}_c^2$
0.0	1.0	.268	.214	.0002
.020	.951	.261	.211	.0097
.038	.847	.263	.224	.0163
.059	.663	.252	.225	.0193
.080	.500	.230	.200	.0197
.100	.337	.211	.170	.0142
.121	.259	.181	.147	.0110
.142	.191	.136	.118	.0051
.166	.116	.084	.007	.0021
.185	.083	.063	.051	.0010

Particle-Laden Jet SMD = 79 μm LR = 0.2

Gas-Phase Properties

x/d = 1

r/x	$\bar{u}/\bar{u}_c$	$\left(\overline{u'^2}\right)^{\frac{1}{2}}/\bar{u}_c$	$\left(\overline{v'^2}\right)^{\frac{1}{2}}/\bar{u}_c$	$\overline{u'v'}/\bar{u}_c^2$
0.0	1.0	.085	.032	.00007
.073	.991	.085	.034	.00037
.165	.979	.086	.037	.00080
.257	.948	.083	.045	.00114
.349	.878	.088	.050	.00178
.440	.815	.135	.072	.00428
.514	.570	.159	.116	.01109
.578	.395	.151	.134	.01020
.624	.213	.128	.117	.00833
.670	.146	.076	.082	.00477
.716	.035	.049	.054	.00138

Gas-Phase Properties

x/d = 20

r/x	$\bar{u}/\bar{u}_c$	$\left(\overline{u'^2}\right)^{\frac{1}{2}}/\bar{u}_c$	$\left(\overline{v'^2}\right)^{\frac{1}{2}}/\bar{u}_c$	$\overline{u'v'}/\bar{u}_c^2$
0.0	1.0	.286	.171	.0004
.016	.970	.289	.173	.0081
.034	.860	.271	.181	.0132
.053	.751	.255	.188	.0168
.071	.595	.238	.191	.0192
.089	.469	.215	.181	.0181
.108	.350	.185	.155	.0128
.126	.244	.161	.132	.0097
.145	.136	.137	.102	.0061
.167	.071	.081	.081	.0024

Particle-Laden Jet SMD = 79 μm LR = 0.2

Gas-Phase Properties

x/d = 40

r/x	$\bar{u}/\bar{u}_c$	$\left(\overline{u'^2}\right)^{\frac{1}{2}}/\bar{u}_c$	$\left(\overline{v'^2}\right)^{\frac{1}{2}}/\bar{u}_c$	$\overline{u'v'}/\bar{u}_c^{\,2}$
0.0	1.0	.312	.183	.0002
.014	.946	.313	.183	.0083
.032	.818	.275	.190	.0119
.051	.681	.235	.185	.0159
.069	.531	.216	.178	.0166
.087	.415	.197	.152	.0137
.106	.257	.180	.140	.0078
.124	.170	.144	.114	.0062
.142	.103	.112	.100	.0040
.161	.051	.083	.080	.0024
.179	.022	.059	.061	.0010

Solid-Phase Properties

x/d = 1

r/x	$\bar{u}_p/\bar{u}_{p_c}$	$\left(\overline{u_p'^2}\right)^{\frac{1}{2}}/\bar{u}_{p_c}$	$\left(\overline{v_p'^2}\right)^{\frac{1}{2}}/\bar{u}_{p_c}$	r/x	$\bar{G}/\bar{G}_c$
0.0	1.0	.083	.027	0.0	1.0
.184	.985	.088	.031	.073	.981
.321	.927	.088	.037	.165	.930
.413	.882	.095	.049	.257	.862
.477	.818	.116	.059	.349	.815
.523	.621	.151	.092	.440	.725
.569	.437	.124	.105	.514	.485
.615	.305	.107	.096	.578	.170
.661	.185	.095	.090	.624	.101
.706	.129	.079	.083	.670	.002

Particle-Laden Jet SMD = 79 μm LR = 0.2

Solid-Phase Properties

x/d = 20

r/x	$\bar{u}_p/\bar{u}_{p_c}$	$\left(\overline{u_p'^2}\right)^{\frac{1}{2}}/\bar{u}_{p_c}$	$\left(\overline{v_p'^2}\right)^{\frac{1}{2}}/\bar{u}_{p_c}$	r/x	$\bar{G}/\bar{G}_c$
0.0	1.0	.223	.036	0.0	1.0
.011	.911	.240	.040	.014	.934
.023	.747	.224	.062	.021	.781
.034	.591	.191	.076	.030	.505
.046	.508	.169	.084	.039	.271
.057	.429	.155	.095	.048	.119
.069	.362	.136	.095	.057	.048
.080	.304	.125	.093	.067	.027
.092	.260	.113	.087	--	--
.115	.187	.094	.076	--	--

Solid-Phase Properties

x/d = 40

r/x	$\bar{u}_p/\bar{u}_{p_c}$	$\left(\overline{u_p'^2}\right)^{\frac{1}{2}}/\bar{u}_{p_c}$	$\left(\overline{v_p'^2}\right)^{\frac{1}{2}}/\bar{u}_{p_c}$	r/x	$\bar{G}/\bar{G}_c$
0.	1.0	.259	.056	0.0	1.0
.011	.896	.267	.080	.014	.865
.023	.724	.255	.091	.021	.665
.032	.597	.215	.103	.030	.347
.041	.515	.168	.113	.039	.133
.051	.472	.150	.108	.048	.039
.060	.419	.141	.110	.057	.018
.069	.365	.126	.107	.062	.009
.078	.327	.122	.102	--	--
.087	.296	.114	.100	--	--
.096	.260	.109	.094	--	--
.106	.215	.104	.090	--	--

Particle-Laden Jet SMD = 119 μm LR = 0.2

Gas-Phase Properties

x/d = 1

r/x	$\bar{u}/\bar{u}_c$	$\left(\overline{u'^2}\right)^{\frac{1}{2}}/\bar{u}_c$	$\left(\overline{v'^2}\right)^{\frac{1}{2}}/\bar{u}_c$	$\overline{u'v'}/\bar{u}_c^{\,2}$
0.0	1.0	.063	.039	.00013
.046	.986	.065	.038	.00053
.138	.976	.066	.036	.00052
.229	.931	.067	.040	.00057
.333	.888	.072	.046	.00136
.413	.804	.096	.058	.00226
.459	.718	.120	.079	.00486
.505	.621	.147	.098	.00789
.551	.473	.154	.114	.01040
.596	.295	.136	.113	.00887
.642	.215	.114	.096	.00602
.688	.115	.077	.075	.00384
.734	.059	.058	.073	.00126

Gas-Phase Properties

x/d = 20

r/x	$\bar{u}/\bar{u}_c$	$\left(\overline{u'^2}\right)^{\frac{1}{2}}/\bar{u}_c$	$\left(\overline{v'^2}\right)^{\frac{1}{2}}/\bar{u}_c$	$\overline{u'v'}/\bar{u}_c^{\,2}$
0.0	1.0	.271	.181	.0003
.023	.927	.270	.182	.0116
.046	.738	.269	.190	.0159
.067	.555	.230	.177	.0164
.092	.392	.197	.156	.0135
.115	.252	.156	.128	.0098
.138	.171	.120	.095	.0046
.161	.119	.084	.070	.0028
.174	.078	.057	.055	.0008

Particle-Laden Jet SMD = 119 μm LR = 0.2

Gas-Phase Properties

x/d = 40

r/x	$\bar{u}/\bar{u}_c$	$\left(\overline{u'^2}\right)^{\frac{1}{2}}/\bar{u}_c$	$\left(\overline{v'^2}\right)^{\frac{1}{2}}/\bar{u}_c$	$\overline{u'v'}/\bar{u}_c^{\,2}$
0.0	1.0	.309	.190	.0002
.020	.968	.290	.191	.0111
.038	.813	.268	.196	.0168
.059	.641	.242	.207	.0179
.080	.440	.214	.185	.0165
.100	.313	.188	.153	.0113
.121	.215	.159	.139	.0089
.142	.180	.123	.104	.0050
.166	.092	.073	.062	.0035
.185	.068	.052	.038	.0006

Solid-Phase Properties

x/d = 1

r/x	$\bar{u}_p/\bar{u}_{p_c}$	$\left(\overline{u_p'^2}\right)^{\frac{1}{2}}/\bar{u}_{p_c}$	$\left(\overline{v_p'^2}\right)^{\frac{1}{2}}/\bar{u}_{p_c}$	r/x	$\bar{G}/\bar{G}_c$
0.1	1.0	.059	.030	0.0	1.0
.110	.994	.059	.028	.046	.976
.202	.980	.065	.029	.138	.960
.248	.972	.066	.031	.229	.969
.294	.963	.068	.034	.333	1.022
.339	.951	.073	.035	.413	1.039
.385	.934	.077	.037	.505	.877
.431	.920	.078	.034	.551	.680
.477	.910	.101	.033	.596	.321
.523	.872	.102	.033	.642	.148
.569	.638	.133	.068	.688	.020
.615	.458	.115	.107	--	--
.661	.317	.102	.098	--	--

Particle-Laden Jet SMD = 119 μm LR = 0.66

Gas-Phase Properties

x/d = 1

r/x	$\bar{u}/\bar{u}_c$	$\left(\overline{u'^2}\right)^{\frac{1}{2}}/\bar{u}_c$	$\left(\overline{v'^2}\right)^{\frac{1}{2}}/\bar{u}_c$	$\overline{u'v'}/\bar{u}_c^{\,2}$
0.0	1.0	.100	.048	.00012
.046	.981	.100	.038	.00030
.138	.952	.103	.035	.00088
.229	.932	.104	.039	.00099
.333	.906	.108	.044	.00098
.413	.816	.101	.063	.00180
.459	.764	.113	.077	.00372
.505	.673	.142	.109	.00600
.551	.516	.164	.119	.01156
.596	.323	.153	.123	.01060
.642	.225	.124	.107	.00880
.688	.128	.085	.084	.00420
.734	.060	.063	.080	.00189

Gas-Phase Properties

x/d = 20

r/x	$\bar{u}/\bar{u}_c$	$\left(\overline{u'^2}\right)^{\frac{1}{2}}/\bar{u}_c$	$\left(\overline{v'^2}\right)^{\frac{1}{2}}/\bar{u}_c$	$\overline{u'v'}/\bar{u}_c^{\,2}$
0.0	1.0	.279	.148	.0004
.023	.952	.289	.138	.0057
.046	.686	.275	.159	.0101
.067	.484	.204	.155	.0117
.092	.323	.175	.129	.0109
.115	.183	.131	.103	.0066
.138	.115	.096	.074	.0031
.161	.101	.075	.054	.0014
.174	.062	.046	.044	.0008

Particle-Laden Jet SMD = 119 μm LR = 0.2

Solid-Phase Properties

x/d = 20

r/x	$\bar{u}_p/\bar{u}_{p_c}$	$\left(\overline{u_p'^2}\right)^{\frac{1}{2}}/\bar{u}_{p_c}$	$\left(\overline{v_p'^2}\right)^{\frac{1}{2}}/\bar{u}_{p_c}$	r/x	$\bar{G}/\bar{G}_c$
0.0	1.0	.130	.030	0.0	1.0
.014	.975	.139	.031	.011	.932
.028	.898	.134	.033	.023	.850
.041	.823	.122	.039	.034	.673
.055	.747	.125	.044	.046	.428
.069	.642	.126	.064	.057	.209
.083	.536	.121	.074	.069	.068
.096	.487	.108	.073	.080	.020
.110	.468	.100	.072	—	--

Solid-Phase Properties

x/d = 40

r/x	$\bar{u}_p/\bar{u}_{p_c}$	$\left(\overline{u_p'^2}\right)^{\frac{1}{2}}/\bar{u}_{p_c}$	$\left(\overline{v_p'^2}\right)^{\frac{1}{2}}/\bar{u}_{p_c}$	r/x	$\bar{G}/\bar{G}_c$
0.0	1.0	.176	.033	0.0	1.0
.012	.975	.177	.035	.010	.808
.023	.937	.165	.036	.020	.536
.034	.883	.156	.046	.029	.302
.046	.851	.147	.057	.038	.147
.057	.795	.144	.642	.049	.053
.069	.747	.136	.070	.059	.025
.080	.722	.128	.070	--	--

Particle-Laden Jet SMD = 207 μm LR = 0.66

Gas-Phase Properties

x/d = 1

r/x	$\bar{u}/\bar{u}_c$	$\left(\overline{u'^2}\right)^{\frac{1}{2}}/\bar{u}_c$	$\left(\overline{v'^2}\right)^{\frac{1}{2}}/\bar{u}_c$	$\overline{u'v'}/\bar{u}_c^2$
0.0	1.0	.113	.032	.00017
.055	.993	.113	.033	.00054
.156	.986	.115	.038	.00158
.248	.948	.111	.043	.00182
.339	.880	.107	.054	.00229
.431	.786	.122	.081	.00345
.495	.557	.135	.110	.00726
.569	.325	.146	.133	.01064
.624	.177	.113	.110	.00664
.670	.105	.082	.084	.00300
.706	.055	.064	.061	.00150

Gas-Phase Properties

x/d = 20

r/x	$\bar{u}/\bar{u}_c$	$\left(\overline{u'^2}\right)^{\frac{1}{2}}/\bar{u}_c$	$\left(\overline{v'^2}\right)^{\frac{1}{2}}/\bar{u}_c$	$\overline{u'v'}/\bar{u}_c^2$
0.0	1.0	.269	.179	.0004
.010	.979	.268	.176	.0051
.023	.947	.266	.175	.0103
.046	.741	.253	.180	.0173
.069	.588	.228	.181	.0180
.092	.389	.197	.162	.0145
.115	.232	.147	.129	.0096
.138	.141	.116	.103	.0044
.161	.072	.078	.070	.0017

Particle-Laden Jet SMD = 119 μm LR = 0.66

Solid-Phase Properties

x/d = 20

r/x	$\bar{u}_p/\bar{u}_{p_c}$	$\left(\overline{u_p'^2}\right)^{\frac{1}{2}}/\bar{u}_{p_c}$	$\left(\overline{v_p'^2}\right)^{\frac{1}{2}}/\bar{u}_{p_c}$	r/x	$\bar{G}/\bar{G}_c$
0.0	1.0	.110	.021	0.0	1.0
.014	.987	.111	.022	.011	.965
.028	.933	.108	.025	.023	.810
.041	.862	.111	.033	.034	.542
.055	.784	.111	.044	.046	.291
.069	.694	.111	.063	.057	.094
.083	.584	.106	.066	.069	.033
.096	.535	.104	.063	.080	.012
.110	.523	.108	.061	—	—

Solid-Phase Properties

x/d = 40

r/x	$\bar{u}_p/\bar{u}_{p_c}$	$\left(\overline{u_p'^2}\right)^{\frac{1}{2}}/\bar{u}_{p_c}$	$\left(\overline{v_p'^2}\right)^{\frac{1}{2}}/\bar{u}_{p_c}$	r/x	$\bar{G}/\bar{G}_c$
0.0	1.0	.144	.026	0.0	1.0
.012	.954	.153	.029	.010	.811
.023	.887	.151	.037	.015	.688
.034	.817	.144	.042	.020	.507
.046	.780	.141	.050	.029	.272
.057	.734	.134	.058	.038	.122
.069	.714	.130	.063	.049	.046
.080	.694	.118	.064	.059	.022

Particle-Laden Jet SMD = 207 μm LR = 0.66

Gas-Phase Properties

x/d = 40

r/x	$\bar{u}/\bar{u}_c$	$\left(\overline{u'^2}\right)^{\frac{1}{2}}/\bar{u}_c$	$\left(\overline{v'^2}\right)^{\frac{1}{2}}/\bar{u}_c$	$\overline{u'v'}/\bar{u}_c^2$
0.0	1.0	.291	.187	.0003
.010	.981	.288	.189	.0049
.023	.923	.282	.196	.0115
.046	.680	.254	.191	.0183
.064	.533	.228	.184	.0185
.083	.428	.212	.171	.0139
.101	.318	.177	.155	.0112
.122	.190	.139	.124	.0094
.140	.127	.103	.102	.0035
.161	.083	.075	.077	.0019

Solid Phase Properties

x/d = 1

r/x	$\bar{u}_p/\bar{u}_{p_c}$	$\left(\overline{u_p'^2}\right)^{\frac{1}{2}}/\bar{u}_{p_c}$	$\left(\overline{v_p'^2}\right)^{\frac{1}{2}}/\bar{u}_{p_c}$	r/x	$\bar{G}/\bar{G}_c$
0.0	1.0	.107	.036	0.0	1.0
.138	.994	.113	.042	.055	.992
.229	.990	.116	.045	.156	.981
.321	.988	.130	.051	.248	.972
.413	.931	.146	.065	.339	.969
.459	.878	.155	.080	.431	.910
.505	.725	.157	.097	.495	.580
.550	.521	.158	.134	.569	.223
.596	.389	.156	.137	.624	.130
.642	.248	.137	.128	.670	.063
.688	.169	.121	.114	.706	.024

REFERENCES

1. Shuen, J. S., Solomon, A. S. P., Zhang, Q. F. and Faeth, G. M., "The Structure of Particle-Laden Jets and Nonevaporating Sprays," NASA CR-168059, 1983.

2. Shuen, J. S., Chen, L. D. and Faeth, G. M., "Predictions of the Structure of Turbulent, Particle-Laden, Round Jets," AIAA Paper No. 83-0066.

3. Solomon, A. S. P., Shuen, J. S., Zhang, Q. F. and Faeth, G. M., "Measurements and Predictions for Nonevaporating Sprays in a Quiescent Environment," AIAA Paper No. 83-0151.

4. Shuen, J. S., Chen, L. D. and Faeth, G. M., "Evaluation of a Stochastic Model of Particle Dispersion in a Turbulent Round Jet," AIChE J., Vol. 29, 1983, pp. 167-170.

5. Faeth, G. M., "Evaporation and Combustion of Sprays," Prog. in Energy and Combust. Sci., Vol. 9, 1983, pp. 1-76.

6. Modarress, D., Wuerer, J. and Elghobashi, S., "An Experiment Study of a Turbulent Round Two-Phase Jet," AIAA Paper No. 82-0964, 1982.

7. Modarress, D., Tan, H. and Elghobashi, S., "Two-Component LDA Measurement in a Two-Phase Turbulent Jet," AIAA Paper No. 83-0052, 1983.

8. Shearer, A. J. Tamura, H. and Faeth, G. M., "Evaluation of a Locally Homogeneous Flow Model of Spray Evaporation," J. of Energy, Vol. 3, 1979, pp. 271-278.

9. Mao, C-P., Szekely, G. A., Jr. and Faeth, G. M., "Evaluation of a Locally Homogeneous Flow Model of Spray Combustion," J. of Energy, Vol. 4, 1980, pp. 78-87.

10. Mao, C-P., Wakamatsu, Y. and Faeth, G. M., "A Simplified Model of High Pressure Spray Combustion," Eighteenth Symposium (International) on Combustion, The Combustion Institute, Pittsburgh, 1981, pp. 337-347.

11. El Banhawy, Y. and Whitelaw, J. H., "Calculation of the Flow Properties of a Confined Kerosene Spray Flame," AIAA J., Vol. 18, December 1980, pp. 1503-1510.

12. Mongia, H. C. and Smith, K., "An Empirical/Analytical Design Methodology for Gas Turbine Combustors," AIAA Paper No. 78-998, 1978.

13. Boyson, F. and Swithenbank, J., "Spray Evaporation in Recirculating Flow," Seventeenth Symposium (International)

on Combustion, The Combustion Institute, Pittsburgh, 1979, pp. 443-453.

14. Yuu, S., Yasukouchi, N., Hirosawa, Y. and Jotaki, T., "Particle Turbulent Diffusion in a Dust Laden Round Jet," AIChE J., Vol. 24, 978, pp. 509-519.

15. Dukowicz, J. K., "A Particle-Fluid Numerical Model for Liquid Sprays," J. Comp. Phys., Vol. 35, 1980, pp. 229-253.

16. Gosman, A. D. and Ioannides, E., "Aspects of Computer Simulation of Liquid-Fueled Combustors," AIAA Paper No. 81-0323, 1981.

17. Lockwood, F. C. and Naguib, A. S., "The Prediction of the Fluctuations in the Properties of Free, Round Jet, Turbulent, Diffusion Flames," Combustion and Flame, Vol. 24, 1975, pp. 109-124.

18. Gosman, A. D., Lockwood, F. C. and Syed, S. A., "Prediction of a Horizontal Free Turbulent Diffusion Flame," Sixteenth Symposium (International) on Combustion, The Combustion Institute, Pittsburgh, 1977, pp. 1543-1555.

19. Bilger, R. W., "The Structure of Diffusion Flames," Comb. Sci. Tech., Vol. 13, 1976, pp. 155-170.

20. Bilger, R. W., "Turbulent Jet Diffusion Flames," Prog. Energy Combust. Sci., Vol. 1, 1976, pp. 87-109.

21. Schlichting, H., Boundary Layer Theory, McGraw-Hill Book Co., New York, 1979, p. 599.

22. Hinze, J. O., Turbulence, 2nd Ed., McGraw-Hill, New York, 1975, p. 427; also pp. 724-734.

23. Al Tawell, A. M. and Landau, J., "Tubulence Modulation in Two-Phase Jets," Intl. J. Multiphase Flow, Vol. 3, 1977, pp. 341-351.

24. Hinze, J. O., "Turbulent Fluid and Particle Interaction," Progress in Heat and Mass Transfer (G. Hetsroni, S. Sideman and J. P. Hartnett, ed.), Vol. 6, Pergamon Press, Oxford, 1972, pp. 433-452.

25. Crowe, C. T., "Review-Numerical Models for Dilute Gas-Particle Flows," J. Fluid Engrg., Vol. 104, 1982, pp. 297-303.

26. Faeth, G. M. "Current Status of Droplet and Liquid Combustion," Prog. Energy Combust. Sci., Vol. 3, 1977, pp. 191-224.

27. Panchev, S., Random Functions and Turbulence, Pergamon Press, Oxford, 1971.

28. Faeth, G. M., "Recent Advances in Modeling Particle Transport Properties and Dispersion in Turbulent Flow," Proceedings of the ASME-JSME Thermal Engineering Conference, Vol. 2, ASME, New York City, 1983, pp. 517-534.

29. Laats, M. K. and Frishman, F. A., "Assumptions Used in Calculating the Two-Phase Jet," Fluid Dynamics, Vol. 5, 1970, pp. 333-338.

30. Laats, M. K. and Frishman, F. A., "Scattering of an Inert Admixture of Different Grain Size in a Two-Phase Axisymmetric Jet," Heat Transfer-Soviet Res., Vol. 2, 1970, pp. 7-12.

31. Levy, Y. and Lockwood, F. C., "Velocity Measurements in a Particle Laden Turbulent Free Jet," Combustion and Flame, Vol. 40, 1981, pp. 333-339.

32. Peskin, R. L. and Kau, C. J., "Numerical Simulation of Particle Motion in Turbulent Gas-Solid Channel Flow," J. Fluid Engrg., Vol. 101, September 1979, pp. 319-325.

33. Melville, W. K. and Bray, K. N. C., "A Model of the Two-Phase Turbulent Jet," Int. J. Heat Mass Transfer, Vol. 22, 1979, pp. 647-656.

34. Danon, H., Wolfshtein, M. and Hetsroni, G., "Numerical Calculations of Two-Phase Turbulent Round Jets," Int. J. Multiphase Flow, Vol. 3, 1977, pp. 223-234.

35. Elghobashi, S. E. and Abou-Arab, T. W., "A Two-Equation Turbulence Model for Two-Phase Flows," Phys. Fluids, Vol. 26, 1983, pp. 931-938.

36. Tennekes, H. and Lumley, J. L., A First Course in Turbulence, The MIT Press, Cambridge, MA, 1972.

37. Daly, B. J. and Harlow, F. H., "Transport Equations in Turbulence," Phys. Fluids, Vol. 13, 1970, pp. 2634-2649.

38. Szekely, G. A., Jr. and Faeth, G. M., "Reaction of Carbon Black Slurry Agglomerates in Combustion Gases," Nineteenth Symposium (International) on Combustion, The Combustion Institute, Pittsburgh, 1983, pp. 1077-1085.

39. Shearer, A. J., "Evaluation of a Locally Homogeneous Flow Model of Spray Evaporation," Ph.D. Thesis, The Pennsylvania State University, University Park, PA, 1979.

40 Abramovich, G. N., The Theory of Turbulent Jets, MIT Press, Cambridge, MA, 1963.

41. Becker, H. A., Hottel, H. C. and Williams, G. C., "Mixing and Flow in Ducted Turbulent Jets," Ninth Symposium (International on Combustion, The Combustion Institute, Pittsburgh, 1962, pp. 7-20.

42. Spalding, D. B., GENMIX; A General Computer Program for Two-Dimensional Parabolic Phenomena, Pergamon Press, Oxford, 1971.